Republic of Iraq
Ministry of Higher Education and Scientific Research
University of Babylon
College of Education for
Pure Sciences
Department of Physics

Fabrication and Characterization of (PVP-PVA-Ferrite) Nanocomposites and their Applications

A Thesis

Submitted to the Council of the College of Education for Pure Sciences , University of Babylon in Partial Fulfillment of the Requirements for the Degree of Master in Education / Physics

By

Ali Jasim Mohammed Masarie

B. Sc. in Physics
(University of Babylon- 2007)

Supervised by

Prof. Dr. Sameer H. Al- Nesrawy

2022 A.D. 1443 H.D.

بسم الله الرحمن الرحيم

أَمَّن يُجِيبُ ٱلْمُضْطَرَّ إِذَا دَعَاهُ وَيَكْشِفُ ٱلسُّوٓءَ
وَيَجْعَلُكُمْ خُلَفَآءَ ٱلْأَرْضِ ۗ أَءِلَٰهٌ مَّعَ ٱللَّهِ ۚ قَلِيلًا مَّا
تَذَكَّرُونَ ﴿62﴾ أَمَّن يَهْدِيكُمْ فِي ظُلُمَٰتِ ٱلْبَرِّ
وَٱلْبَحْرِ وَمَن يُرْسِلُ ٱلرِّيَٰحَ بُشْرًۢا
بَيْنَ يَدَيْ رَحْمَتِهِۦٓ ۗ أَءِلَٰهٌ مَّعَ ٱللَّهِ ۚ تَعَٰلَى ٱللَّهُ عَمَّا
يُشْرِكُونَ ﴿63﴾

صدق الله العلي العظيم

سورة النمل الآية (62-63)

ACKNOWLEDGEMENTS

First of all praise be to “ALLAH” for giving me the strength to complete this work.

I would like to submit my sincere gratitude to my supervisor Prof. Dr. **Sameer H. Al- Nesrawy** for his helpful advice, valuable suggestions, and encouragement throughout this study

Special thanks to the Deanery of College of Education for Pure Sciences and the Head of the physics department and to all my professors gave me everything.

Finally, my deep gratitude and dedication go to my wife, my family and my friends for their love, support, guidance, and endless patience throughout all my endeavors.

Ali jasim

2022

Dedication

TO .....

MARTYRS OF IRAQ AND THE POPULAR CROWD AND SECURITY FORCES

SOUL OF MY FATHER....

MY MOTHER....

MY WIFE,

MY CHILDREN,

MY BROTHERS AND MY SISTERS,

MY SUPERVISOR,

MY HEART THROB, IRAQ,

WITH ALL THE LOVE AND APPRECIATION

Ali Jassim

2022

Abstract

In the present study, $Cu_xNi_{1-x}FeO_3$ with x=0.1 and 0.3 at a temperature of 1200 C° was ware by the Co-Precipitation method because it gives great homogeneity to the powder particles.

The XRD obtained that the formation of the face center cubic spinel phase (FCC) at the degree of calcination of powder ferrite $Cu_xNi_{1-x}FeO_3$ with x=0.1 and 0.3. Then added different concentrations of this ferrite (1,3 and 5)wt% to the Polyvinyl pyrrolidone (PVP)/ Poly(vinyl alcohol) (PVA) nanocomposite.

From the field emission scanning electron microscope (FESEM) and the optical microscope images showed the ferrite $Cu_xNi_{1-x}FeO_3$ with x=0.1 and 0.3 form a continuous network inside the PVP/PVA composites shift in certain bonds and changes in the intensities of particular bonds seen in the Fourier transformation infrared spectroscopy (FTIR) spectrum, demonstrating that there are no interactions between the polymer matrix (PVP/PVA) and ferrite.

From the optical properties, **t**he absorbance increases with increasing the concentration of ferrite($Cu_xNi_{1-x}FeO_3$ with x=0.1 and 0.3) and it is decrease with increasing wavelength for all samples of nanocomposites , while the transmittance decrease with the increasing of the ferrite concentration and it is increase with increasing wavelength. The energy gap for decrease with the increasing of the ferrite $Cu_xNi_{1-x}FeO_3$ with x=0.1 and 0.3 inside (PVP/PVA) polymer matrix. Increasing in absorption coefficient, extinction coefficient, refractive index, real and imaginary of dielectric constants and optical conductivity with increase ferrite

concentration of $Cu_x Ni_{1-x}FeO_3$ with x=0.1 and 0.3 (PVP/PVA) inside of the polymer matrix.

The AC electrical properties such as the dielectric constant and loss increase with increasing the concentration of ferrite $Cu_x Ni_{1-x}FeO_3$ with x=0.1 and 0.3 inside (PVP/PVA) polymer matrix and decrease with the increase of frequency of the applied electric field, while the A.C electrical conductivity increase with the increase of the ferrite concentration $Cu_x Ni_{1-x}FeO_3$ with x=0.1 and 0.3 inside (PVP/PVA) polymer and also increase with frequency. Attenuation of microwaves within the frequency range (4-7) GHz for different concentration of $Cu_x Ni_{1-x}FeO_3$ with x=0.1 and 0.3 inside (PVP/PVA) polymer. The ability of this nanocomposite to attenuators of microwaves emitted within the S-band.

List of Symbols

Symbol	Physical Meanings	Units
A	Absorbance	
A.C	Alternation Conductivity	
B	FWHM	degree
C	Velocity of light	m/s
C.B	Conduction band	
C_0	Vacuum capacitor	µF
C_p	Parallel capacitance	µF
D	Average crystallite size	Nm
d_{hkl}	Interplanner Spacing	
E_g	Energy Band gap	eV
$E^{opt}g$	Optical energy gap	eV
E_P	Photon energy	eV
h	Planck s Constant	6.63×10^{-34}J.s
hv	Photon Energy	eV
I_0	Incident intensity of light	mw/cm^2
I_A	Absorbed intensity of light	mw/cm^2
K_0	extinction coefficient	m^2
K_P	Boltzman constant	J/K
M	Molecular concentration	
n	refractive index	-
N	number of moles	Mol.

R	Reflectance	
S_{11},S_{21},S_{12},S_{22}	The dispersion coefficients S11 (related to the radiative emission from port 1 and collected in port 1) and S21 (the dispersion coefficient related to the radiative emission from port 1 and collected in port 2) .... etc.	
T_0	Transmittance	
t	Thickness	Nm
T	Temperature	Kelvin
V.B	Valence band	
VNA	Vector Network Analyzer	
ω	Angular frequency	Gm
W	Weight	g/mol.
w_m	molecular weight	
Γ_j	Reflection coefficient	
ε^*	Complex permittivity.	F/cm
ε_0	Vacuum permittivity	f/cm
ε''	Dielectric loss	%
A	absorption coefficient	cm^{-1}
ε_i	Imaginary Part of Dielectric Constant	-
ε_r	Real Part of Dielectric Constant	-
θ	Diffraction angle	Degree
λ	Wavelength	Nm
$\sigma_{A.C}$	A.C electrical conductivity	$(ohm.cm)^{-1}$
σ_{op}	Optical Conductivity	$(ohm.cm)^{-1}$
υ	Frequency	Hz

List of Abbreviations

OMCs	Organic Matrix Composites	
MMCs	Metal matrix composite	
CMCs	Ceramic Matrix Composites	
PMCs	polymer matrix composites	
FRP	Fiber composites	
PVP	Polyvinyl pyrrolidone	
PVA	Polyvinyl alcohol	
Cd O	cadmium Oxide	
Zn O	zinc Oxide	

Mn O	manganese Oxide		
Ni O	nickel Oxide		
Mn,Zn,Fe_2O_4	Manganese–zinc ferrite		
XRD	X-ray Diffraction		
VNA	vector network analyzer		
SEM	Scanning Electron Microscope		
FTIR	Fourier Transforms Infrared Spectroscopy		
VSM	Vibrating Samples Magnometer		
TEM	Transmission electron microscopy		
MNPS	magnetic nano-particles		
EDS	Energy-Dispersive X-Ray Spectroscopy		
PVC	Polyvinyl chloride		
Pb O	lead(II) oxide		
$FeCl_3$	Ferric chloride		
$Cu(NO_3)_2.3H_2O$	Copper nitrate		
PEG	Poly-Ethylene Glycol		
$Ni(No_3)_2.6H_2O$	Nickel nitrate		
$FeCl_3$	Ferric chloride		
NaOH	Sodium hydroxide		
CMC	Carboxyl methylcellulose		
SDS	sodium dodecyl sulfate		
CTAB	Cetrimonium bromide		
FE-SEM	Field emission scanning electron microscope		
FWHM	Full Width at Half Maximum		

List of Figures

Chapter One

Introduction and Literature Review

1.1 Introduction:

In general, most polymers were only employed to make low-cost items that were only used for a few functions. However, due to fast technological advancements, certain industrial materials have had to be replaced by newer materials for superior specifications [1,2]. Later on the progress increased substantially. Scientists are actively working on low-cost, flexible, and versatile polymers. They may be utilized in homes, autos, and industries. Electrical equipment and components have greatly benefited from the use of these materials. When it comes to electrical properties, polymers are often more stable than their mechanical counterparts because of their chemical structure rather than their microstructure. Optically, there are several applications that may benefit from optical features. Polymers are excellent insulators because of their high electrical resistance. The conductivity of a polymer's surface layer may be affected by both humidity and surface contaminants. Surface resistivity may be determined by measuring the current flowing between two electrodes that are in contact with the polymer's surface [3].

Each molecule is made up of thousands of atoms joined by covalent chemical bonds, and the polymer is made up of enormous organic molecules (Large molecules) of repeating tiny structural units (monomers) bonded together in a process called polymerization. Molecules in a polymer are attracted to one another by forces that vary depending on the polymer type [4].

1.2 Composite materials

Composite materials are those in which a second component with quite different qualities is mixed in with the polymer so that both contribute to the product's properties. The added component is thought to reinforce the product by increasing its strength or hardness[5]. Composite

materials originate in a number of shapes and sizes, and they're made in a diversity of ways. Carbon and glass fibers are the greatest common, and they can be mixed with a diversity of polymer matrices [6]. Their high specific strength, low density, stiffness, excellent fatigue endurance, and low thermal coefficient make them ideal for aerospace and military applications (in the fiber direction), advanced composite materials possess seen increased use in the aerospace, marine, and automobile industries in recent decades [7]. A composite material system is made up of two or more distinct phases that, when combined, provide aggregate qualities that are unique from their component properties. Composites may be quite useful. [8]. Polymer nanocomposites have a wide range of uses, including protective coatings and computer chip packing (insulation) their high strength, temperature stability, process ability and chemical resistance. Improvements in mechanical characteristics and thermal stability [9,10].

The following two levels of classification are often used to classify composite materials [11]:

The first level of categorization is usually classified using the matrix component. OMCs, MMCs, and CMCs are the three main types of composites: (CMCs). Polymer matrix composites (PMCs) and carbon matrix composites (also known as carbon-carbon composites) are examples of matrix organic composites. composites Fiber reinforced, composites laminar and composites are particle included in the level second of classification because of their reinforcing properties. Discontinuous and continuous fiber composites (FRP).

1.3 Nanomaterials

Nanomaterials are the foundations of nanoscience; they are defined as materials with dimensions less than 100 nm that have at least one unique property that distinguishes them from bulk materials. These properties can be used in a variety of fields, including pharmaceuticals, cosmetics, and nanoelectronics [12]

Nanomaterials are recently produced materials in which the nanoscale structure under control has a significant impact on the material's or device's desired behavior. There are three types of nano-materials: discrete nano-materials, nano-scale device materials, and bulk nano-materials. Discrete nano-materials are those that are individually packaged. Nano-scale deivce materails are nano-scale materail elemants that are contianed within devicas, usuall as thin films. Bulk nano-materials are materials with structure controlled at the nano-scale that are accessible in bulk quantity (defin here as at least 3 mm volume) [13]. Nanostructures of nano-materials can be classified according to their primary spatial dimensions (X, Y, and Z) [14]:

1-zero-dimension (0-D) (represent for quantum dots or nanoparticles).

2-one-dimension (1-D) (indicate to nanofibres, nanorods, nanobelts, nanotubes and nanowires).

3-two-dimension (2-D) (refer to nanosheets, nanowalls and nanoplates)

4-three-dimension (3-D) (represent to nanoflowers and other complex structures such as nanotetrapods) .

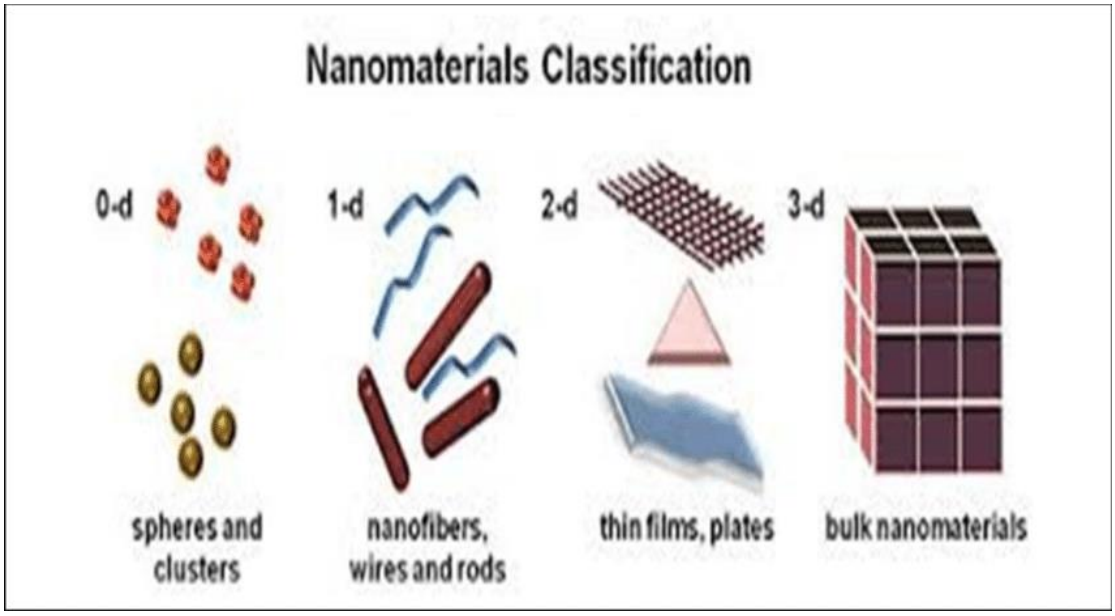

Figure(1-1) : Types of nanomaterial[14]

1.4 Nanocomposite

Nanocomposites are a key component in the development of innovative advanced materials for a wide range of applications, including electrical engineering. Nanocomposites have piqued the attention of both academia and industry [15]. Since each kind of composite has its own special characteristics and those characteristics may shift from one material to another, a composite's traits are different from those of its constituent parts. The matrix (the fundamental material) and the additives are the two main components of the compound. To build a compact system, the matrix surrounds other components and makes them more cohesive[16]. Material systems made up of two or more different materials are called composites; the features of a composite are unique from their elements. The matrix (the fundamental ingredient) and the additives are the two main components of the compound. Created by the matrix, this tiny system is held together by other parts[15,16]. The properties of polymer nanocomposites are influenced by the nature of the polymer matrix and filler, dispersion state of the particles, filler- matrix interaction, filler size and surface modification of the filler [17].

1.5. Polyvinyl pyrrolidone (PVP)

There are several uses for the hydrophilic Polyvinyl Pyrolidone and separation procedures to improve the hydrophilic character of the blended polymeric materials [18,19]. Due to its water solubility and exceedingly low concentration [20]. PVP has gotten a lot of interest among the conjugated polymers because of its outstanding environmental stability, ease of processing, and transparency. PVP is a potential material with a high charge storage capacity , electrical and optical characteristics that are depending on the dopant. PVP has been shown to be chemically inert, non-toxic, and intriguing. [21]. It has a great proclivity for forming complexes with a broad range of smaller compounds. [22]. In table (1) some physical properties of the PVP. Povidone, or Polyvinylpyrrolidone, is a synthetic polymer made by radical polymerizing the monomer, N-vinylpyrrolidone [23].

Table (1-1): Some of the physical and chemical characteristics of (PVP) [24, 25]

Properties	PVP
Appearance	Water soluble amorphous(white to yellow)powder
Molecular formula	$(C_6H_9NO)_n$
Density	1.2g/cm^3
Melting point	(150-180)°C
Boiling point	217.6 °C
Glass Transition Temperature (Tg)	(165-175) °C
molecular weight	40000

1.6 Polyvinyl alcohol (PVA)

PVA is a water soluble polymer that comes in a variety of molecular weight and viscosity grades. [26]. PVA was elected as a polymer matrix due to its water-dispensability and hydrophobicity, which give it an excellent compatibility [27] .Poly(vinyl alcohol) is a typical bio plastic with good properties such as oil and chemical resistance, as well as the ability to withstand practically all organic solvents. PVA is also ideal for use as a paper adhesive and in packaging. [28,29]. In the early twentieth century, PVA, a man-made polymer, was widely employed for a number of uses resins, Lacquers, threads surgical and food packaging materials that come in to direct touch with food have all produced been using it in the medical, commercial, industrial and sectors food [30]. Due to its structure compatible and hydrophilic capabilities, this polymer is often mixed with other polymers such as biopolymers and other polymers hydrophilic. It is used in many industrial applications to improve film mechanical properties [31].

Table (1.2): Some physical and chemical properties of (PVA)[32,33]

Properties	PVA
Appearance	**White to cream granular powder**
Molecular formula	**$(CH_2CH(HO))_n$**
Density	**1.19–1.31 g/cm3**
Melting point	**200°C (392°F-473K)**
Glass Transition Temperature T_g	**$(75\text{-}85)C^0$**
molecular weight	**18000**

1.7 Ferrite

Ferrite is one of magnetic oxide compounds, which comprise iron oxide as a major component[34]. For the most part, ferrites are made from iron oxides and are ferromagnetic ceramic compounds [35]. They have a dark brown or gray hue to them, and their physical properties describe them as being very hard and brittle [36]. Ferrites have dielectric characteristics, which means that although electromagnetic waves may flow through them, they cannot readily carry electricity. Because these metals conduct electricity, they offer an advantage over iron, nickel, and other transition metals that exhibit magnetic characteristics in many applications [37].

Ferrite is a chemical compounds (ferromagnetic materials) that contains oxygen and at least two magnetic ions, (A) and (B) represent various metal cations consisting of different combinations of iron oxides. Added mineral oxides such as CdO, ZnO, MnO, and NiO. Other oxides (manganese, cadmium, zinc, nickel, etc.) are less likely. More than that, these low-cost materials are easier to build and more formable than metals and amorphous magnetics [38].

1.7.1 Types of Ferrites according to Magnetic Properties :

Hard and soft ferrites are classified by their magnetism. This categorization is based on ferrite's magnetization or demagnetization. Soft ferrites are readily magnetized or demagnetized, but hard ferrites are not[39].

1.7.1.1 Soft Ferrites

It is a type of ceramic that can be easily magnetized This indicates that magnetic materials have a low coercive field and high magnetization is required in many applications, and the hysteresis loop is long and narrow and therefore the energy loss is very low in these magnetic

materials [40]. Soft ferrites have certain advantages over other electromagnetic materials including high electrical resistance, eddy current losses over a wide range and high and stable transmittance temperatures. Many examples of Spinel ferrites like manganese–zinc ferrite $(Mn,Zn,Fe)O_4$ system are commercially important soft magnets. In addition, lithium ferrite, nickel ferrite, and garnets are other examples of soft ferrites [41, 42].

1.7.1.2 Hard Ferrites:

Hard ferrites have a high coactivity and restrain applied field to demagnetize, which is why this is the case., which is necessary for a permanent magnet. They are also magnetically permeable. Ceramic magnets are inexpensive and commonly utilized in household items like refrigerator magnets. Hard ferrite magnets include iron oxide and barium or strontium carbonate. Common hard ferrites: It is utilized in tiny electric motors, microwave devices, magneto-optic media, electronics, and telecommunications[43] [44].

1.8 Literature review

In 2016, J. M. Al-Issawe *et.at.* [45] preparation ferrite using precipitation method. The X-ray diffraction was used to confirm the spinel phase formation of the prepared samples. Ferrite has been added to silicone rubber. Microwave attenuation measurements were performed using VNA to determine the sensitivity of materials intended for microwave attenuation.waves. The results showed that the prepared materials have a high microwave absorption capacity .Waves in the frequency range (3-5) GHz.

In 2016, A. K. Thanigai *et.al*. [46] synthesis Polymer co-precipitation yields uniform nan sheets. To co-doped ferrites magnetic nanoparticles,

pure (0 g), 0.2 g, and 0.5 g polyvinyl alcohol were added. They used XRD, SEM, FTIR, and Raman spectroscopy. XRD verified $NiCoFe_2O_4$ spinel structure. FTIR verified $NiCoFe_2O_4$ and PVA. Also, PVA was verified by Raman modes.

In 2017 S. Mirzaee *et. al.* [47] Co-precipitation of Cobalt Ferrite - Poly(vinyl) Alcohol nanocomposites with and without ultrasonic treatment . (XRD), (VSM), (FTIR), and (TEM) were explored. According to the findings, ultrasonic irradiation enhances magnetic anisotropy energy of(7nm) magnetic nanoparticles (MNPS). The lattice strain caused diffraction peak widening and shift to angle lower. These photos demonstrate nano crystallite cobalt ferrite totally disseminated and embedded in PVA matrix in the ultrasonic irradiated sample.

In 2018, M. T. Ramesan *et. al.* [48] Sol-gel was mixed by spontaneous combustion of ferrite nanoparticles ($ZnFe_2O_4$) at different concentrations. Infrared (FTIR) and X-ray (FTIR peak shift offsets confirm the chemical interactions between the polymer and $ZnFe_2O_4$. XRD data show that adding $ZnFe_2O_4$ nanoparticles to the polymer mixture increases the crystalline character of the mixture. SEM images of the nanocomposites show the dispersion of nanoparticles in the PIN/PVA mixture, while TEM images show spherically formed nanoparticles with an average size of 15 nm.

In 2018 S. Mallesh *et. el.* [49] The prepared of Mn-Zn-ferrite nanoparticles by sol-gel process and for different concentrations ($0\leq x\leq 1.0$) at 1200 °C. The results showed that it is in the cubic spinel and the stability of the spin ferrite phase in the concentration of (Mn) and annealing temperature, in air, oxygen and air argon. The magnetic and structural properties of argon and air were compared and it was found that the partial pressure of oxygen plays a significant role instability as well as

in magnetic properties effect of the depletion of Fe^{+3} ions from the spinel structure that affects the action distribution. While the magnetic properties are controlled by controlling the conditions of operation.

In 2019, T. Kaewmanee *et .al.* [50] prepared the ferrite compound hydrothermal method with oleic acid anti-agglomeration all samples were spherical in form, firmly aggregated, and energy-dispersive in nature, as shown by XRD. EDS confirms that no element was lost in the produced samples. The modified nanoparticles were confirmed super paramagnetic using a vibrating sample magnetometer (VSM).

In 2020, R. Sagayaraj *et.al.* [51] prepared type hexaferrites Co-precipitation of nanoparticles samples were examined by XRD, SEM, FT-IR, antimicrobial, and magnetometer tested (VSM). XRD shows polycrystalline sample with hexagonal crystal structure. It shows octahedral and tetrahedral coordination. Pure and doped materials' band energy gabs are semiconductors. The SEM micrograph shows the hexagonal structure and spongy shape of BHFs. The incorporation of zinc (Zn^{2+}) in VSM enhances the magnetic characteristics of the samples, enhancing their antibacterial activity. While doped ferrite has a band energy gap of 2.4 eV.

In 2020, T.A. Taha *et. al.* [52] prepared $Ni_{0.5}Zn_{0.5}Fe_2O_4$ nanoparticles prepared using green sol-gel auto-combustion method. PVA Solution cast $Ni_{0.5}$ $Zn_{0.5}$ Fe_2O_4 nano-composites were successfully made for dielectric spectroscopy. They observed dielectric characteristics of PVA-$Ni_{0.5}$ $Zn_{0.5}$ Fe_2O_4nano-composites at (323–403K).The PVA matrix with $Ni_{0.5}$ Z $n_{0.5}$ Fe_2O_4 nanoparticles has a higher dielectric constant. The specimen with 15% nano-$Ni_{0.5}$ $Zn_{0.5}$ Fe_2O_4 had the maximum dielectric loss at all temperatures.

In 2021, A. H. Alshammari *et.al.*[53] prepared polymer blend from Polyvinyl chloride (PVC)/Polyvinylpyrrolidone (PVP) with nano-zinc ferrite by using the solution casting method. The nanocomposites are examined by the XRD, SEM and FTIR analysis, thermal and dielectric properties. They found cubic crystal structure of $ZnFe_2O_4$ nanoparticles. A uniform dispersion of nanostructured zinc ferrite was confirmed by SEM morphology. PVC/PVP with $ZnFe_2O_4$ additions FTIR spectra indicated distinct absorption bands. All polymer mixes showed three phases of heat breakdown. A higher proportion of $ZnFe_2O_4$ in the polymer results in a lower dielectric constant. All samples AC conductivity rises with frequency.

In 2021, M. S. Toman *et.al.* [54] prepared (PbO/PVA/PEG) nanocomposites by combining lead oxide weight concentrations (0,1,3,5,7)% wt. The optical microscopy, FTIR and electrical properties of nanocomposites (PVA-CMC/PbO) were studied. The dielectric constant dropped with decreasing dielectric loss, whereas the frequency increased with introducing an electric field. The dielectric loss and constant dielectric of all increased samples with the quantity of lead oxide.

In 2021, A. A. Abid. *et.al.*[55] prepared polymer blend (PVA-PVP) Casting carbon black nanocomposites has been studied. Electrical and optical qualities have been examined using FTIR. The loss dielectric of the sample decreased with increasing frequency, whereas the A.C electrical conductivity increased. The concentration of carbon black enhanced the electrical conductivity (A.C), loss dielectric, and constant dielectric of all samples.

In 2022, S. Kittipon *et.al.*[56] The cobalt ferrite nanoparticles ($Co_xFe_{1-x}Fe_2O_4$) were generated by co-precipitation technique employing several

surfactants notably sodium dodecyl sulfate (SDS), hexadecyltrimethy lammonium bromide (CTAB). This work explored the magnetic and electrical properties of cobalt ferrite nanoparticles. Co_xFe_{1-x} Fe_2O_4 nanoparticles varied in size from 16 to 43 nm. Usage CTAB and SDS, the saturation magnetization of $CoFe_2O_4$ was decreased. The rise with Fe^{2+} mole ratio in $Co_xFe_{1-x}Fe_2O_4$ produced using the SDS template at 1.2 CMC. The Fe_3O_4 had the highest Ms of 100.4 emu/g employing the SDS template. The Fe_3O_4 nanoparticle could be used in various actuators and biological devices.

1.9 The Aims of Project

1. Preparation the ferrite Compound(FeO_3) using co-precipitation technique.
2. Synthesis of (PVP-PVA-FeO_3) nanocomposites that it used in a wide variety of industrial applications.
3. Study the structural, morphological, optical and A.C electrical properties of the nanocomposites prepared. This nanocomposite for microwave attenuation was used.

Chapter Two

Theoretical Part

2.1 Introduction

This chapter explains the main properties which make (PVP/PVA/ferrite) nanocomposite a good candidate for certain application. The study of structural and morphological properties were performed with X-ray diffraction (XRD), field emission scanning electron microscope (FESEM), Fourier transform infrared (FTIR) spectroscopy, optical properties of nanocomposite (absorbance, transmittances, electronic transitions and optical constants), AC electrical properties and microwave attenuation.

2.2 Structural and Morphological Properties:

2.2.1 X-Ray Diffraction (XRD)

It is a well-known technique into analyzing the structure of size and thin films (XRD) X-ray diffraction [57]. When a solid, such as a single crystal or polycrystalline powder, has a long-range (at least m) periodic atomic order, it is bombarded by X-rays and acts as an extended periodic grating, producing a pattern of diffraction with numerous sharp points known as Bragg diffraction peaks [58] . when the X-ray beam is incident at a specific angle on the crystalline material Because of the coherent scattering from the atoms, diffraction occurs at the intersecting planes. Because the wavelength of an X-ray is similar to the distance between atoms, diffraction from a variety of planes produces a certain diffraction pattern. The required condition for diffractions emanating from separate planes is provided by Bragg's law below. The diffraction Bragg's law can be stated as [57]:

$$m\lambda = 2d_{hkl}\, sin\theta \quad \ldots\ldots\ldots\ldots\ldots\ldots (2-1)$$

The wavelength of the incoming, X-ray beam the Bragg's diffraction angle (θ) of the XRD peak and the interlinear distance (d_{hkl}) may all be used to calculate the distance [57].

Fig.(2.1) demonstrates that the (XRD) meets Bragg's requirement

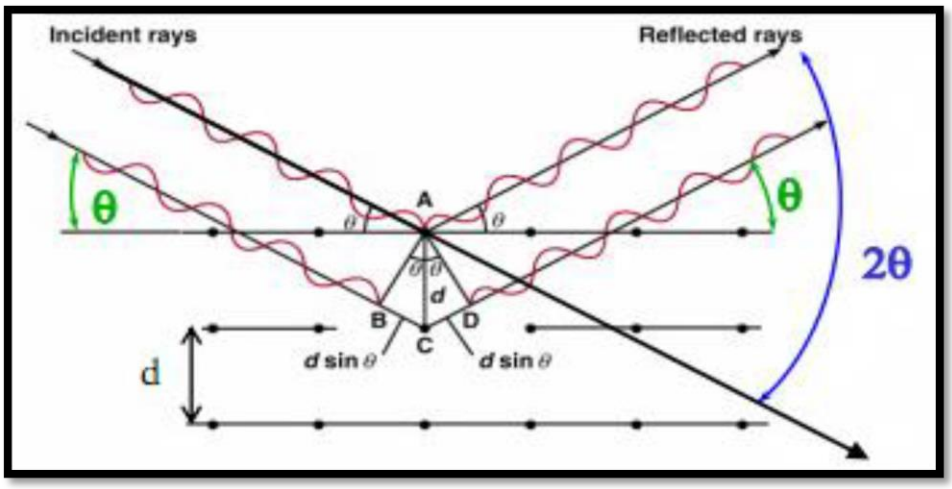

Figure(2.1) diffraction Bragg [59].

2.2.1.1 Average crystallite size (D)

The average crystallite size (D) can be estimated using Scherrer's method. Crystallite size can be calculated from peak broadening using XRD [60]. X-ray line broadening method was used to determine the particle size of ferrite by using Scherrer's equation. [61][62][63]:

$$D = \frac{K\lambda}{\beta cos\theta_{\beta}} \quad \text{.....(2-2)}$$

where K is 0.9 depend on the structure, (λ) Wavelength of incident X-ray radiation(1.54056Å), (β):Full width at half maximum of the peak (radian). θ_{β} θ_{β}Bragg diffraction angle of the XRD peak (degree).

2. 2.2 Field emission scanning electron microscope (FESEM)

The (FE-SEM) uses a high-energy beam of electrons to raster scan across a sample surface. Surface topography, composition, as well as other qualities such as electrical conductivity, may be gleaned from signals generated by electrons interacting with atoms in the sample. There are two classes of emission source: thermionic emitter and field emitter [64]. The primary distinction between a SEM and a Field Emission Scanning Electron Microscope (FESEM) is the kind of emitter used (FE-SEM). Tungsten (W) and Lanthanum hexaboride (LaB6) are the most often utilized filament materials in Thermionic Emitters (TEs). When the filament material's work function is exceeded, electrons are released from the filament. Thermionic sources operate with a low level of brightness, cathode material evaporation, and thermal drift. By utilizing Field Emission, you may avoid these problems. The filament is not heated by a Field Emission Source (FE-SEM), also known as a cold cathode field emitter. When the filament is placed in a massive electrical potential gradient , the emission occurs. Tungsten (W) wire is often used to make the FES, which is then shaped into a sharp point. With developments in secondary electron detector technology, the FE source is compatible with scanning electron microscopes (SEMs)[65,66]. Cathode and anode voltages are typically between 0.5 to 30 kV, and the microscope needs an extreme vacuum (10–6 Pa) in the column of the microscope, as seen in figure (2.2)[67].

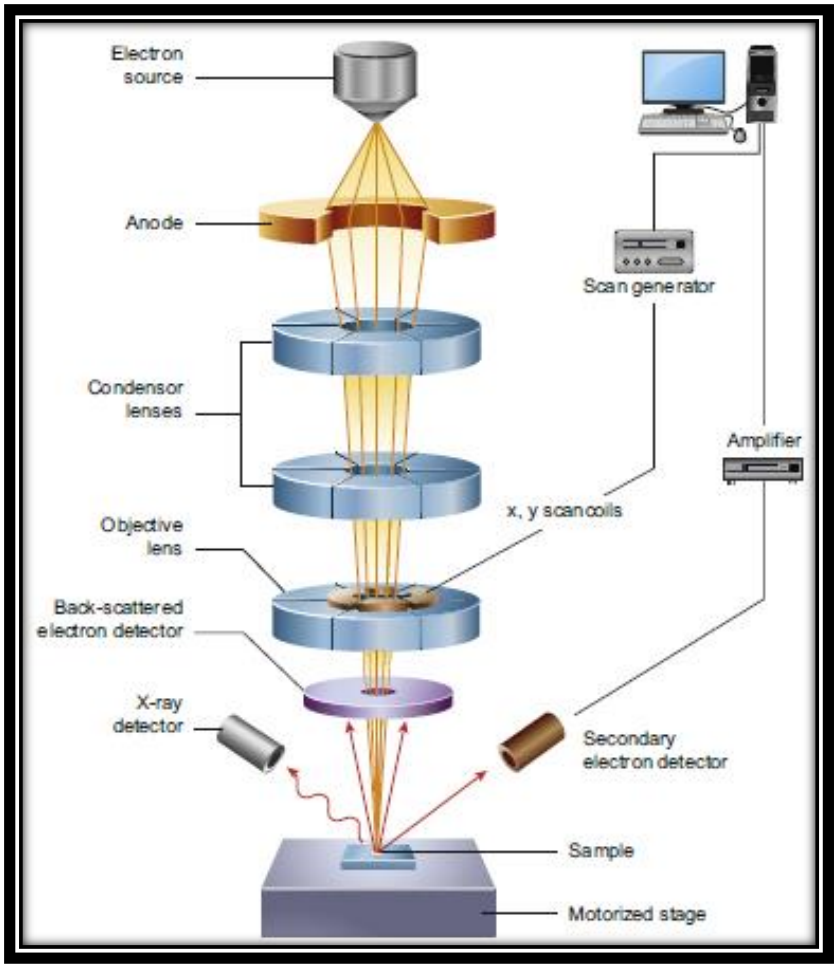

Fig.(2.2): Schematic diagram of the field scanning emission electron microscopy[68].

2.2.3 Optical Microscope

The study of optical absorption useful for clarification of indirect transitions, determine direct and the electronic structure. The addendum of nanoparticles in improves polymer the electrical, mechanical properties and optical of the materials [69]. The microscopy is most widely used for minute light diffracting specimens (such as bacterial flagella, bacteria, diatoms, flagella, microtubules, and polymers) and isolated organelles (such as cilia, actin filaments, gold particle and silver grains in his to chemical labeled cells and tissues). The number of scattering objects in the specimen is a significant aspect, as the

scattering of light from too many objects can obscure details and over- brighten the background [70].

2.2.4 Fourier Transforms Infrared (FTIR) Spectroscope

The Fourier transformation Infrared (FTIR) Spectroscopy is a non-destructive chemical characterization method. This spectral region is classified into three regions: far-infrared, mid infrared and near-infrared which are between (4~400cm^{-1}), between (400~4000cm^{-1}) and lastly, between (4000~14000 cm^{-1}), respectively. FTIR spectroscopy is a vibrational spectroscopic method that can be used for the optical study of molecular shifts. The allowable existence of this technology relies on the identification of vibration in the sample by the chemical functional group. Wherever an interaction takes place between infrared light and matter, the chemical bonds will stretch. [71]. Thus, a molecule is only absorbed at frequencies corresponding to its molecular vibration modes in the region of the electromagnetic spectrum between the visible (red) and the short (microwave) waves when exposed to radiation emitted by the thermal emission of a hot source (the source of IR energy) [72] .

2.3 The Optical Properties

2.3.1 Absorbance (A)

Absorbance is defined as the ratio of absorbed light intensity (I_A) to incident light intensity (I_o) by a substance [73].

$$A = \frac{I_A}{I_O} \quad \dots\dots\dots\dots\dots\dots\dots (2-3)$$

2.3.2 Transmittance (T)

It is determined by the proportion of the intensity of the rays (I_T) that transmits to the of the incident sunlight (Io) intensity as follows through the film [74]:

$$T = I_T / Io \qquad (2.4)$$

2.3.3 Fundamental Absorption Edge

The fundamental absorption edge can be defined as the rapid increasing in absorbance when absorbed energy radiation is almost equal to the band energy gap; therefore, the fundamental absorption edge represents the less difference in the energy between up point in valance band to bottom point in conduction band [75].

2.3.4 Absorption Regions

Absorption regions can be classified to three regions [76]:

A) High absorption Region:

This region is shown in Figure (2.3). The magnitude of the absorption coefficient (α) is larger or equal to (10^4 cm^{-1}). From this region the magnitude of forbidden optical energy gap (E_g opt.) can be introduced.

B) Exponential Region

This region is shown as in Figure (2.3). In (B), the absorption coefficient (α) is equal to ($1\ cm^{-1} < \alpha < 10^{\ 4} cm^{-1}$). It refers to transition between the extended levels from the Valens band (V.B.) to the local level in the conductive band (C.B.) and vice versa, transited from local levels in (V.B.) to the extended levels in the bottom of conductive band (C.B.)

C) Low absorption Region

The absorption coefficient (α) in this region is very small, it is about ($\alpha<1cm^{-1}$). The transition happens in this region because of state density inside space motion resulted from faults structural[80] as shown in Fig.(2.3), the part (C).

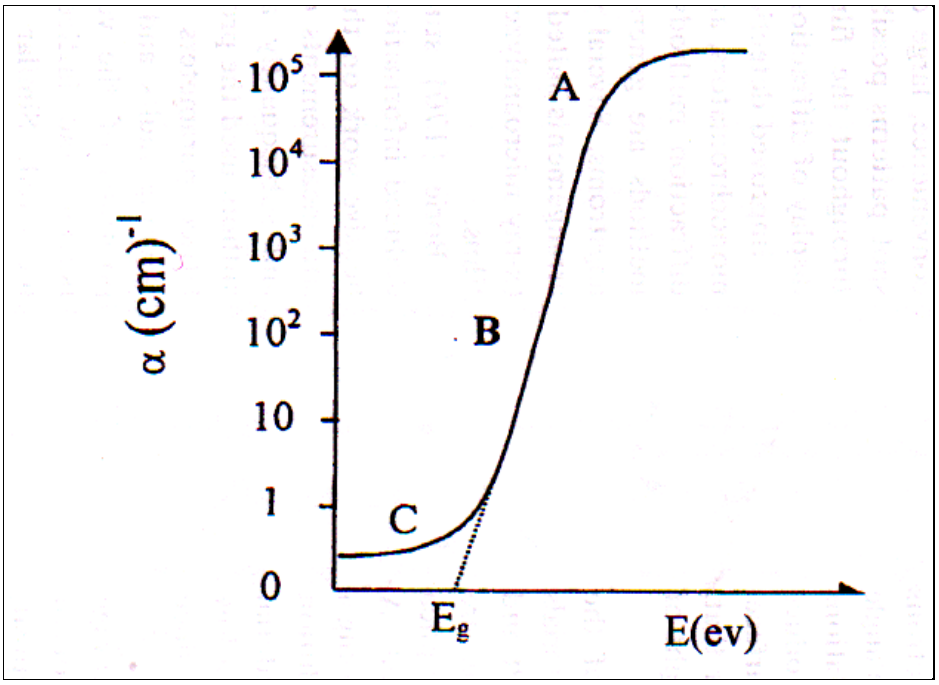

Figure (2 .3)The variation of absorption edge with absorption regions [77].

2.3.5 The electronic transitions

The electronics transformations can essentially stay divided in to two type [78]:

2 .3.5.1 Direct transition

This transition occurs in semiconductors when the conductive bottom $(C.B)$is exactly above the valence band $(v.B)$.This means they have the same wave vector value (ΔK=0), the absorption occurs in this state when $(E_g = h\nu)$.This form of transition involves the laws of energy and momentum conservation. There are two forms of direct transformations, [79] these are :

A) Allowed direct transition

Fig. (2-4-a) shows that this transition occurs from the top points in the $(V.B)$ and the bottom point in the $(C.B)$. The equation (2-4) provides the Tauc empirical relationship for this type of transition [80]:

$$\alpha h\vartheta \approx (h\vartheta - E_g)^{1/2} \quad \cdots\cdots\cdots\cdots\cdots\cdots (2\text{-}5)$$

B) Forbidden direct transitions .

The transition from near the top points of $(V.B)$and the bottom points of $(C.B)$is shown in Fig .(2-4-b) . The equation (2-5) gives the empirical relationship that corresponds to this transition[81]:

$$\alpha h\vartheta \approx (h\vartheta - E_g)^{1/3} \quad \cdots\cdots\cdots\cdots\cdots\cdots (2\text{-}6)$$

2.3.5.2 Indirect transitions

When the bottom of $(C.B)$is not above the top of $(V.B)$ in the curve(E-K), this transformation occurs. Where the value of the electron wave vector before and after transition is not equal ($\Delta K \neq 0$), the electron transits from (V.B) are not perpendicular. This form of transformation happens with the aid of a related particle called "Phonon," for energy and momentum law conservation. Hence, a phonon 's support is required to maintain the momentum,[81]:

$$hv = E_g \pm E_P \quad \cdots\cdots\cdots\cdots\cdots\cdots (2\text{-}7)$$

$$hkf = \text{hki} \pm \text{hkp} \quad \cdots\cdots\cdots\cdots\cdots\cdots (2\text{-}8)$$

Where the strength of the absorbed or emitted phonon is Ep.

c) Allowed Indirect Transitions

Fig.(2-4-c) indicates the change between the top of (C.B) and the bottom of (V.B) located in the area of(K-space)gap, so that[81]:

$$\alpha hv \approx (hv - E_g)^2 \cdots\cdots\cdots\cdots\cdots (2\text{-}9)$$

D) Forbidden Indirect Transitions

Fig.(2-4-d) indicates that this transition occurs between close points at the top of (C.B) and close points at the bottom of (V.B). The absorption coefficient for the phonon-absorption transition is defined by the following equation[82]:

$$\alpha hv \approx (hv - E_g)^3 \cdots\cdots\cdots\cdots\cdots (2\text{-}10)$$

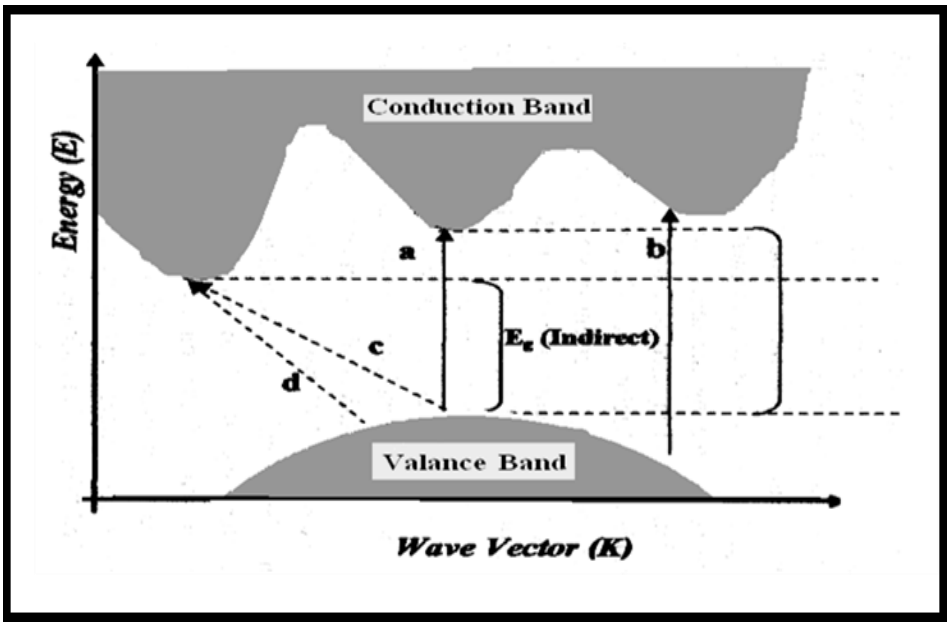

Figure.(2-4) : Electronic transitions [83]

(A) allowed direct transition . (C) allowed indirect transition.

(B) forbidden direct transition. (D) forbidden indirect transition.

2.4 Optical Constants :

Optical constants are parameters which are very imperative since they explain the materials' optical, behavior. An area of common interest [70] is the extraction of optical constants from various methods of optical measurement. The refractive index (n), extinction coefficient (k), real (ε_r) and imaginary (ε_i) portions of the dielectric constant were included in the optical constants [84].

$$n = \left(\frac{4R}{(R-1)^2} - k^2 \right)^{1/2} + \frac{(R+1)}{(R-1)} \qquad \text{..... (2-11)}$$

The reflectance (R) has been determined from values of transmission (T), and absorbance (A), using the relationship [53]:

A + R + T =1 ……..(2-12)

The Extinction Coefficient (k) is defined as the quantity of the energy in thin film or the extinction that happen in electromagnetic wave inside the material. It also represents the imaginary part of the complex refractive index.And is connected with absorption coefficient by the following relation [85]:

$$k_0 = \alpha\lambda/4\pi \ \ldots\ldots\ldots\ldots\ldots (2-13)$$

Where k_0 is the Extinction Coefficient, λ is wavelength of incident photon and (α) is absorption coefficient which given by the following equation [86]:

$$\alpha = 2.303\, A/t \ \ldots\ldots\ldots\ldots\ldots\ldots\ldots (2-14)$$

(A) is absorbance and (t) is thickness of sample

the following equations were used to calculate the real and imaginary (ε_1 and ε_2) part of dielectric constant [87]:

$\varepsilon_1=n^2-k^2$ ……..... (2-15)

$\varepsilon_2=2nk$ ……..… (2-16)

The optical conductivity (σ) can be calculated by using the equation [88]:

σ= αnc/4л …….(2-17)

In which c denotes the light speed, (n)the refractive index and is the absorption coefficient

2.5 The A.C Electrical Properties

Dielectric materials can be used to store electrical energy in the form of charge separation when the electron distributions around constituent atoms or molecules are polarized by an external electric field. The complex permittivity of a material can be expressed as [89]:

$$\varepsilon^* = \acute{\varepsilon} - j\varepsilon'' \ldots\ldots\ldots\ldots\ldots\ldots (2-18)$$

where ε'' and $\acute{\varepsilon}$ are the imaginary and real part of the complex permittivity and $j = \sqrt{-1}$.

The real part of the permittivity is by given [89]:

$$\acute{\varepsilon} = \varepsilon_0 \varepsilon^- \ldots\ldots\ldots\ldots\ldots\ldots (2-19)$$

The magnitudes of ε'' and $\acute{\varepsilon}$ depend on the hesitation ω of the field electric applied. The magnitude of $\acute{\varepsilon}$ (or the dielectric constant ε^-) indicates the ability of the material to store energy from the applied electric field [89].

The capacitance of a capacitor constructed of two plates parallel is given by the equation [90]:

$$c = \varepsilon^{-}\varepsilon_0 \frac{A}{t} \dots\dots\dots\dots\dots\dots (2-20)$$

Where :, έ is dielectric constant ,t thickness of the sample and $\varepsilon_\circ$ is vacuum permittivity . The is t dielectric constant by given [91]

$$\varepsilon^{-} = \frac{C_p}{C_0} \dots\dots\dots\dots\dots\dots . (2-21)$$

Where: c_p: is parallel capacitance and C_0 is vacuum capacitor . As the polarization of a material under an electric field varies, some of the applied electric field energy is dissipated due to charge migration (i.e., conduction) or conversion into thermal energy (e.g., molecular vibration). Ceramic capacitors based on highly polarizable inorganic materials have traditionally been used to meet the need for pulse power applications [92]. The dielectric loss (ε″) is given by. The *dielectric loss* (ε'') is by given [93]:

$$\varepsilon^{''} = \varepsilon^{-} D \dots\dots\dots\dots\dots (2-22)$$

Where $D\ is\ dispersion$ fac tor. And this is a measure of the amount of electrical energy that is lost in the sample as a result of the applied field. The alternating potential, which is a function of the alternating conductivity, represents the dissipated power in the insulator. [94]:

$$\sigma_{A.C} = w\,\varepsilon''\,\varepsilon_0 \dots\dots\dots\dots\dots . (2-23)$$

2.6 Microwave Attenuation

Microwave attenuation is a measure of the reduction in power level experienced by a signal as it passes through a circuit across the nanocomposite Attenuation plays a vital role in both telecommunications and ultrasonography. The attenuation coefficient of the medium in question is used to evaluate attenuation in decibels per unit length of medium (dB/cm, dB/km, etc.).In today's wireless telecommunications environment, attenuation is a significant factor. Every day, it affects people, as they increasingly depend on mobile phones, televisions and the internet through satellite. The range of radio waves is reduced by attenuation [95].

2.6.1 Vector Network Analyzer (VNA)

The VNA vector network analyzer has become an essential tool for microwave measurements. The device's principal function is to measure S-Parameters and other non-linear properties of components, and it was developed for laboratory use. [96].

2.6.2 Scattering parameter

Input waves at ports 1 and 2 are referred to as a_1 and a_2, respectively, in fig. (2.5), whereas output waves at port 1 are given the same names as input waves at $port\,1$. Both b_1 and b_2 refer to the output waves at $port\,1$ and $port\,2$, respectively. In other words, they might be either current or voltage coefficients (i.e., the current or voltage coefficients). Both sorts of coefficients are used interchangeably in most cases. The s-parameter is often used to represent the connection between input and output waves. [97,98].

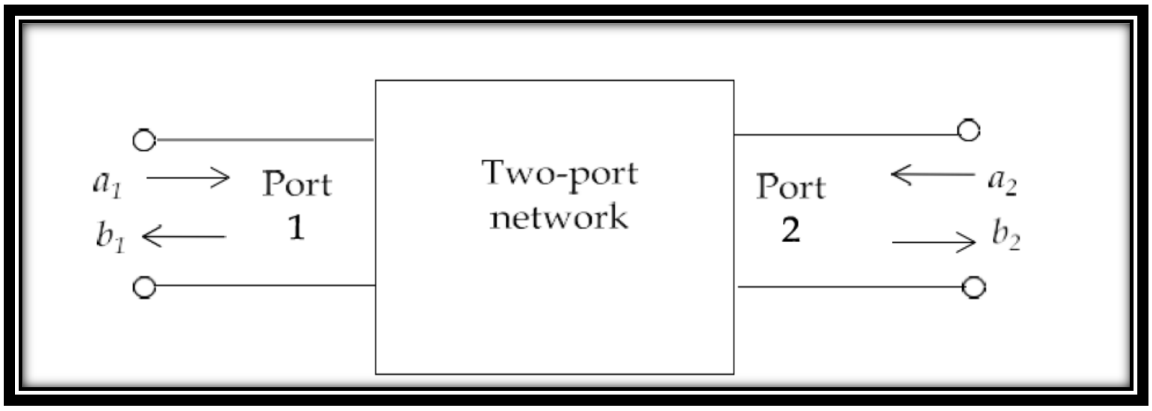

Fig.(2-5) Two network entries ("a" s, "b" s) [98]

$$[b] = [S]\,[a] \quad \ldots\ldots\ldots\ldots\ldots\ldots\ldots\ldots (2-24)$$

where [a] = [a1, a2] T and [b] = [b1, b2] T can be defined with a coefficient matrix S.

$$S = \begin{bmatrix} s11 & s12 \\ s21 & s22 \end{bmatrix} \ldots\ldots\ldots\ldots\ldots\ldots\ldots (2\text{-}25)$$

$$S_{jj}\frac{a_j}{b_j} \ldots\ldots\ldots\ldots\ldots\ldots\ldots (2-26)$$

$$S_{ij}\frac{a_i}{b_j} \quad (i \neq j\,;\; i = 1\,,2\,;\; j = 1,\; 2) \ldots\ldots\ldots\ldots (2-27)$$

Whereas, Equation (2-23) states that when $port\ j$ is connected to a source and the other port is connected to a corresponding load , the reflection coefficient at $port\ j\ is\ equal\ to\ S_{jj}$:

$$\Gamma_j = S_{jj}\frac{a_j}{b_j} \ldots\ldots\ldots\ldots\ldots\ldots\ldots (2-28)$$

$$\Gamma_{ij} = S_{ij}\frac{a_i}{b_j} \ldots\ldots\ldots\ldots\ldots\ldots\ldots (2-29)$$

Chapter Three

Experimental Procedures

&

Measurements

3.1 Introduction

This chapter deals with an explanation of the experimental stages of preparing spindle ferrite compounds of the (inverse spin) type with the formula $Cu_x Ni_{_(1-x)} FeO_3$where (x=0.1, 0.3) through the raw materials used to prepare the samples and the method of calculating weights, method of preparation, measuring some magnetic and structural properties, adding them to the polymer mixture in proportions (1, 3, 5)%wt, measuring some optical properties, electrical properties, and microwave attenuation properties. Figure (3-1) shows a diagram of the mentioned work stages.

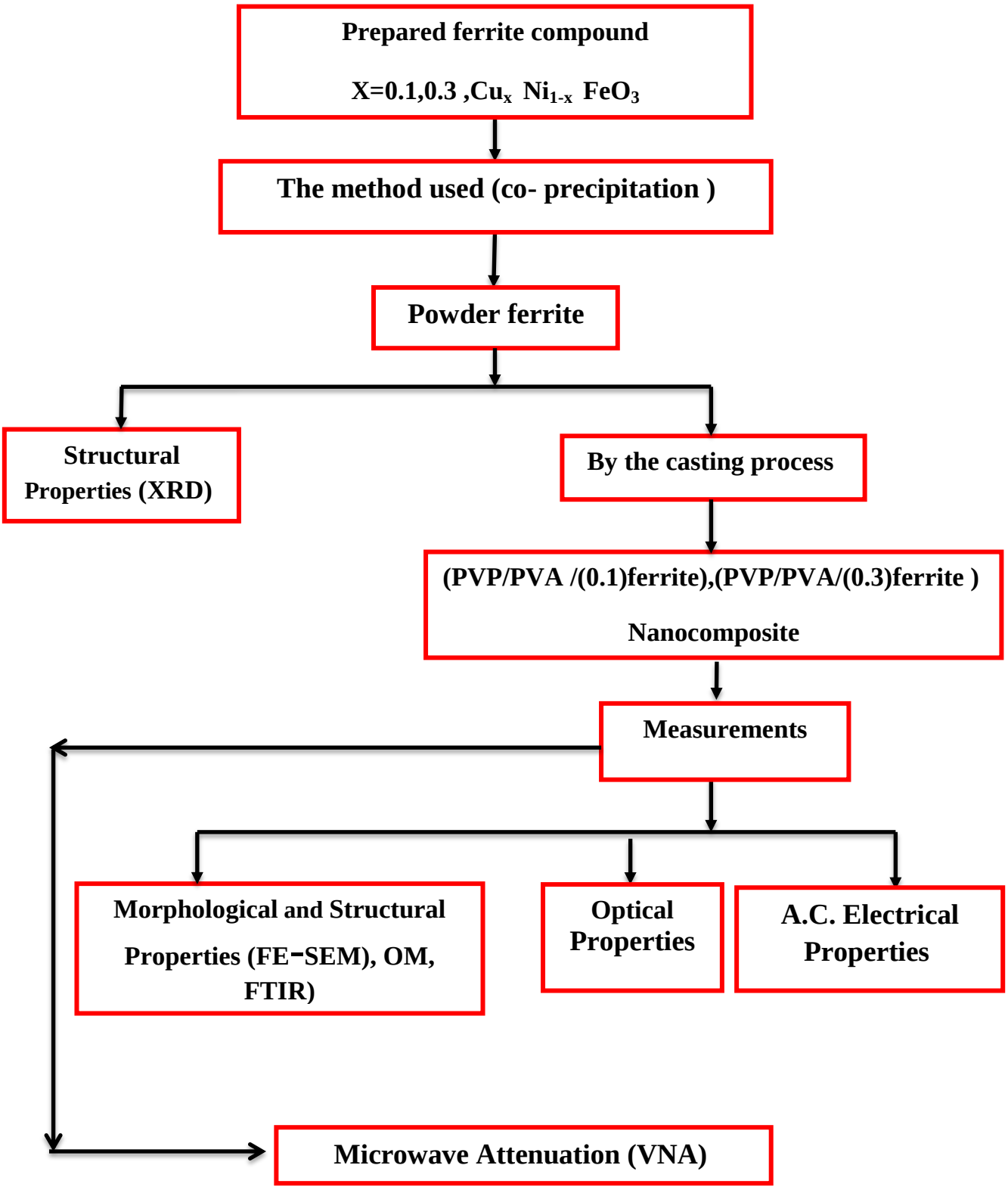

Figure(3.1)Schematic diagram of experimental work

3.2 Raw materials for ferrite

The raw materials were selected with high purity because this leads to the production of pure ferrite materials free of impurities, which in turn gives good magnetic and electrical properties. The table(3-1) shows a complete description of the materials involved in the reaction.

Table(3-1) Information about the raw materials involved in the reaction

material name	Chemical formula	molar mass g/mol	Purity	manufacturing country	Company
Ferric chloride	$FeCl_3$	162.20	99.9%	Spain	RBL Sr.No.9066
Nickel nitrate	$Ni(No_3)_2.6H_2O$	290.81	98%	Korea	Gyeonggi-do
Copper nitrate	$Cu(NO_3)_2.3H_2O$	241.60	98%	Spain	Barcelona

3.3 Ferrite preparation $Cu_x Ni_{1-x} FeO_3$

The following steps were followed to prepare ferrite, according to the scheme shown in Figure (3.1).

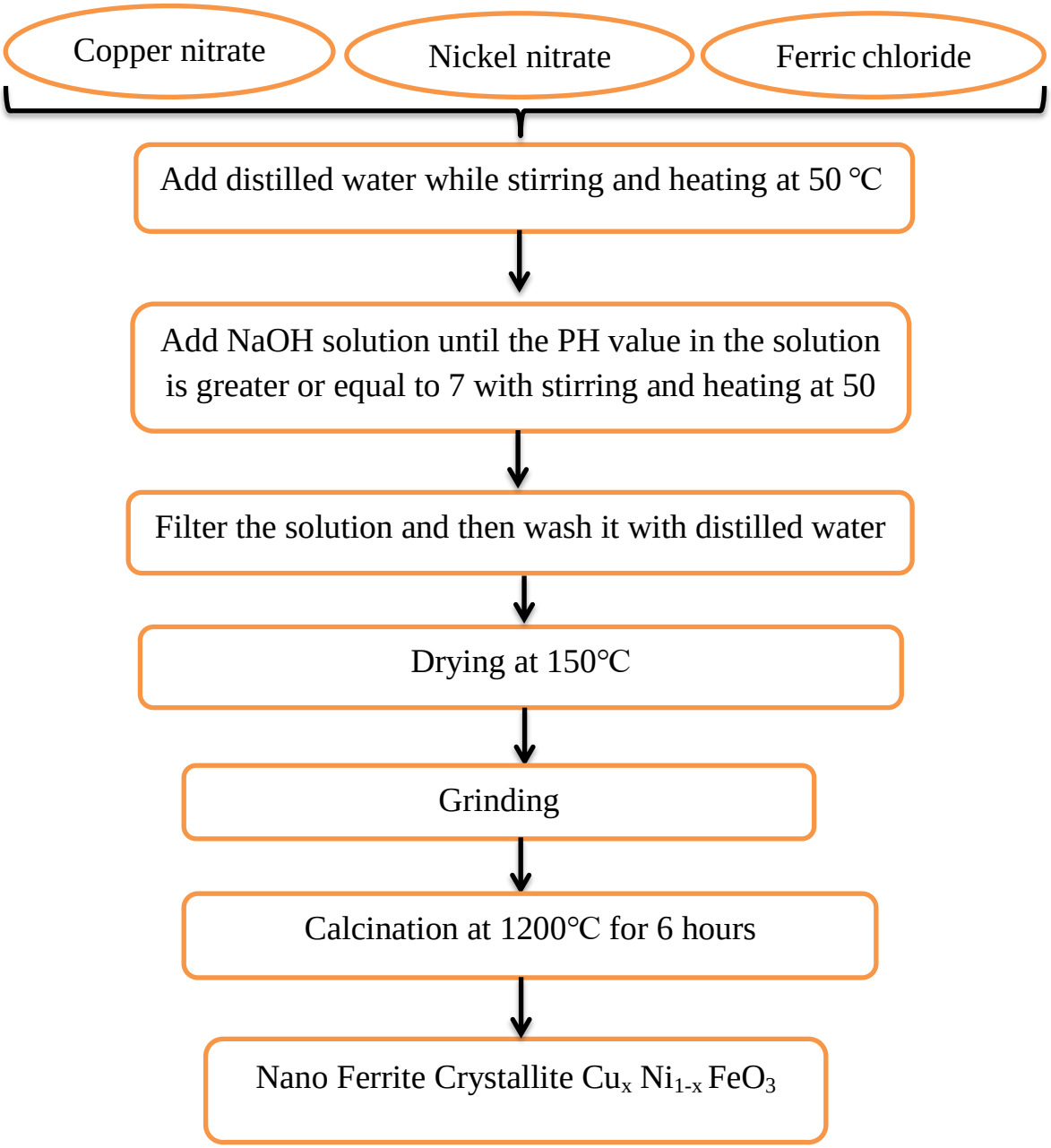

Figure(3.2) is a diagram showing the stages of preparing frites

3.3.1 Calculation of masses

The mass that is calculated in this paragraph is the initial mass, so the proportions of the components are determined for one mole in terms of the atomic weights of each element, which calculating from the following equation:

$$n = \frac{w}{W_m} \dots\dots\dots\dots\dots (3-1)$$

where n is the number of moles, w is the weight to be calculated, and $W_m$is the molecular weight.

Assuming that n = 1, the equation will be (3-1)

$$w = w_m \dots\dots\dots\dots\dots (3-2)$$

The molar mass of nickel nitrate $Ni(NO_3)_2.6H_2O$ was calculated as follows :-

58.693+2(14+3×16)+6(2×1+16) = 290.6939 g/mol

The same way for the rest of the materials whose values are shown in Table (3-1)

3.3.2 Calculating the masses of the reactants

To prepare 30 g of the ferrite compound $Cu_x\ Ni_{(1-x)}FeO_3$ at the ratio x=0.1, the compound becomes as $Cu_{0.1}\ Ni_{(0.9)}FeO_3$.

We follow the same steps to find other compounds of values (x =0.1)

1- Amount of $FeCl_3$

$$\frac{0.1\times162.2\times100}{1000} = 1.622\ g \qquad (3-3)$$

2- Amount $Ni(NO_3)_2\ 6(\ H_2O)$

$$\frac{0.9 \times 290.8 \times 100}{1000} = 26.172\ g \qquad (3-4)$$

3- Amount $Cu(NO_3)_2.3H_2O$

$$\frac{0.1 \times 241.6 \times 100}{1000} = 2.416\ g \qquad (3-5)$$

We follow the same steps to find other compounds of values (x=0.3).

3.3.3 Mixing and drying process

The prepared quantities were put together in a glass container and dissolved by adding 800 ml of distilled water and then placed in the magnetic stirrer at a temperature of 50 ℃ and continuously mixing resulted in a homogeneous solution, then NaOH was added until the PH value reached greater than or equal to 7, where it turns viscose solution. The volume is then completed to one liter by adding distilled water. After that, the filtration process was carried out using filter paper and put it in a Buchner filter and then put the solution inside the filter and then wash the product with distilled water several times to get rid of the suspended impurities, and thus get metal hydroxides instead of ions, which disintegrate easily when the temperature is raised to the metal oxide in the spinel phase. This is followed by the drying process, as the product is placed in an oven at a temperature of 150 ℃ for 24 hours .

3.3.4 Grinding and calcination process

The grinding process is carried out in a ceramic mortar for a period of /6/ hours. After the grinding stage, the powder resulting from grinding was placed in a ceramic pulp that bears very high heat, and the powder was placed in the electric oven. The temperature of the oven was gradually raised at a rate of (10) ℃ per minute to That the temperature of

the furnace reaches (1200) ℃ and the furnace remains at this temperature for (6) hours and then leaves the oven until it cools gradually (this process is called calcination) and then the material is taken out to be ground again, and to ensure that the spinel ferrite phase is achieved, an examination is conducted XRD for output. The following equations obtain to get the ferrite.

$$X\ Cu(NO_3)_2\ 6H_2O + (1-X)Ni(NO_3)_2.3H_2O\ +\ FeCl_3 + H_2\ O \longrightarrow xCu^{+2} + (1-x)Ni^{+2} + Fe^{+3} + +4NO_3\ + CL_3^-\ + 10H_2\ O$$

$$X\ Cu^{2+} + (1-X)Ni^{2+} + Fe^{3+} + 4NO_3^- + Cl_3^- + 10H_2O + 8NaOH \xrightarrow{1200\ ℃} XCu(OH)_2 + (1-X)Ni(OH)_2 + Fe(OH)_3\ + 4NaNO_3 + 3NaCl + 10H_2\ O$$

$$X\ Cu(OH)_2 + (1-X)Ni(OH)_2 + Fe(OH)_3 \xrightarrow{1200\ ℃} Cu_xNi_{1-x}Fe\ O_3 + 4H_2O$$

3.4 Preparation of (PVP/PVA/Cu_x Ni_{1-x} FeO_3)(with x=0.1 and 0.3)

The nanocomposites of (PVP -PVA- Cu_x Ni_{1-x} FeO_3) at x=0.1 and x=0.3are prepared by dissolving 1g (70 wt.% PVP and 30 wt.% PVA) in 50 ml of distilled water and in order to achieve a more uniform solution, a magnetic stirrer was used to mix the polymers for 1 hour. Varying concentrations of ferrite nanoparticles (1, 3, and 5) wt.% are added to a polymer mixture are shown in table (3-2). PVP/PVA/ferrite nanocomposites are placed on a petri dish using the casting method. The thickness for all samples of (PVP/PVA/ $Cu_{0.1}$ $Ni_{0.9}$ FeO_3)(with x=0.1 and0.3) nanocomposite were (120) μm .

Table (3.2) Weight Percentages of nanocomposite $Cu_xNi_{1-x}FeO_3$

PVP (gm)	PVA(gm)	$Cu_{0.1}Ni_{0.9}FeO_3$ and $Cu_{0.3}Ni_{0.7}FeO_3$	Weight of Sample
0.7	0.3	0	1g
0.7	0.29	0.01	
0.7	0.27	0.03	
0.7	0.25	0.05	

3.5 X-Ray Diffraction (XRD)

The main aim of these measurements is to study the form of structure of the prepared films. Determining the general structure of bulk solids, including lattice constants, identifying unknown materials, orienting single crystals, orienting polycrystalles , flaws and stresses. has long been used in this experimental technique. X-ray diffraction by the X-ray diffract meter device (^{o}XRD-60000) from SHIMADZU, which records a measure of the intensity as a function the angle of Bragg. The system's circumstances were:

CuK emits radiation with a wavelength of 1.5406 nm from a CuK sourc

Target: Cu current is equal to 30 mA.

The voltage is equal to 40 kV.

The scanning speed is 0.25 degrees per minute.

A total of two X-ray scans) are done (between) the two-point values of zero and eighty degrees as shown in fig.(3.3).

Figure.(3.3) The system of the XRD.

3.6 Field Emission Scanning Electron Microscope (FESEM).

Via high – resolution photographs and magnification, describe the essence and morphology of the prepared films' surface, as well as the internal structure of the films' substance. Photons with X-ray wavelengths are produced when primary electrons reaction with the sample. The atomic ratio in the sample can be measured using energy dispersive spectroscopy after this emission is detected by (ΣIGMA, JSM-7610F,Carl Zeiss, Germany) image operating at an accelerating voltage of 10 kV . The element ratio and surface morphology of the thin film that were produced were examined utilizing FE-SEM can be observed Fig.(3.4).

Figure (3.4). FESEM System

3.7 FTIR Spectrometer

The FTIR spectra of (PVP/PVA/Cu_x Ni $_{1-x}$ FeO_3) nanocomposites at x=0.1 and x=0.3 were acquired by an FTIR in strument (Bruker company, German origin, type vertex -70) FTIR was implemented The University of Babylon/ College of Education for Pure Sciences / Department of Physics. The findings of this investigation show that considered wave number range is (400-4500) $cm^{-.1}$as shown in Fig.(3.5)

Figure(3.5) Image of the FTIR device

3.8 Microscopic Examination

The (PVP/PVA/ Cu_x Ni_{1-x} FeO_3) at x=0.1and x=0.3nanocomposites specimen were examined by an optical microscope by the Olympus name (Top View) type (Nikon-73346), and fitted with an automatic camera operated by light intensity under magnification (100x) this measurement was carried out for Pure Sciences at the University of Babylon-College of Education, in Babylon, as seen in Figure (3.6).

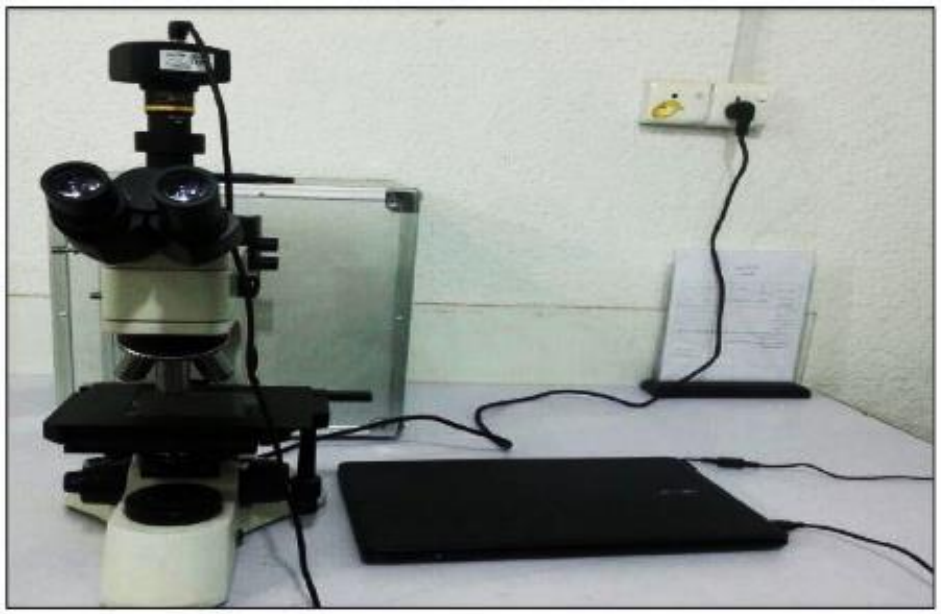

Figure(3.6) Optical Microscope

3.9 Optical Properties

The optical properties of (PVP-PVA/ Cu_x Ni_{1-x} FeO_3)at x=0.1and x=0.3 double beam spectrophotometer (Shimadzu, UV -18000A) with a measure nanocomposites in this study (220-820) nm. The Department of Physics at the University of Babylon / College of Education for Pure Sciences, as seen in fig. (3.7). At room temperature, the absorption spectra has been measured and analyzed. The absorption coefficient, optical constants, extinction coefficient, refractive index and energy gaps

were calculated with the use of a computer software, which may be found here.

Figure(3.7)) The photographic of UV-VIS.NIR spectrophotometer

3.10 A.C Electrical Properties

The A.C electrical properties of(PVP/PVA/ Cu_x Ni_{1-x} FeO_3) at x=0.1and x=0.3nanocomposites are determined by calculating capacity (Cp) and8 dissipation factor (D) with an LCR meter of the type (HIOKI 3532-50 LCRHI-TESTER) at room temperature with different frequencies rangingfrom (100 Hz–5 MHz) as shown in the figure. Fig.(3.8).

Figure(3-8) Schematic diagram for A.C electrical properties measurement

3.11 Vector Network Analyzer Application Measurements of Nanocomposites

The Vector Network Analyzer application of (PVP/PVA/Cu_x Ni_{1-x} FeO_3) at x=0.1and x=0.3 nanocomposites to measure microwave attenuation with in the S-band with a is frequency range (4-7) GHz, Vector Network Analyzer (VNA) model Anritsu-MS4642A (10MHz-20GHz) of American origin was used, which is located in the Industrial Research and Development Center of the Ministry of Science and Technology and shown In Fig.(3-9)

In this devices, we can measure each of the scattering coefficients of electromagnetic waves (S11, S21, S12, and S22), and we can use the results to calculate the complex permittivity and complex transmittance at various frequencies within the S-Band and K-Band bands, as each band has its own waveguide where the guide model differs wave form for each dimensional packet.

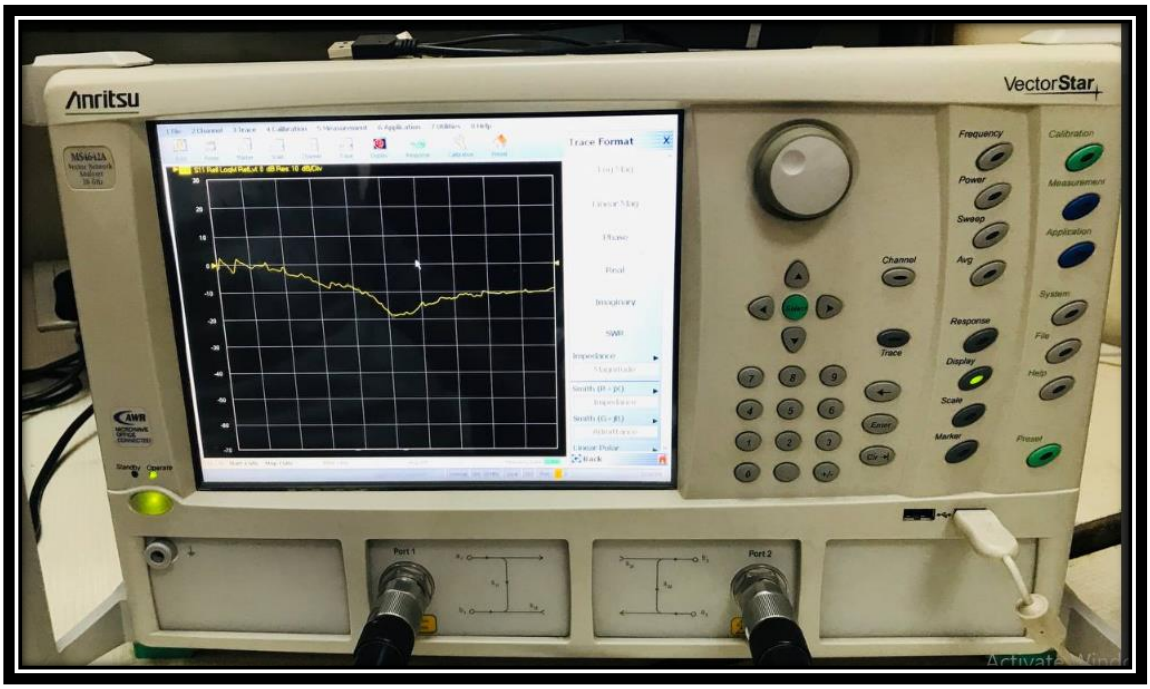

Figure(3.9)Vector network analyzer(VNA)

Chapter Four

Results& Discussions

4-1 Introduction

This chapter emphases on the results and discussion of the X-ray diffraction (XRD) for the ferrite nanocomponent when x (0.1) for the group A and x (0.3) for the group B and then study the Fourier transform technique (FT-IR), Scanning electron microscopy (FESEM), Optical microscope, UV-Visible spectroscopy and AC electrical of the PVP/PVA/ferrite nanocomposites with different content of the ferrite by the casting method and then apply to attenuate microwave.

4.2 Structural and Morphological Properties

4-2-1 X-ray Diffraction (XRD)

The X-ray diffraction of the (PVP/PVA/$Cu_xNi_{1-x}FeO_3$) at x=0.1 and x=0.3are shown in Fig.(4.1) after treatment in the same condition of preparing catalyst that calcination at 1200 ^{0}C for 6 hours.

From the figure, shows the peaks at 2θ (30.36, 35.73°, 37.19°, 43.22°, 57.53°, 63.34°, 75.81° and 79.24°) for the group A and (30.3°, 35.68°, 37.22°, 43.24°, 57.36°, 63.12°, 75.27°, 79.25°) for the group B identical to the card (JCPDS 00-047-1049) [99] confirming the face center cubic spinel phase (FCC) and all samples prepared without the presence of impurities or secondary phases and this proves that the method of preparation includes the incorporation of positive ions into the spinel structure [100]. The average crystallite size have been calculated from the Debye–Scherer e

quation (2-2). It is increase from 26.08 nm for group A to 46.92 nm for group B due to the crystal size of the particles and since the copper ionic radius Cu^{+2} (0.73 Å**)** is greater than the ionic radius of nickel Ni^{+2} (0.69 Å) therefore the copper occupies the tetrahedral sites and its presence at this site leads to an increase in the

size of the particles [101,102]. The intensity of all the peaks decrease with increasing concentration due to the copper ion is replaced with a nickel ion and this decrease is due to saturation of the active level[100]. The dspacing are listed in Table (4.1).

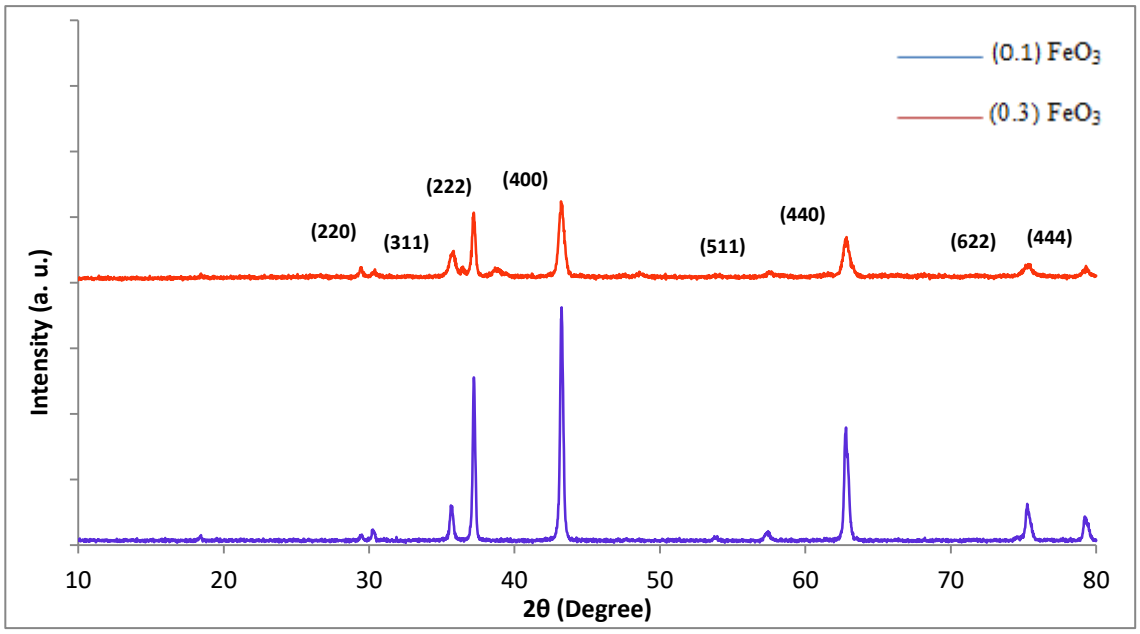

Figure (4.1): XRD pattern of the different concentration of ferrite nanocomponent

Table (4.1): The obtained result of the XRD for of the different concentration of nanocomponent ferrite

FeO_3	2θ (degree)	(hkl)	FWHM (degree)	d(Å)	Crystallite size (nm)	Average Crystallite size (nm)
A	30.36 35.73 37.19 43.22 57.53 63.34 75.81 79.24	(220) (311) (222) (400) (511) (440) (622) (444)	0.37 0.478 0.299 0.434 0.41 0.24 0.28 0.423	2.940 2.510 2.415 2.091 1.600 1.467 1.253 1.207	22.25 17.46 27.95 19.66 22.10 38.89 35.95 24.36	26.08
B	30.3 35.68 37.22 43.24 57.36 63.12 75.27 79.25	(220) (311) (222) (400) (511) (440) (622) (444)	0.236 0.256 0.182 0.207 0.373 0.08 0.252 0.256	2.946 2.514 2.413 2.090 1.604 1.471 1.261 1.207	34.88 32.59 46.06 41.20 24.25 116.53 39.74 40.14	46.92

4.2.2 Field Emission Scanning Electron Microscope (FESEM).

FE-SEM of the (PVP/PVA/$Cu_xNi_{1-x}FeO_3$) at x=0.1 and x=0.3 nanocomposite with different concentration of the ferrite are shown in figs.(4.2),(4.3). from the figures, the symbol A_o,A_1,A_2 and A_3 indicate to blend PVP/PVA, PVP/PVA/1%wt./ ferrite, PVP/PVA/3%wt. / ferrite and PVP/PVA /5%wt. /ferrite for (0.1) respectively and also B_o, B_1, B_2 and B_3 indicate to blend PVP/PVA,PVP/PVA//1%wt./ ferrite, PVP/PVA//3%wt./ferrite and PVP/PVA /5%wt./ ferrite for (0.3) respectively. From this figures, it is observed that the pure PVP/PVA was homogenous and smooth this indicate a good method for prepared films. Also the uniform morphology dispersed of ferrite inside the PVP/PVA blend with shaped nanoparticles. The uniform dispersion of nanoparticles in the polymer

blend is due to the strong interfacial adhesion between the nanoparticles and blend components. From the Table (4-2), it was obtained that the average particle size increased with increasing of concentration of ferrite, it is increased from 32.37 nm for A_1 to 44.83 nm for A_3 and from 40.69 nm for B_1 to 64.43 nm for B_3 individually. This result are agreement with previous studied [103-105].

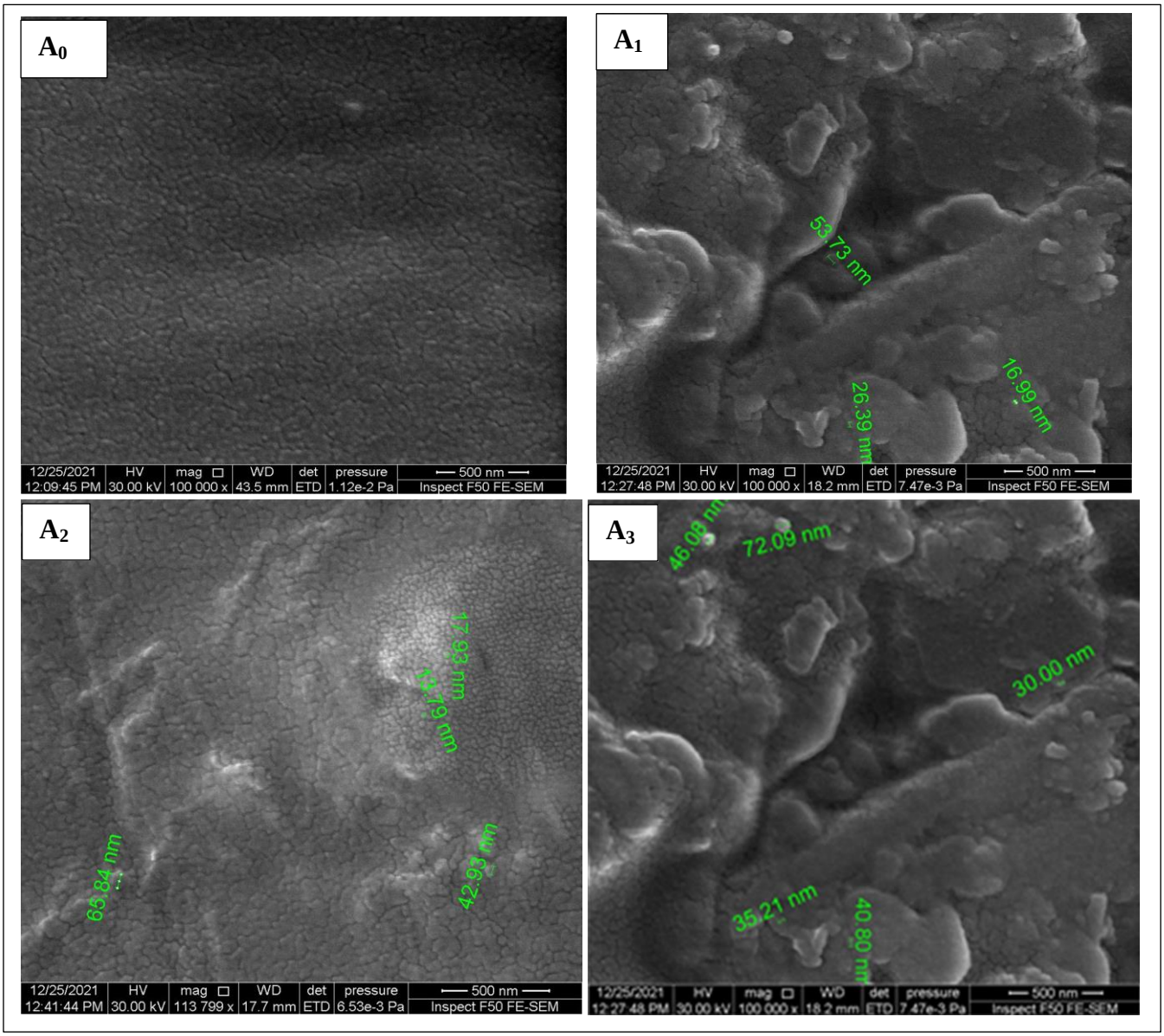

Figure (4.2): FESEM images of (PVP-PVA) blend), $Cu_{0.1}Ni_{0.9}FeO_3$ (A_0) 0 wt. % (A_1) 1 wt. % (A_2) 3 wt. % (A_3) 5 wt. % with different ratios of Ferrite

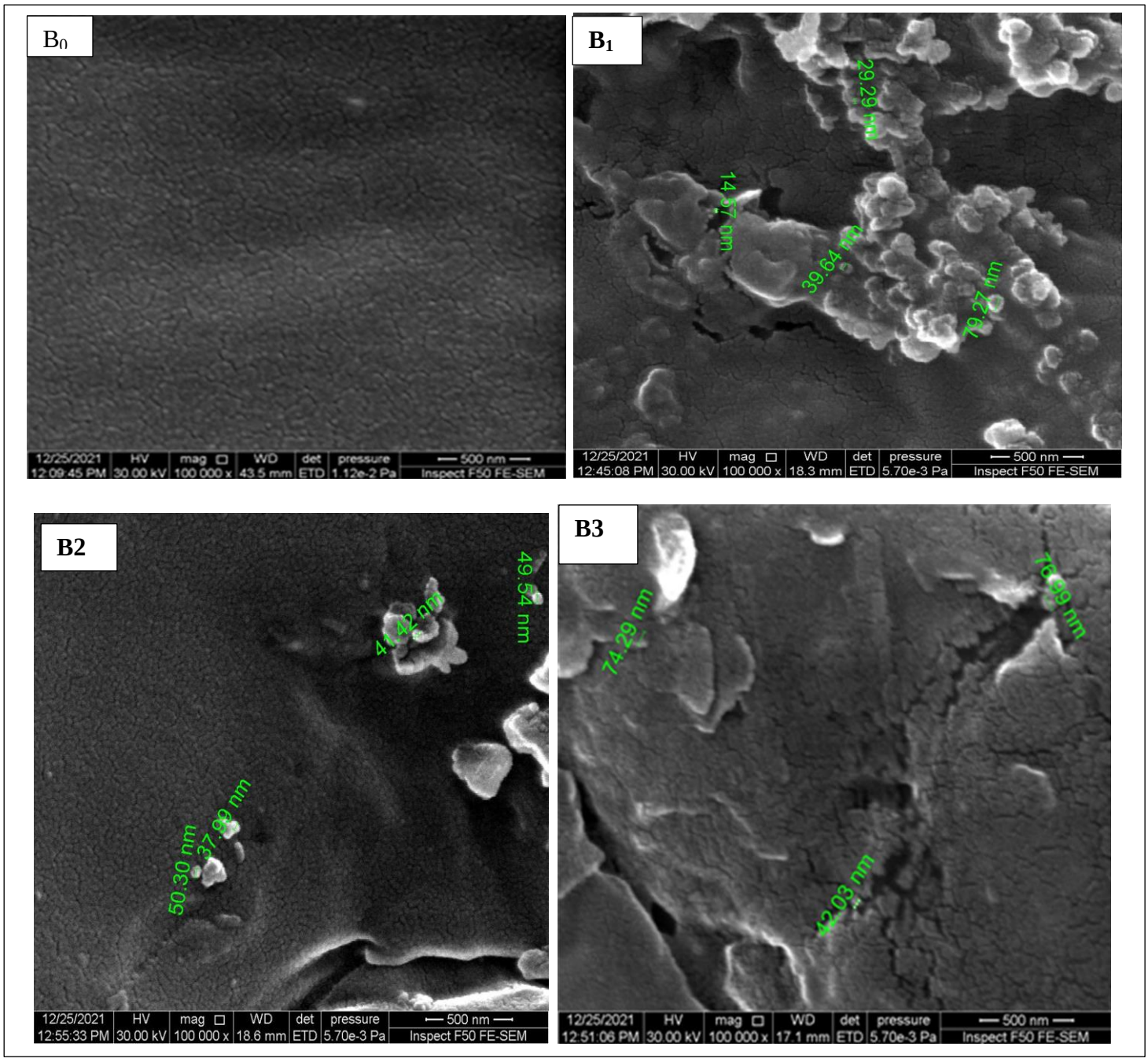

Figure (4.3): FESEM images of Bo (PVP-PVA) blend, $Cu_{0.3}Ni_{0.7}FeO_3$ (B_0) 0 wt. % (A_1) 1 wt. % (B_2) 3 wt. % (B_3) 5 wt. % with different ratios of Ferrite

Table (4-2): The average grain size for all the sample prepared

Composites	Sample	Average grain size (nm)
(PVP/PVA)	A_0	0
(PVP/PVA/(1 %wt)ferrite) at x=0.1	A_1	32.37
(PVP/PVA/(3%wt)ferrite) at x=0.1	A_2	35.12
(PVP/PVA/(5% wt) ferrite) at x=0.1	A_3	44.83
(PVP/PVA/(1% wt) ferrite) at x=0.3	B_1	40.69
(PVP/PVA/(3% wt) ferrite) at x=0.3	B_2	44.81
(PVP/PVA/(5% wt)ferrite) at x=0.3	B_3	64.43

4-2-3 Optical microscope

The optical microscope of the (PVP/PVA/ Cu_x Ni_{1-x} FeO_3) at x=0.1 and x=0.3) nanocomposite at magnification power (100x) with different concentrations (1, 3, and 5 wt.%) of ferrite are shown in figs.(4.4)(4.5).from the figures, it is indicated good homogeneity and fine incorporation of ferrite na noparticle in the blend matrix which was improved with the increasing the proportions level. This provided a good preparation process, which shapes the appropriate conditions and uses them to prepare them composite films. This result is agreement with that obtained by [106] about their study on material.

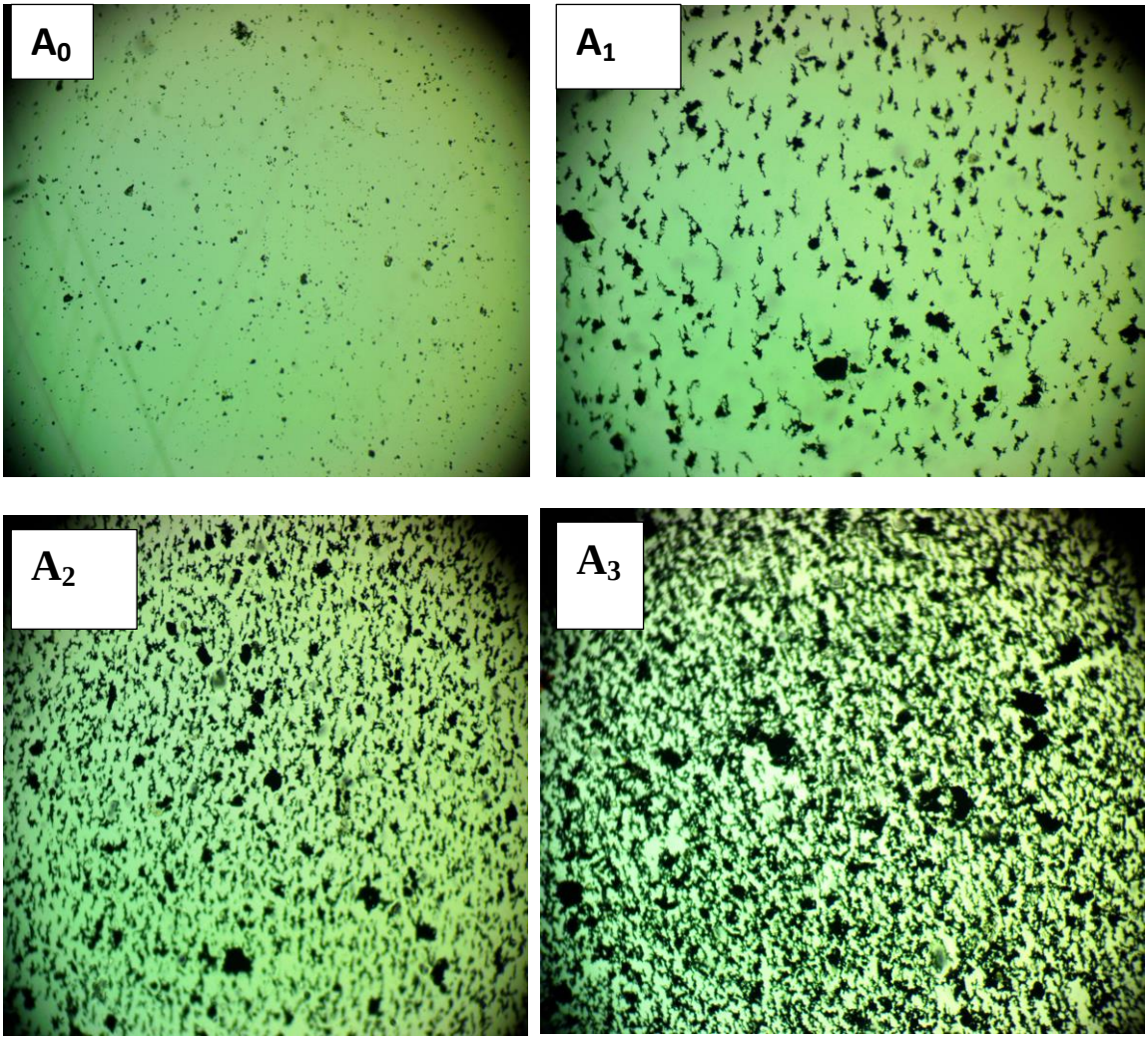

Figure (4.4) Photomicrographs (100x) for (PVP/PVA/) $Cu_{0.1}$ $Ni_{0.9}$ FeO_3) (A_0) 0 wt. % (A_1) 1 wt. % (A_2) 3 wt. % (A_3) 5 wt. % nanocomposites

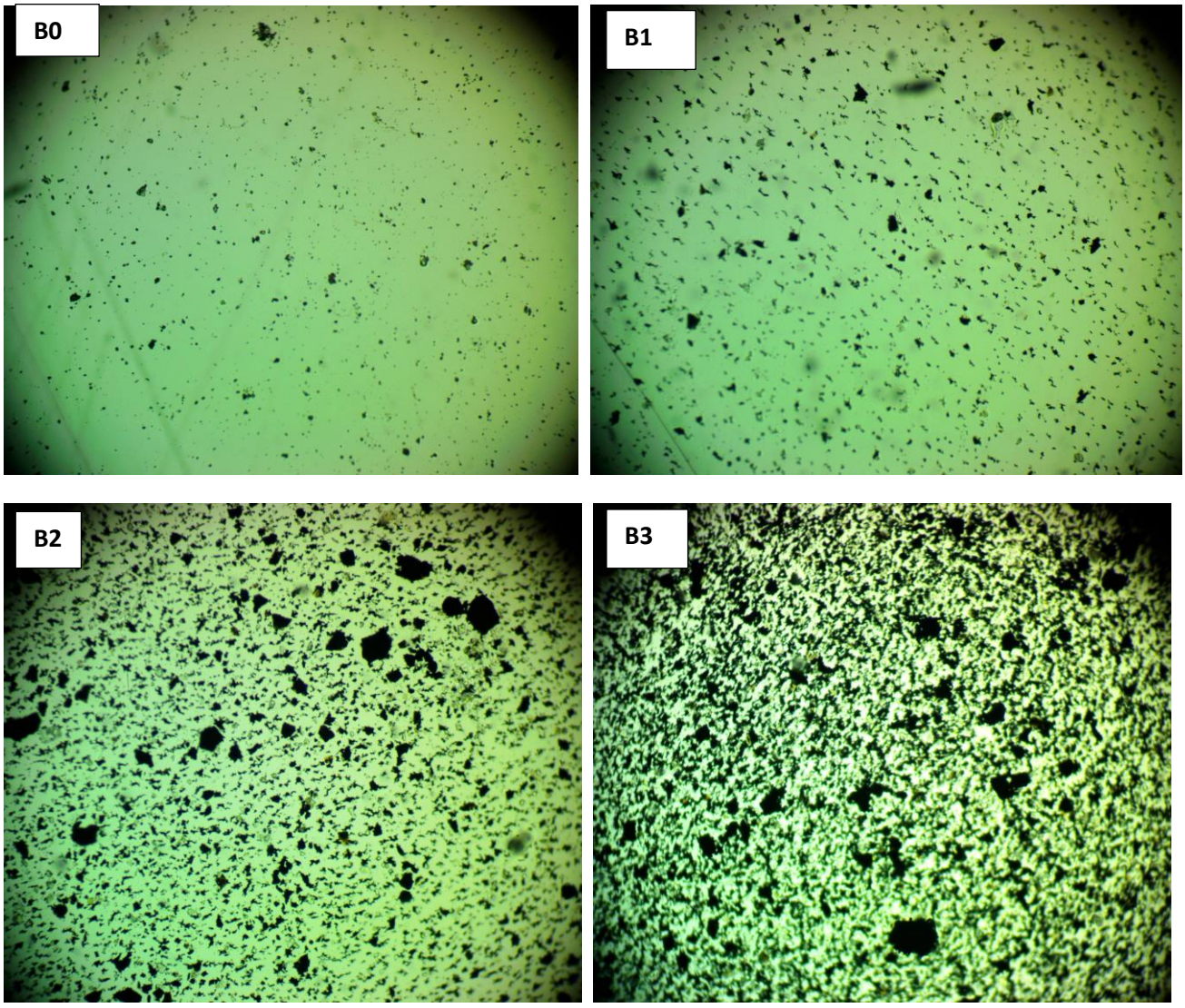

Figure (4.5) Photomicrographs (100x) for (PVP/PVA/ $Cu_{0.3}$ $Ni_{0.7}$ FeO_3) (B_0) 0 wt. % (B_1) 1 wt. % (B_2) 3 wt. % (B_3) 5 wt. % nanocomposites

4-2-4 Fourier Transform Infrared Radiation (FTIR) of Nanocomposites

FTIR spectra of /PVP/PVA/ $Cu_x Ni_{1-x} FeO_3$ / at x=0.1and x=0.3 nanocomposites with different concentration (1, 3, and 5 wt.%) of ferrite are shown in figs. (4.6)-(4.7). The interactions in nanocomposites are revealed by FTIR studies. This apparent broad band at 3365 cm^{-1} is produced for all samples generated of nanocomposites and is attributable to the presence of (OH) sets in the polymer matrix chain. In the CH_2 group, the band seen at 2922 cm^{-1} is indicative of an asymmetric stretching mode, which is represented by the symbol CH_2. The band at (2360) cm^{-1} Adopted in C-H group . There are four strong peaks observed for all the sample of nanocomposite at (1648, 1422 and 1288,1092) cm^{-1} belong to C=O groups, C-O groups, CH_2 bending and (C-0) bonds of matrix polymers respectively. The presence of ferrite nanoparticles causes modifications in the spectral properties of (PVP/PVA), which comprise transformations in bonds some and variations the intensities of some wavelengths. Those modifications are due to interactions between nanoparticles and polymers. It has been shown by FTIR investigations that the (PVP/PVA) polymer matrix and ferrite nanoparticles have no contact with one another. The transmittance in the figures reduces significantly as the concentration of ferrite nanoparticles increases, which may be ascribed to the increased density of nanocomposites in the system. [107]. These result are agree with researchers[108,109].

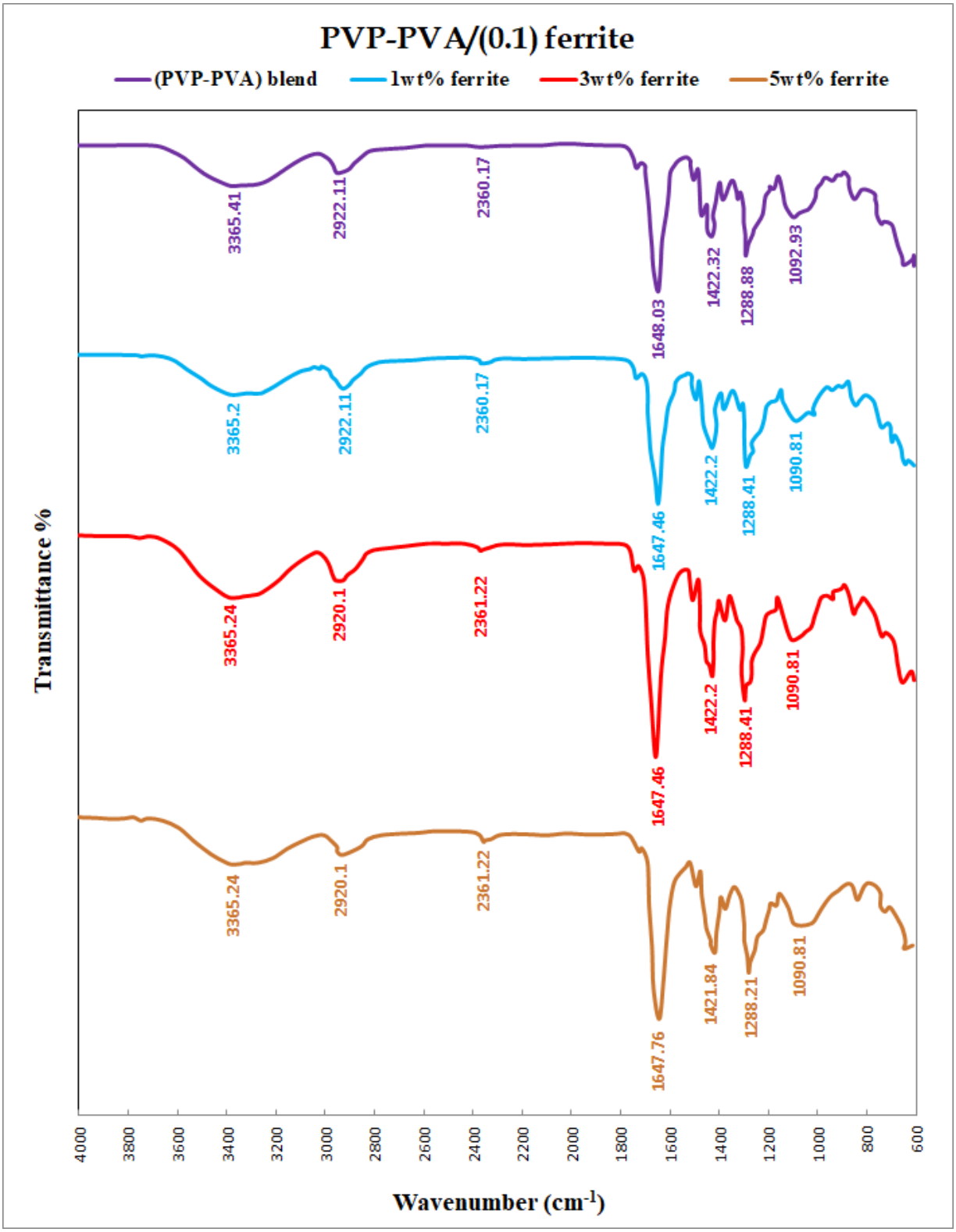

Figure (4.6): FTIR spectra for (PVP-PVA/ $Cu_{0.1}$ $Ni_{0.9}FeO_3$) nanocomposite

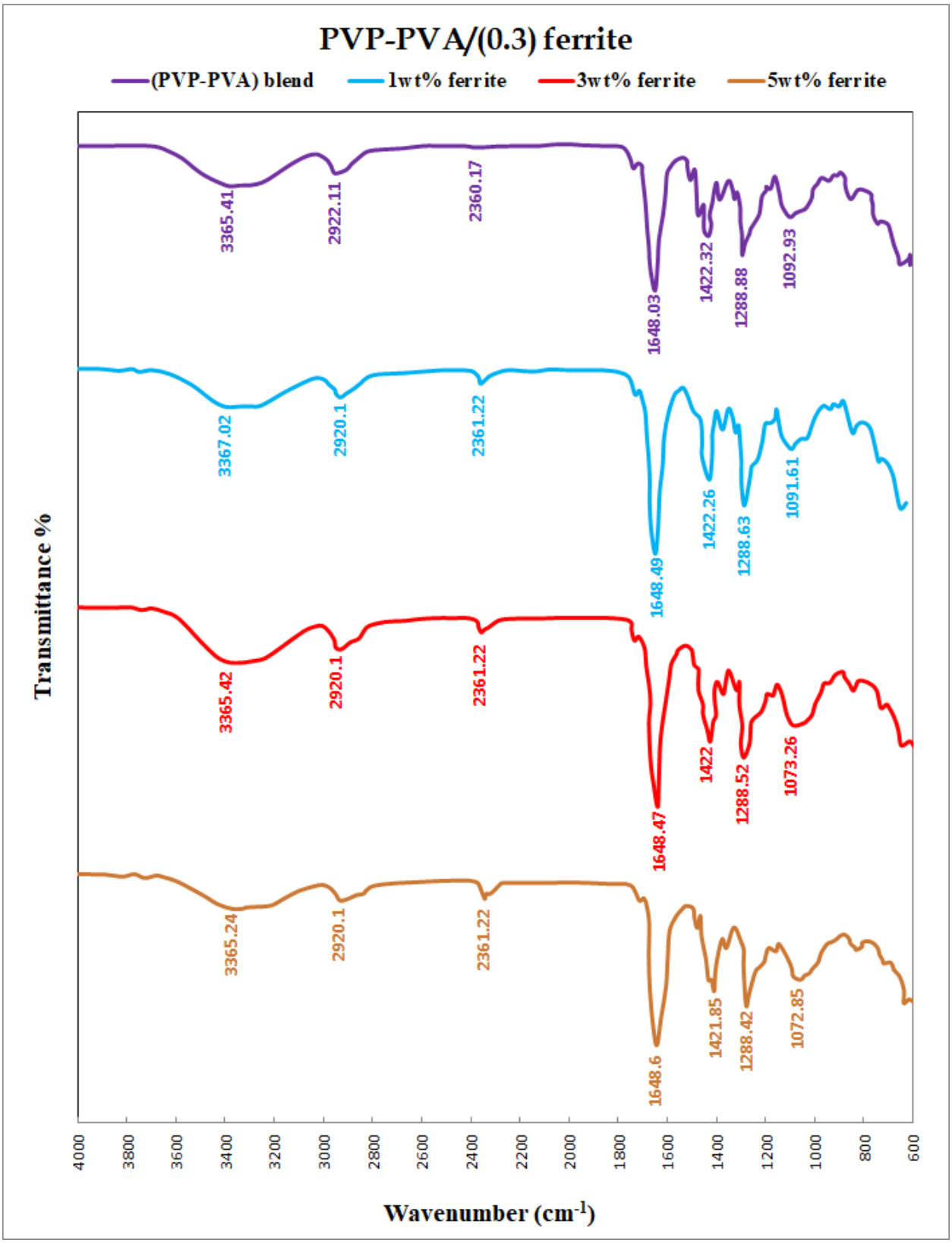

Figure (4.7): FTIR spectra for (PVP-PVA/ $Cu_{0.3}$ $Ni_{0.7}$ FeO_3) nanocomposite

4-3 The Optical Properties of (PVP/PVA/ Cu_x Ni_{1-x} FeO_3) Nanocomposite

4.3.1 The Absorbance

The absorption of (PVP-PVA/Cu_x Ni_{1-x} FeO_3) at x=0.1 and x=0.3 nanocomposites with different concentrations of ferrite has been recorded at wavelengths range (220-820) nm at room temperatures.

Figs.(4.8)-(4.9) show the absorbance of /PVP-PVA/ Cu_x Ni_{1-x} FeO_3 / at . From the figures, it is observe that the absorbance increase with increasing concentration of the ferrite, while the absorbance decrease with increasing wavelength for all samples of nanocomposites. This is attributed to the excitations of donor level electrons to the conduction band at these energies. Also due to the energy of photon enough to interact with atoms; the electron excites from a lower to higher energy level by absorbing a photon of known energy [110]. This result good indicator to apply this nanocomposite for microwave attenuation. This behavior agree with the results of researchers [111-113].

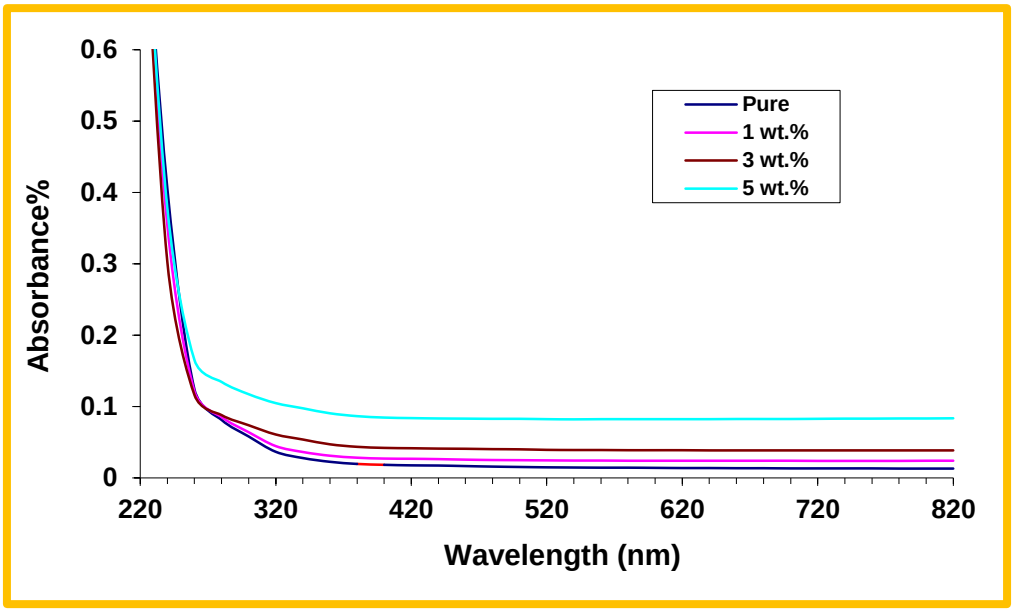

Figure (4 .8) : The absorbance as a function of wavelength of (PVP/PVA / $Cu_{0.1}$ $Ni_{0.9}$ FeO_3) nanocomposites with different concentrations.

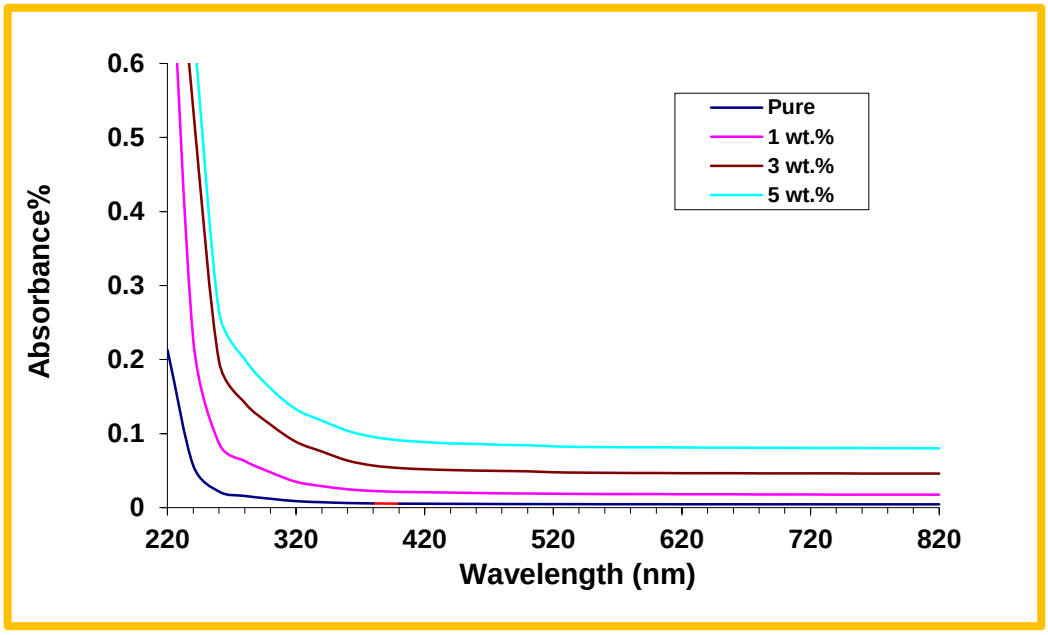

Figure (4 .9) : The absorbance as a function of wavelength of (PVP/PVA/ $Cu_{0.3}$ $Ni_{0.7}FeO_3$) nanocomposites with different concentrations.

4.3.2The Transmittance

The transmittance of(PVP-PVA/$Cu_xNi_{1-x}FeO_3$)at(x=0.1and0.3) nanocomposites with wavelength are shown in Figs.(4.10)-(4.11). From this figures shown, the transmittance decreases with the increasing of the concentrations for the ferrite nanoparticles and transmittance increasing with increasing wavelength, This is due to the conglomerate of nanoparticles with increasing concentration [114].

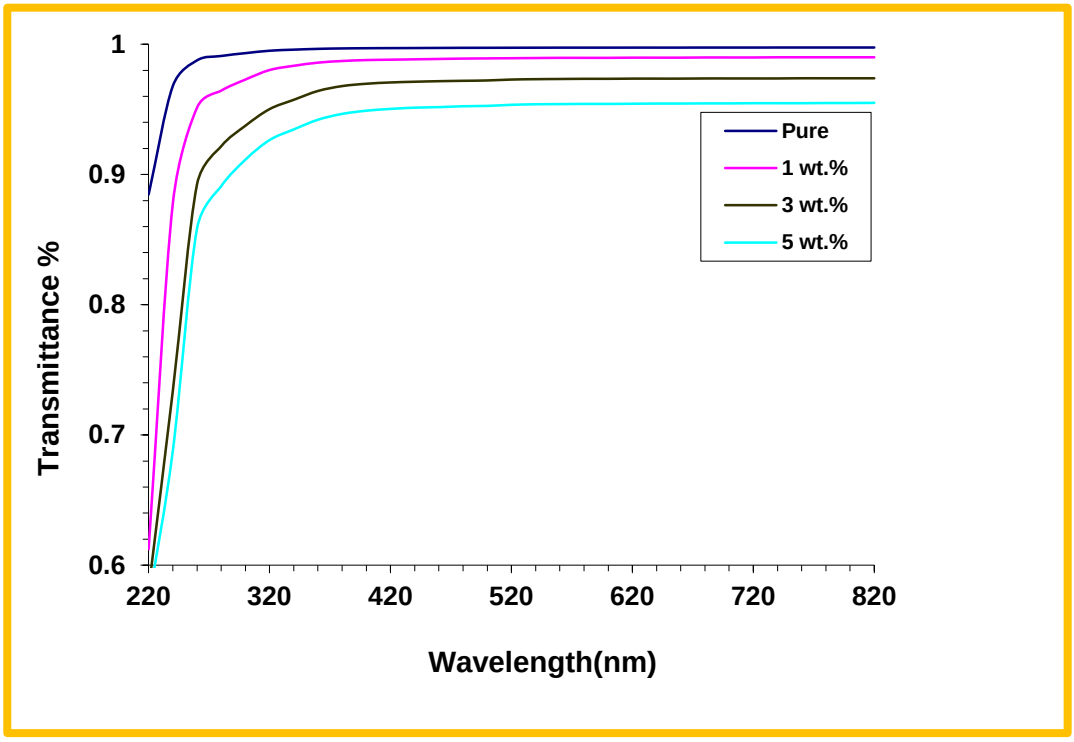

Figure (4.10): The transmittance variation of (PVP/PVA/ $Cu_{0.1}$ $Ni_{0.9}FeO_3$) nanocomposites with the wavelengths.

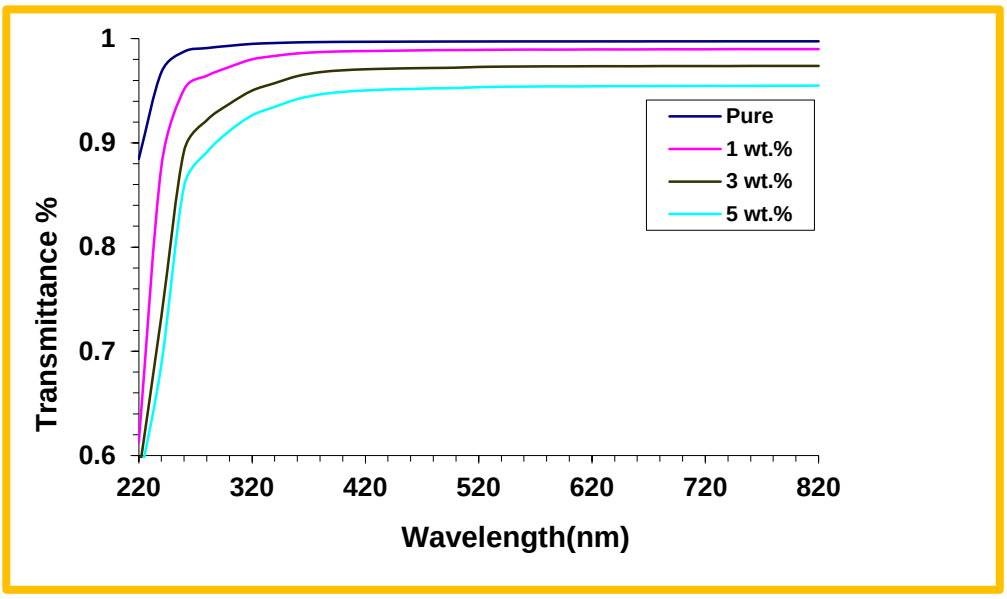

Figure(4.11): The transmittance variation of (PVP/PVA/ $Cu_{0.3}$ $Ni_{0.7}$ FeO_3) nanocomposites with the wavelengths.

4.3.3 Absorption Coefficient (α)

The absorption coefficient of nanocomposites has been calculate by equation (2-12). The absorption coefficient versus photon energy of the incident light are shown in Figs.(4.12)-(4.13) of (PVP-PVA/ Cu_x Ni_{1-x} FeO_3) nanocomposites respectively. From the figures, the absorption coefficient of all samples for nanocomposites is high at high energies. This means that the electron transition has high possibility; i.e. the energy of incident photon is enough to transit the electron from the valence band to the conduction band which due to the energy of the incident photon is greater than the energy band gap. The absorption coefficient assists to know the nature of electron transition [115,116]. When the values of the absorption coefficient of material are high ($\alpha>10^4$) cm^{-1}, it is expected that direct transition of electron. While, when the values of the absorption coefficient of material are low ($\alpha<10^4$) cm^{-1}, it is expected that indirect transition of electron. The values of absorption coefficient of (PVP-PVA/ Cu_x Ni_{1-x} FeO_3) x=0.1and x=0.3 nanocomposites are low ($\alpha<10^4$) cm^{-1}, the transition of electron is indirect. The

absorption coefficient of nanocomposites increases with the increasing of the concentrations of ferrite nanoparticles, this is attributed to the increasing of number of charge carriers, hence, increase the absorbance and absorption coefficient for (PVP-PVA/ Cu_x Ni_{1-x} FeO_3) at x=0.1 and x=0.3 nanocomposites [117].

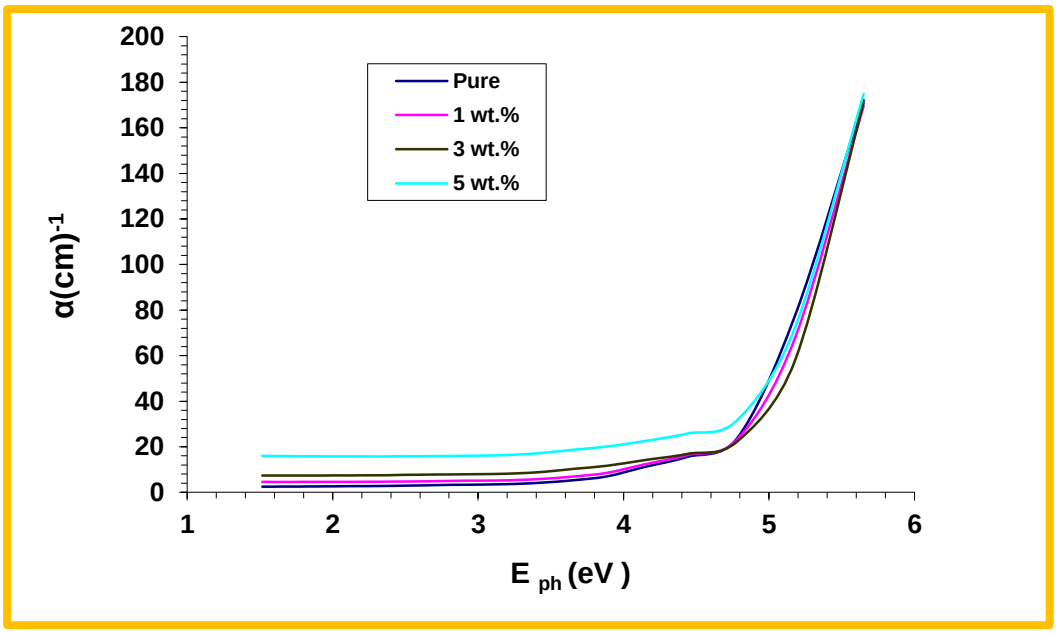

Figure (4.12) :The absorption coefficient variation of (PVP/ PVA/ $Cu_{0.1}$ $Ni_{0.9}$ FeO_3) nanocomposite with the photon energies.

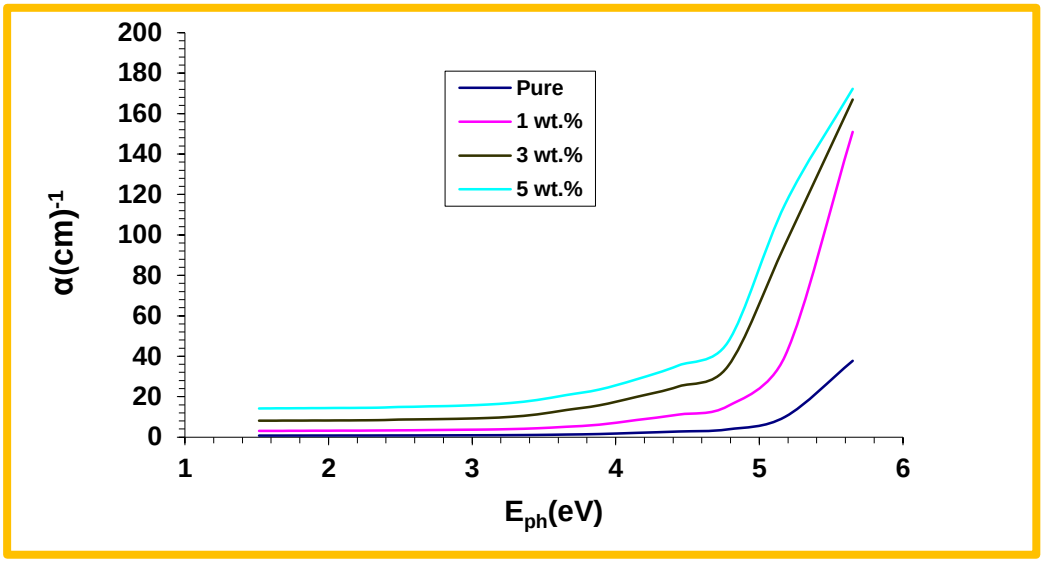

Figure (4.13) : The absorption coefficient variation of (PVP/PVA/ $Cu_{0.3}$ $Ni_{0.7}$ FeO_3) nanocomposite with the photon energies.

4.3.4 Energy gaps (E_g) of the (allowed and forbidden) indirect transition

The E_g were determined from relation (2-8). The E_g permitted indirect transitions of (PVP-PVA / Cu_x Ni_{1-x} FeO_3) nanocomposites x=0.1 and x=0.3 are shown in figs.(4.14)-(4.15) and the forbidden indirect transitions of (PVP-PVA-Cu_xNi_{1-x} FeO_3) nanocomposites x=0.1and x=0.3 are shown in figs.(4.16)-(4.17) respectively. By drawing a straight line from the top of the curve to the (x-axis) we can find the E_g . The E_g reduce with rise of ferrite nanoparticle content. This attributed to formation of local level in the E_g therefore, the transfer of electron from V.B. to local level and then to C.B. [118,119]. The value of the E_g of (PVP-PVA / Cu_x Ni_{1-x} FeO_3) at x=0.1and x=0.3 nanocomposites are listed in Table (4-3) and (4-4).

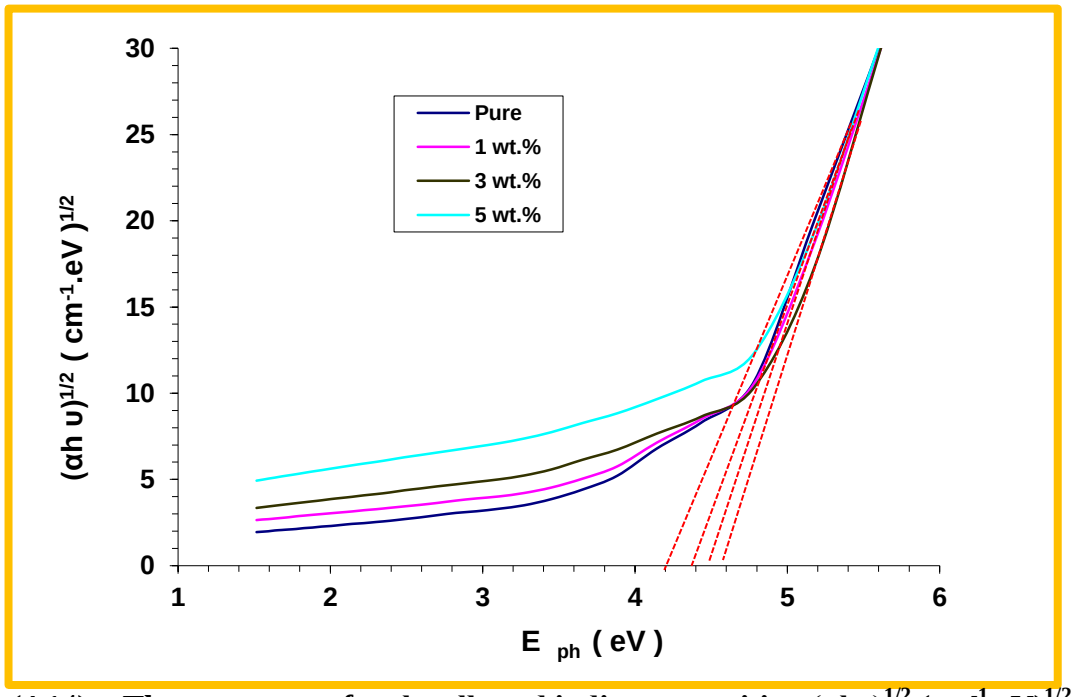

Figure (4.14): The energy gap for the allowed indirect transition $(\alpha h\nu)^{1/2}$ $(cm^{-1}.eV)^{1/2}$ versus photon energy of (PVP-PVA/ $Cu_{0.1}$ $Ni_{0.9}FeO_3$) nanocomposite with different concentration.

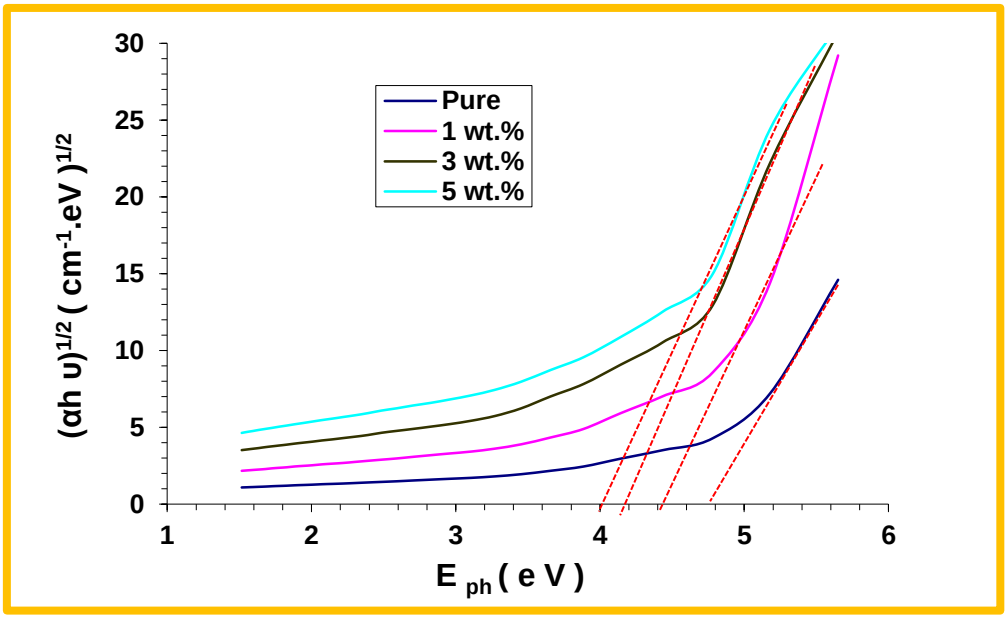

Figure(4.15): The energy gap for the allowed indirect transition $(\alpha h\upsilon)^{1/2}$ $(cm^{-1}.ev)^{1/2}$ versus photon energy of (PVP/PVA / $Cu_{0.3}$ $Ni_{0.7}FeO_3$) nanocomposite with different concentration.

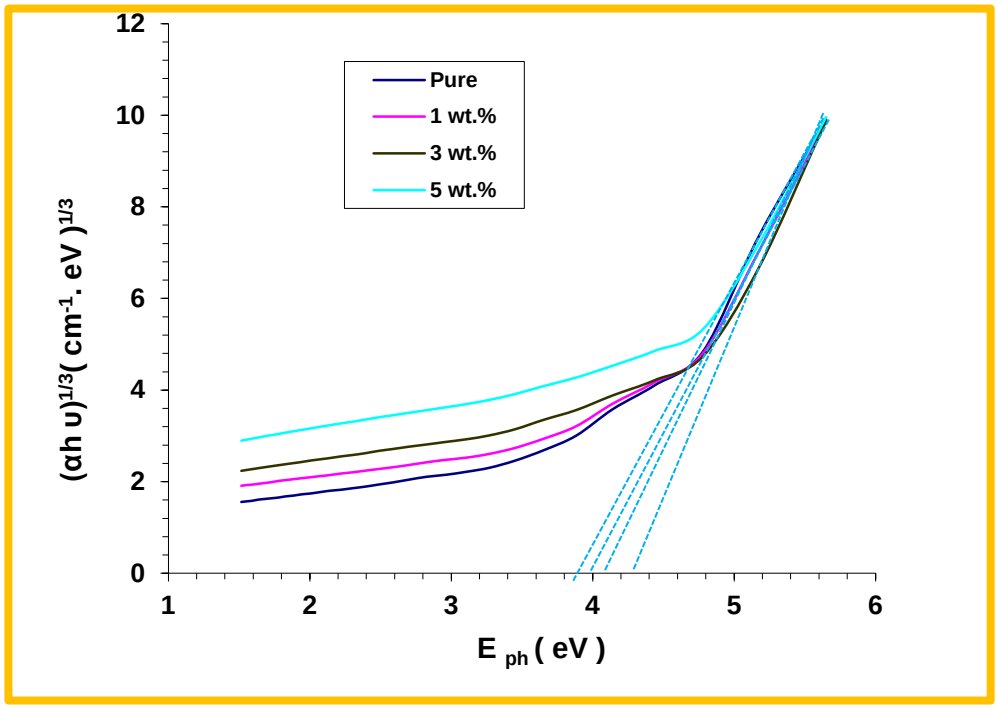

Figure(4.16):The energy gap for the forbidden indirect transition (α hν) $^{1/3}$(cm^{-1}. eV) $^{1/3}$ versus photon energy of the (PVP /PVA/ $Cu_{0.1}$ $Ni_{0.9}$ FeO_3)nanocomposite with different concentration.

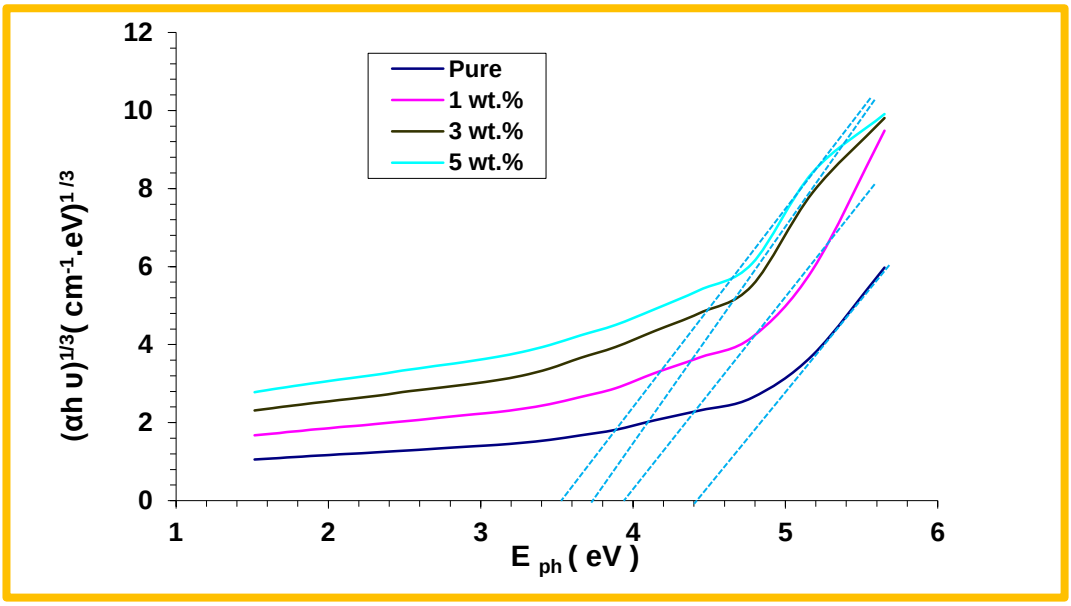

Figure (4.17):The energy gap for the for bidden indirect transition (α hν)$^{1/3}$ (cm^{-1}.eV)$^{1/3}$ versus photon energy of (PVP/PVA/ $Cu_{0.3}$ $Ni_{0.7}$ FeO_3)nanocomposite with different concentration.

Table (4.3): The values of optical energy gap for allowed Indirect transitions of (PVP/PVA/ Cu_x Ni_{1-x} FeO_3) at x=0.1and x=0.3 nanocomposites.

Ferrite wt% Nanoparticle's concentration	Allowed indirect transition for the (PVP/PVA/(0.1)ferrite)	Allowed indirect transition for the (PVP/PVA/(0.3)ferrite)
0	4.8	4.8
1	4.5	4.4
3	4.4	4.2
5	4.2	4

Table (4.4): The values of optical energy gap for forbidden Indirect transitions of (PVP/ PVA/ $Cu_x Ni_{1-x} FeO_3$) at x=0.1 and x=0.3 nanocomposites.

Ferrite wt% Nanoparticle's concentration	Forbidden indirect transition for the (PVP/PVA/(0.1)ferrite)	Forbidden Indirect Transition for the (PVP/PVA/(0.3)ferrite)
0	**4.3**	**4.4**
1	**4.1**	**3.95**
3	**4**	**3.75**
5	**3.9**	**3.55**

4.3.5 The Extinction Coefficient (k_0) of (PVP/PVA/ $Cu_x Ni_{1-x} FeO_3$) Nanocomposite

The $\mathbf{k_0}$ were determined from the formula (2- 11). Figs.(4.18)-(4.19) show the $\mathbf{k_0}$ for (PVP-PVA/ $Cu_x Ni_{1-x} FeO_3$)at x=0.1 and x=0.3 nanocomposites as a function of wavelength respectively. It is observe that $\mathbf{k_0}$ of nanocomposites increases with the increasing of the ferrite nanoparticles concentrations and increases for increasing wavelength, this is due to the increased in absorption optical and photons dispersions in the (PVP- PVA) polymer mixture [120].

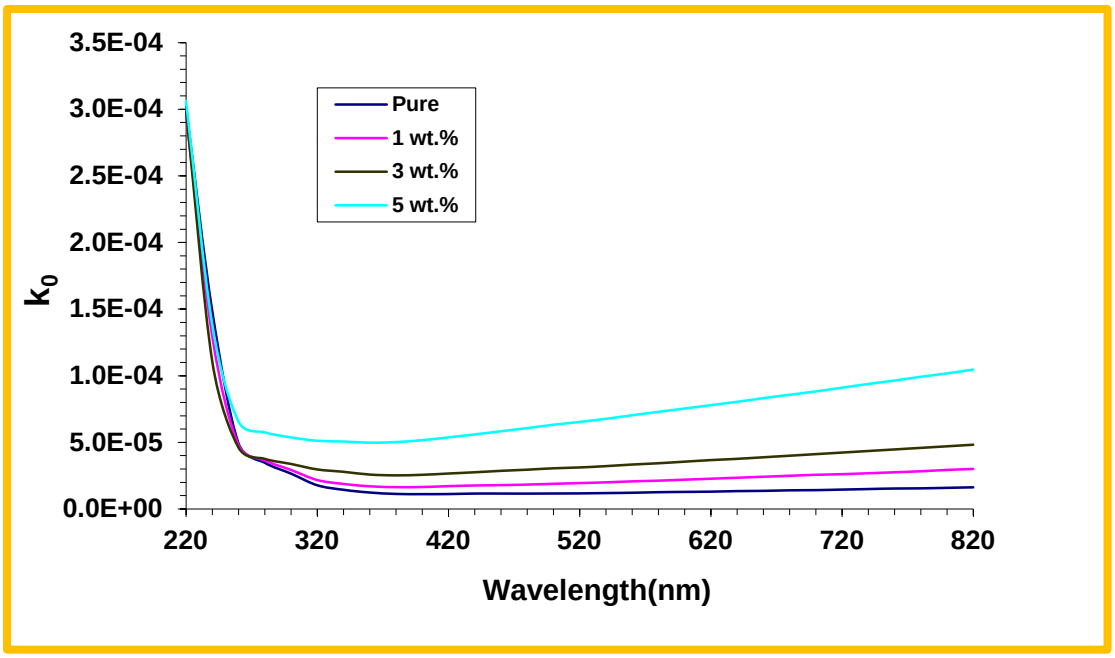

Figure(4.18): variation of Extinction coefficient for (PVP/PVA/ $Cu_{0.1}$ $Ni_{0.9}$ FeO_3) nanocomposites with the wavelengths.

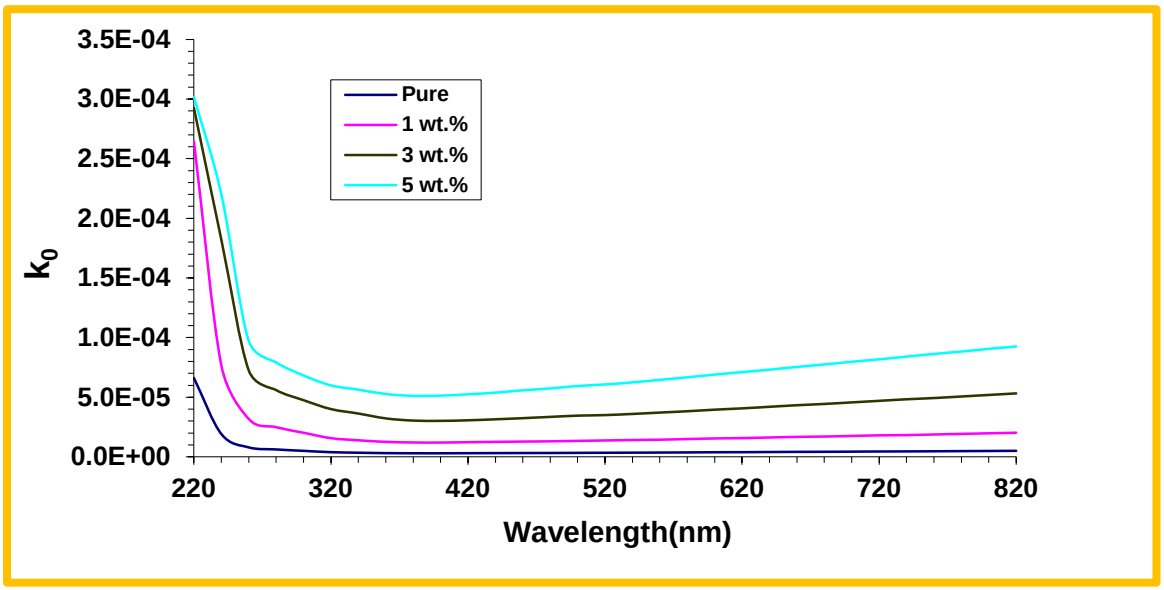

Figure(4.19) : variation of extinction coefficient for (PVP/PVA/$Cu_{0.3}$ $Ni_{0.3}$ FeO_3) nanocomposites with wavelength.

4.3.6 Refractive Index (n)

The refractive index was calculated using equation (2-10). The refractive index of (PVP-PVA/ Cu_x Ni_{1-x} FeO_3)at (x=0.1 and 0.3) nanocomposites as a function of wavelength is shown in figures (4.20)-(4.21) respectively. It is obtain that the refractive index of nanocomposites increases with the increasing of the ferrite nanoparticles concentrations and it is decreased with the increase of the wavelength. This behavior attributed to the increase of the density of nanocomposites. When the incident light interacts with a sample has high refractivity at UV region, hence, the values of refractive index will be increased. [121,122].

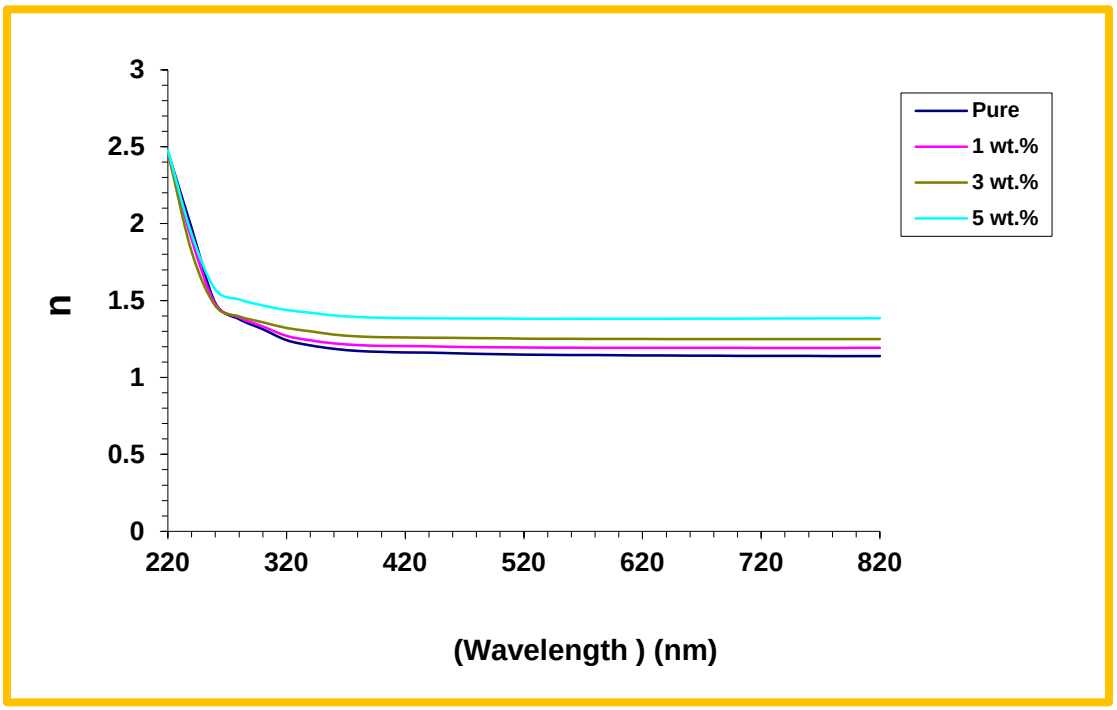

Figure (4.20) : variation of refractive index for (PVP/PVA/ $Cu_{0.1}$ $Ni_{0.9}$ FeO_3) nanocomposites with wavelength

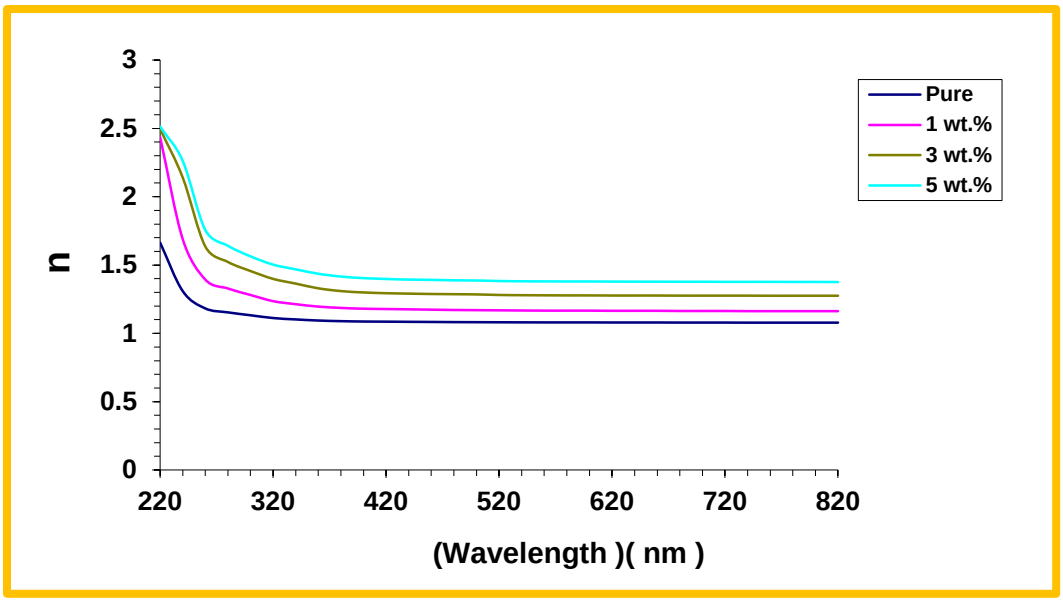

Figure (4.21) : variation of refractive index for (PVP/PVA/($Cu_{0.3}$ $Ni_{0.7}FeO_3$) nanocomposites with wavelength

4.3.7 The Real and Imaginary Parts of Dielectric Constant (ε_1, ε_2) .

By using the equations (2- 13) and (2-14), the real and imaginary parts of dielectric constant can be calculated. The real part versus wavelength for the(PVP-PVA/ Cu_x Ni_{1-x} FeO_3)at x=0.1 and x=0.3 nanocomposites are shown in Figs.(4.22)-(4.23) and imaginary part versus wavelength for the (PVP/PVA/Cu_x Ni_{1-x} FeO_3)at x=0.1and x=0.3 nanocomposites are shown in Figs.(4.22)-(4.23) respectively. From this figures, it is obtain the real and imaginary parts of the dielectric constant of the nanocomposite increase with increasing ferrite nanoparticle concentrations and decrease with increasing wavelength, with the increase in electrical polarization attributed to, the sharing of nanoparticle concentricity in the sample causing this increase, in ε_1, ε_2 of the nanocomposite. [123,124].

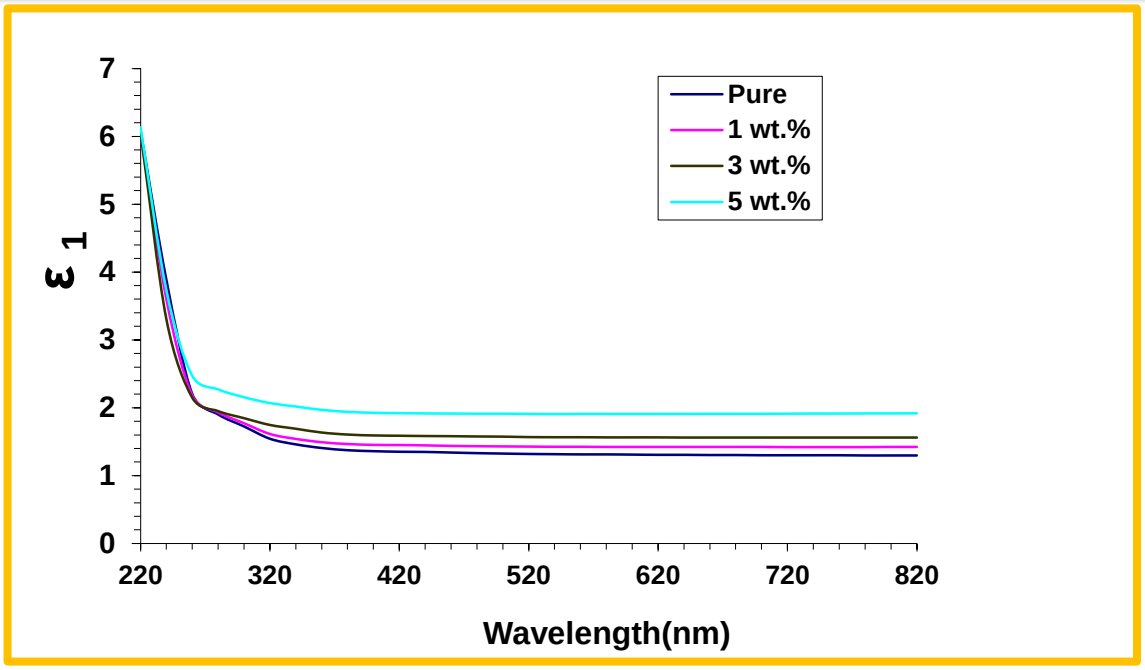

Figure(4.22): Real part variation of the dielectric constant of (PVP /PVA / $Cu_{0.1}$ Ni $_{0.9}$ FeO_3) nanocomposites with the wavelength.

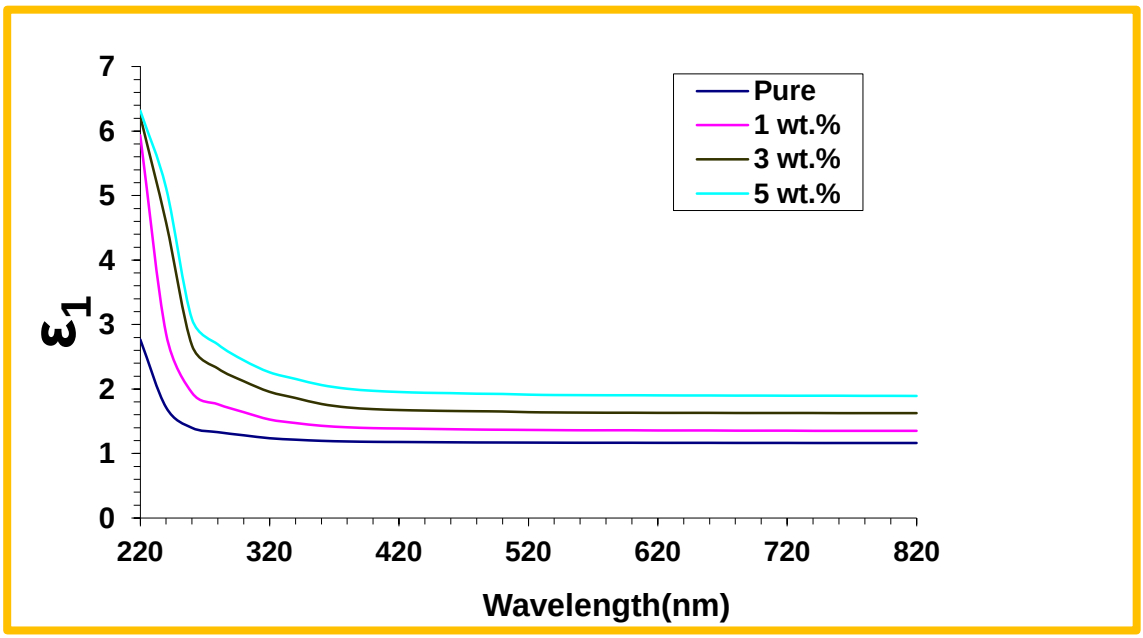

Figure(4.23): Real part variation of the dielectric constant of (PVP/ PVA /$Cu_{0.3}$ Ni $_{0.7}$ FeO_3) nanocomposites with the wavelength.

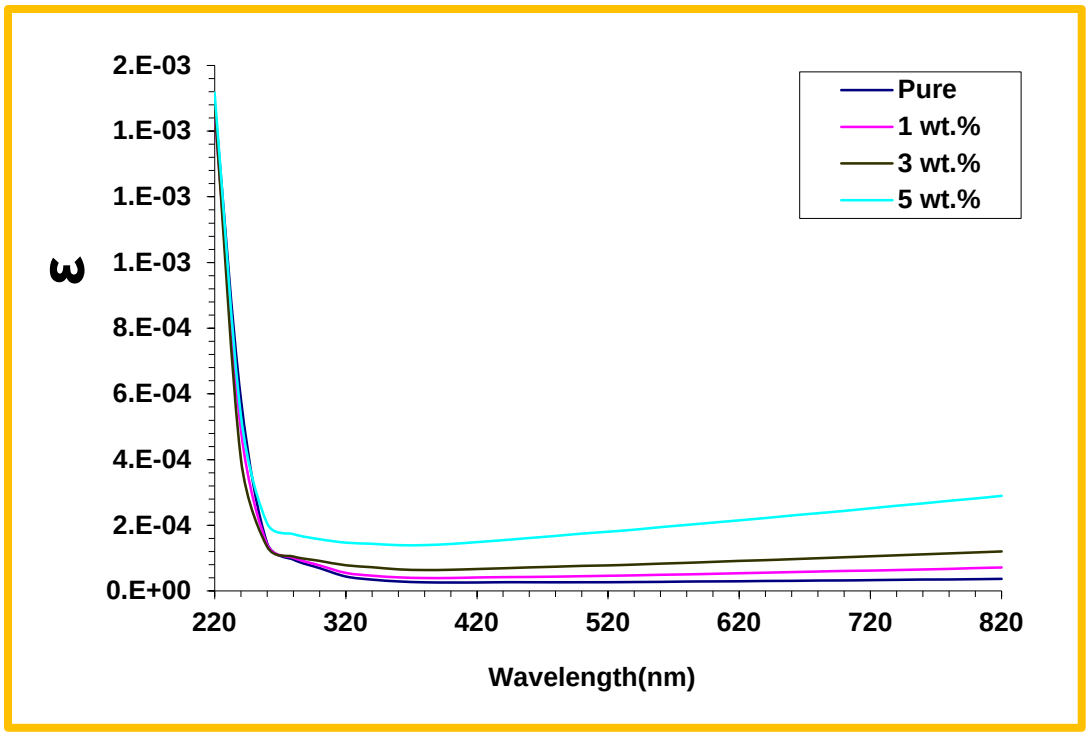

Figure(4.24): Imaginary part variation of the dielectric constant of (PVP/ PVA /$Cu_{0.1}$ Ni $_{0.9}$ FeO_3)nanocomposites with the wavelength.

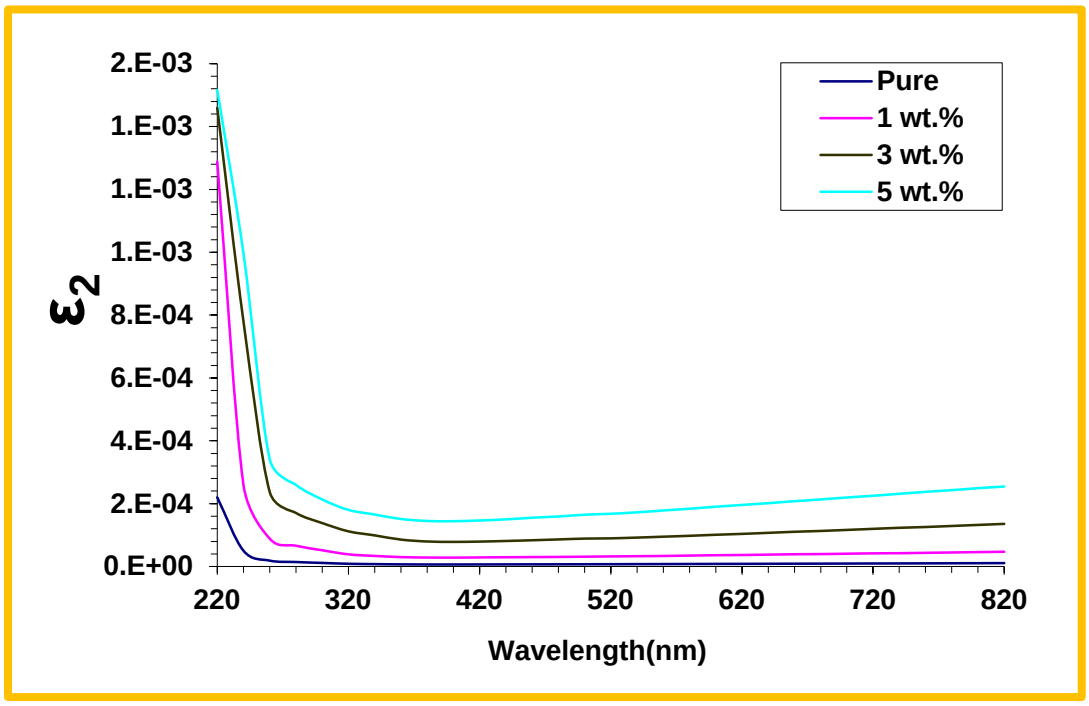

Figure(4.25): Imaginary part variation of the dielectric constant of (PVP/ PVA /$Cu_{0.3}$ Ni $_{0.7}$ FeO_3) nanocomposites with the wavelength.

4.3.8 Optical Conductivity (σ_{op})

The optical conductivity was calculated from the equation (2- 15). The optical conductivity of the ((PVP-PVA /Cu_x Ni $_{1-x}$ FeO_3)at x=0.1and x=0.3 nanocomposites with a wavelength are shown in Figs.(4.24)-(4.25) respectively. It is note that the optical conductivity for all sample decreased with the increased in wavelength, this result due to that the optical conductivity depend on the wavelength of the radiation incident on the nanocomposite specimen. Because the high absorption at low photon wavelength, the optical conductivity is increase at this area, the optical conductivity spectra indicated that the samples are transmittance within the infrared regions, the visible and near. The optical conductivity for nanocomposites is also increased with an increased concentrations of nanocomposites associated with the creation of localized concentrations in the energy gap, the increase in concentrations of nanocomposites induced an increase in the density of localized phases in the band structure; thus, an increase in the absorption coefficient suggests an increase in optical conductivity of the nanocomposites. This result is agree with researches [125].

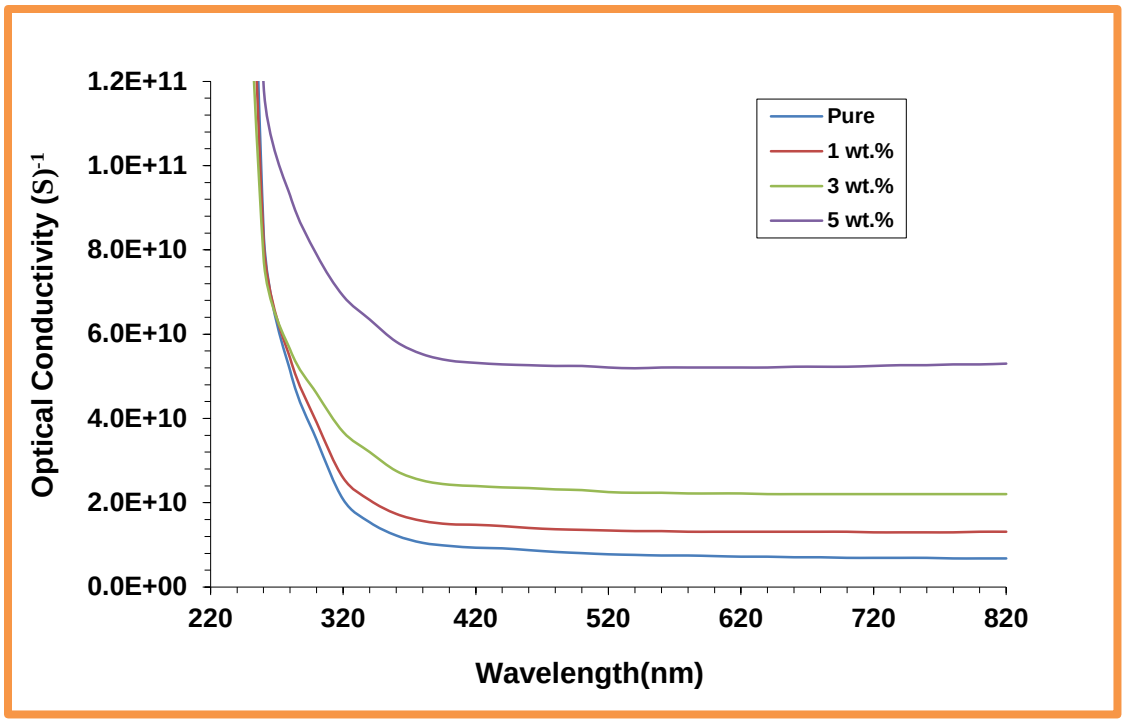

Figure(4.26): Optical conductivity variation for (PVP/PVA /$Cu_{0.1}$ Ni $_{0.9}$ FeO_3) nanocomposites with the wavelengths

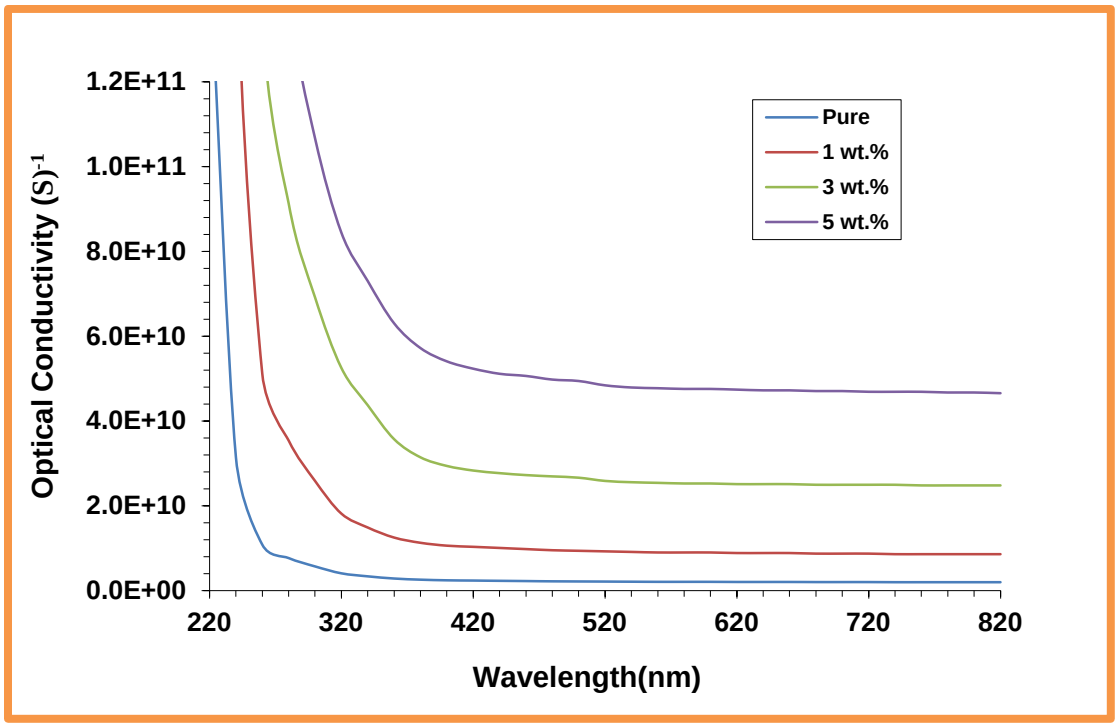

Figure(4.27): Optical conductivity variation for (PVP/PVA/ $Cu_{0.3}$ $Ni_{0.7}$ FeO_3) nanocomposites with the wavelengths.

4.4 The A.C Electrical Properties

The electrical properties of A.C of the (PVP-PVA/ Cu_x Ni $_{1-x}$ FeO_3) at(x=0.1and 0.3) nanocomposites include (dielectric constant, dielectric loss and A.C electrical conductivity) with range of the frequency (100Hz-5MHz) at room temperature

4.4.1 The Dielectric Constant (ε)

The dielectric constant has been calculated from the equation (2- 19). Fig. (4.26) shows the effect of ferrite nanoparticle additive on the dielectric constant. It is note that the dielectric constant increase with the increasing of the concentration of ferrite nanoparticles. This result due to the creation of a continuous network of ferrite nanoparticles within the polymer matrix. This result is agree with the results of researchers [126,127]. The variant of dielectric constant of (PVP-PVA/ Cu_x Ni $_{1-x}$ FeO_3) at (x=0.1 and 0.3) nanocomposites with frequency are shown in figs. (4.27)-(4.28). from this figures, it is observe that the dielectric constant of all samples of nanocomposites decreases with the increasing of the frequency of applied field, this may be attributed to the tendency of dipoles in nanocomposites samples to orient themselves in the direction of the electric applied field and decreasing of space charge polarization to the total polarization [128,129].

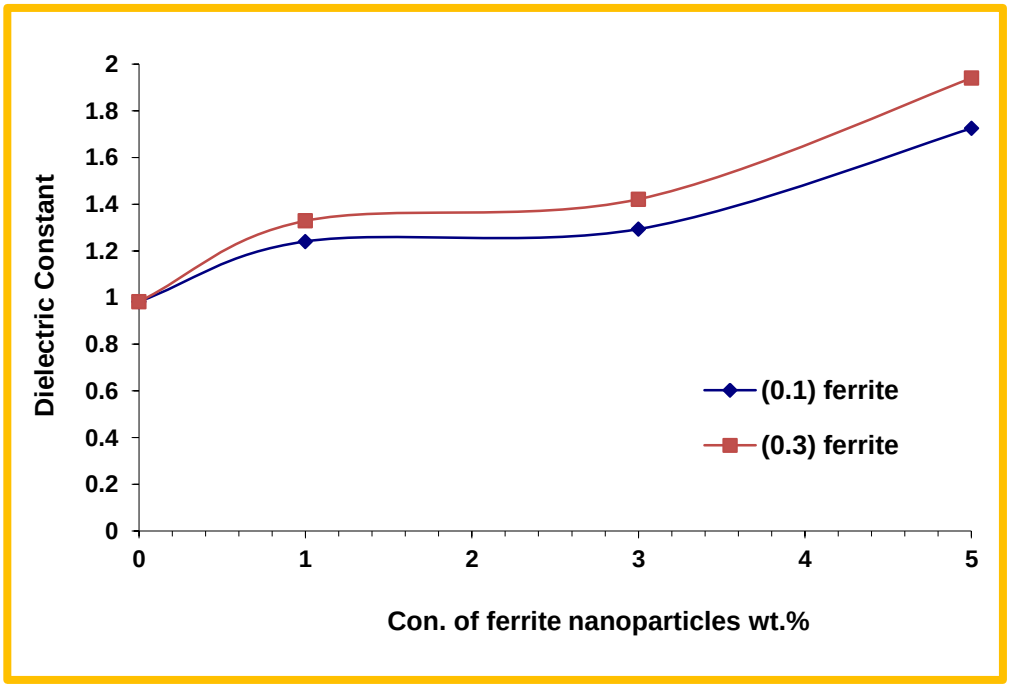

Figure (4.28): Variation of dielectric constant with concentration of nanoparticles at 100Hz of (PVP/PVA / Cu_x Ni $_{1-x}$ FeO_3)at x=0.1and x=0.3 nanocomposites

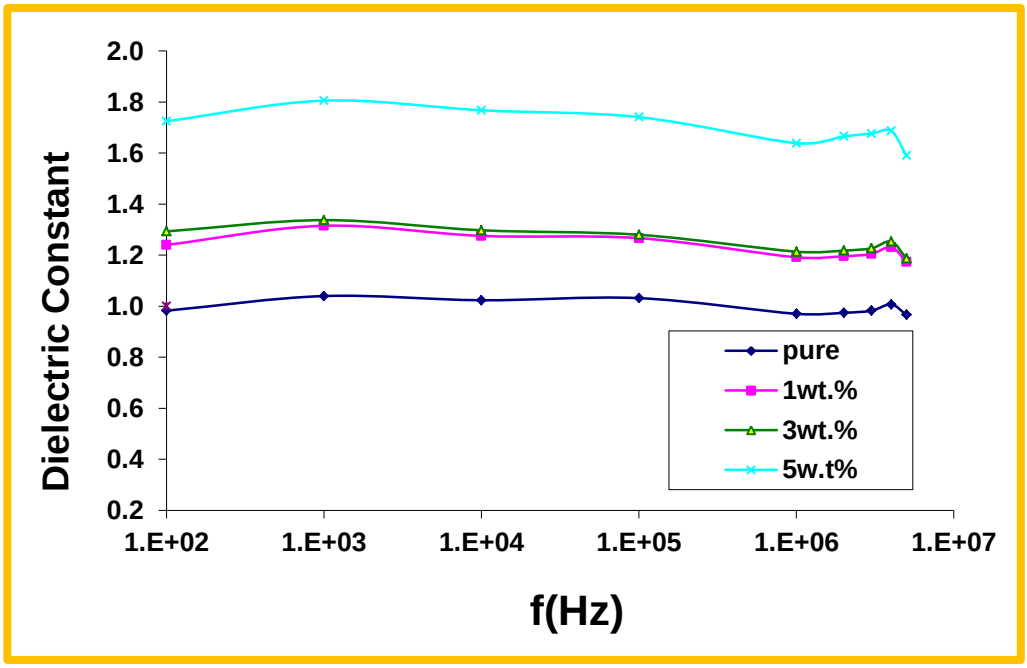

Figure(4.29):Variation of the dielectric constant of (PVP/PVA /$Cu_{0.1}$Ni $_{0.9}$ FeO_3) nanocomposites with frequency.

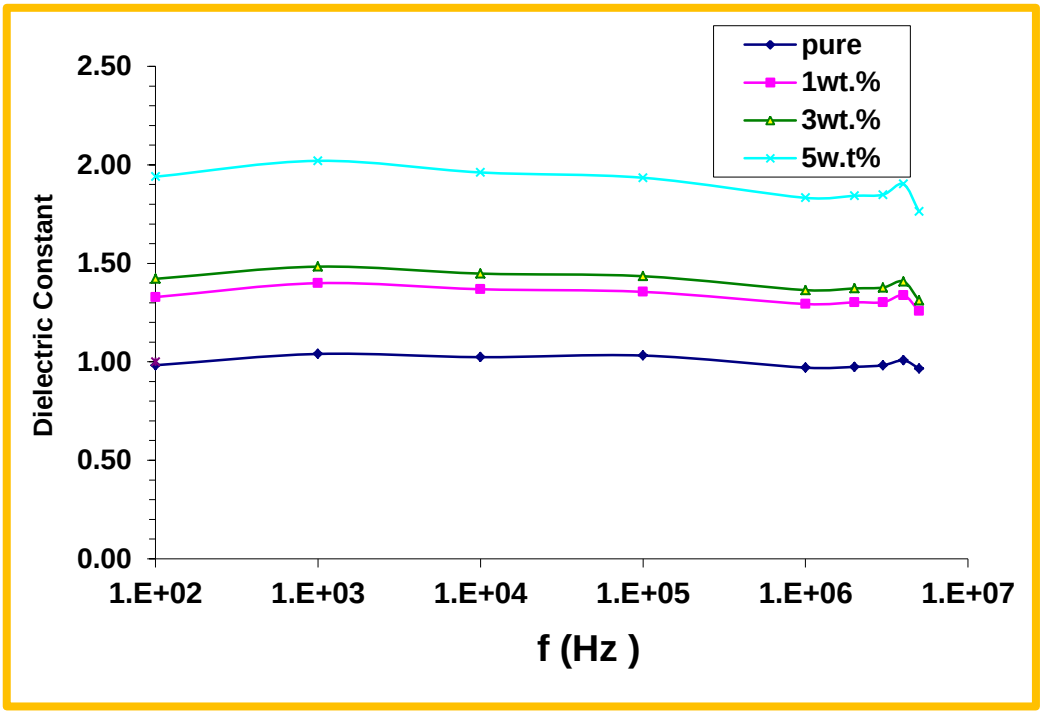

Figure (4.30): Variation of the dielectric constant of(PVP/PVA/ $Cu_{0.3}$ $Ni_{0.3}$ FeO_3) nanocomposites with frequency.

4 .4.2 Dielectric Loss (ε'')

The dielectric loss of the nanocompsite has been calculated using the equation (2-20). The dielectric loss of (PVP-PVA/ Cu_x Ni_{1-x} FeO_3)at (x=0.1and 0.3) nanocomposites shown in the figure (4 -29). From the figure, it's observe that the ε'' increase with increasing concentration of the ferrite nanoparticle. This result is attributable to increased charge on the dipole [130]. This result is similar to researches [131,132].

Figs.(4-30)-(4-31) show the dielectric loss of (PVP-PVA/ Cu_x Ni_{1-x} FeO_3) at (x=0.1and 0.3) nanocomposites with frequency. The dielectric loss of all samples for nanocomposites decreases with the increasing of the frequency. This behavior attributed to the decrease of the space charge polarization contribution. From the figures, at low frequency, the dielectric loss has high value for (PVP-PVA/ Cu_x Ni_{1-x} FeO_3)at(x=0.1 and 0.3)nanocomposites. This is because the electric dipoles

have enough time to align with the applied electric field before the electric field changes direction; as a result, the dielectric constant of nanocomposites is high. Due to the reduced time available for the dipoles to align at high frequencies, the dielectric constant value decreases [133]. These are similar with the results of researchers [134,135].

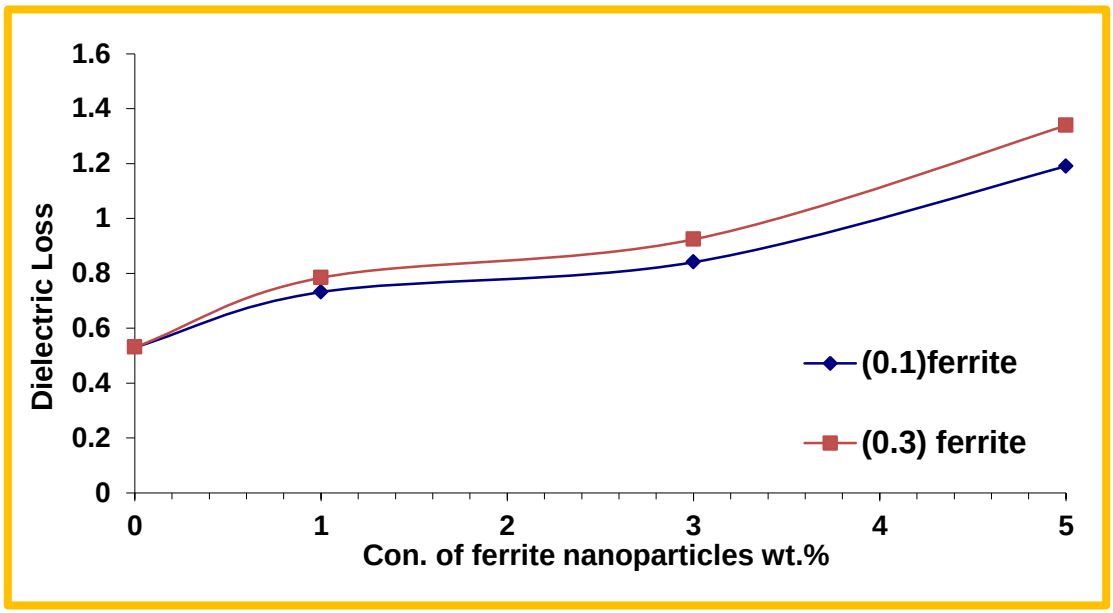

Figure(4.31): Variance of dielectric loss with concentration of nanoparticles for (PVP-PVA/ Cu_x Ni_{1-x} FeO_3) at x=0.1and x=0.3 nanocomposites.

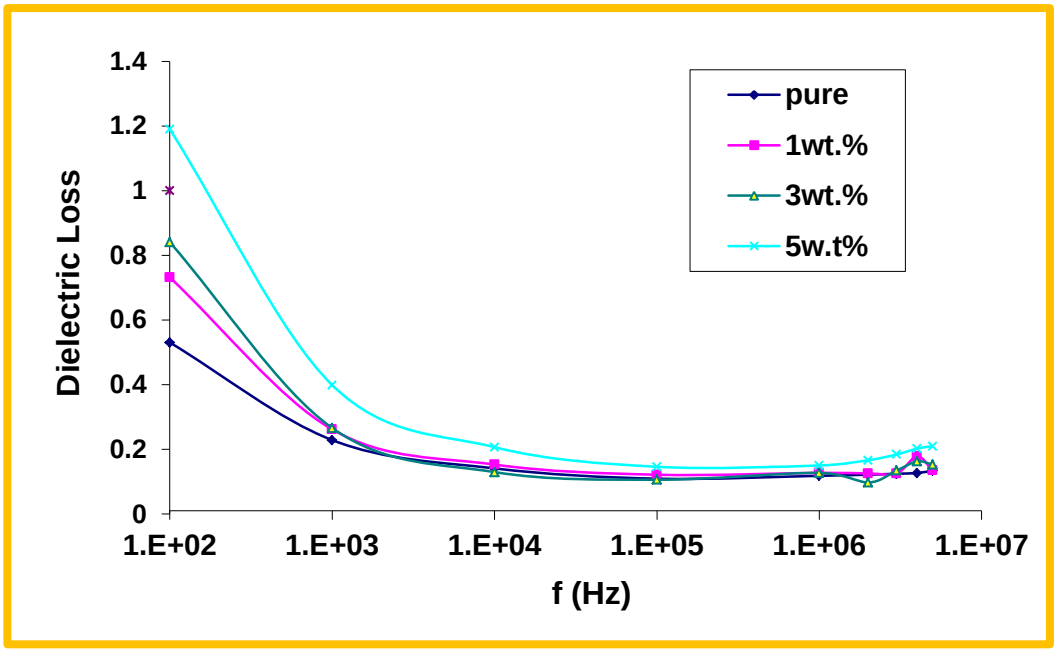

Figure(4.32): Variance of the dielectric loss of (PVP/PVA /$Cu_{0.1}$ Ni $_{0.9}$ FeO_3) nanocomposites with frequency.

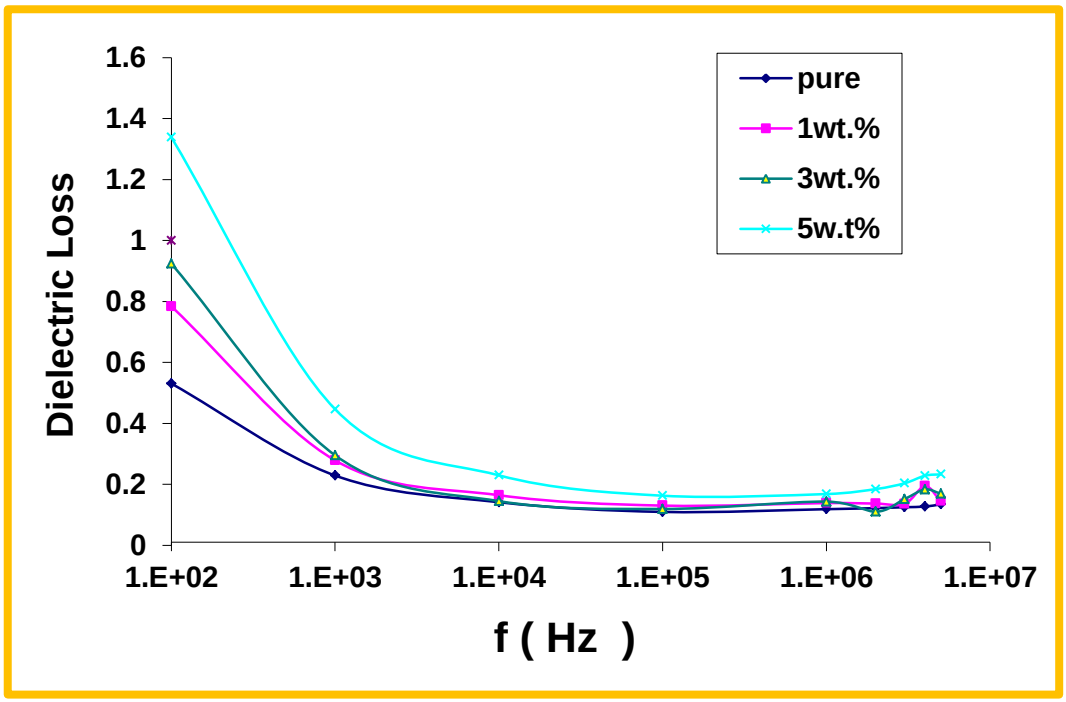

Figure(4.33): Variance of the dielectric loss of (PVP/PVA /$Cu_{0.3}$ $Ni_{0.7}$ FeO_3) nanocomposites with frequency.

4.4.3 The A.C Electrical Conductivity

The A.C Electrical Conductivity has been calculated from equation (2- 21). Fig.(4.32) reveal that the conductivity of nanocomposites increase with increasing of ferrite nanoparticle concentrations as a consequence of an increase in the ionic charge carriers and the formation of a continuous network of ferrite nanoparticles inside polymer matrix [136,137]. Figs.(4.33)-(4.34) show the variation of A.C electrical conductivity of (PVP-PVA/ Cu_x Ni_{1-x} FeO_3)at (x=0.1and 0.3) nanocomposites with frequency respectively at room temperature . The A.C electrical conductivity increases with increasing of the frequency of electric field for all samples of nanocomposites, this behavior attributed to the mobility of charge carriers and the hopping of ions from the cluster. In the low frequency, more charge accumulation occurred at the electrode and electrolyte interface, leading to a decrease in the number of mobile ions and electrical conductivity [138]. The mobility of charge carriers was higher in the high-frequency region; hence the electrical conductivity increases with frequency for ((PVP-PVA/ Cu_x Ni_{1-x} FeO_3)at x=0.1and x=0.3 nanocomposites [139].

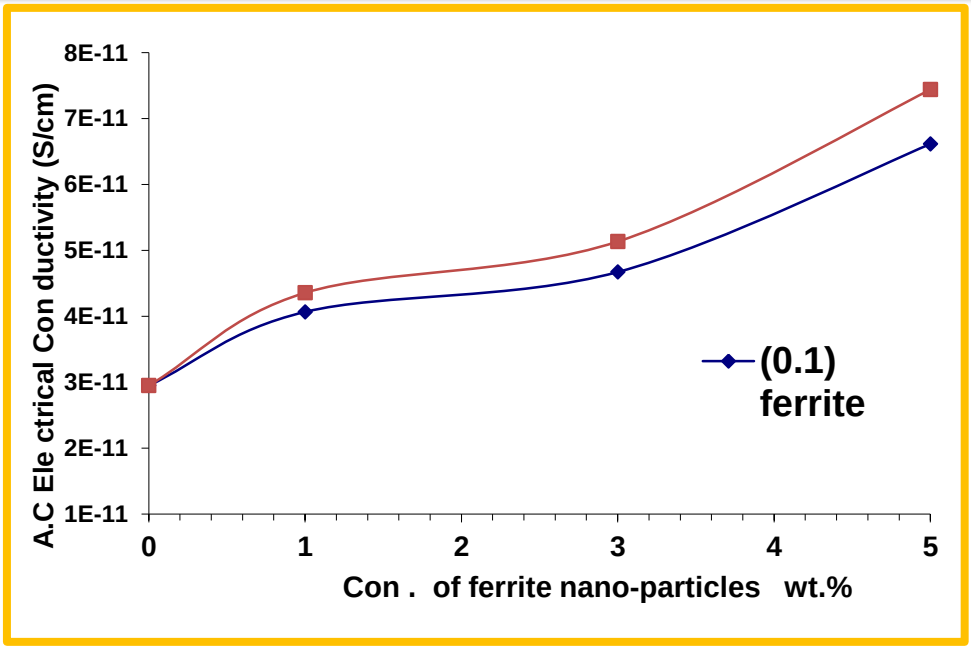

Figure(4.34): Variant of the A.C electrical with concentration of nanoparticles for (PVP/PVA/ $Cu_x Ni_{1-x}FeO_3$)at x= 0.1and x= 0.3 nanocomposites.

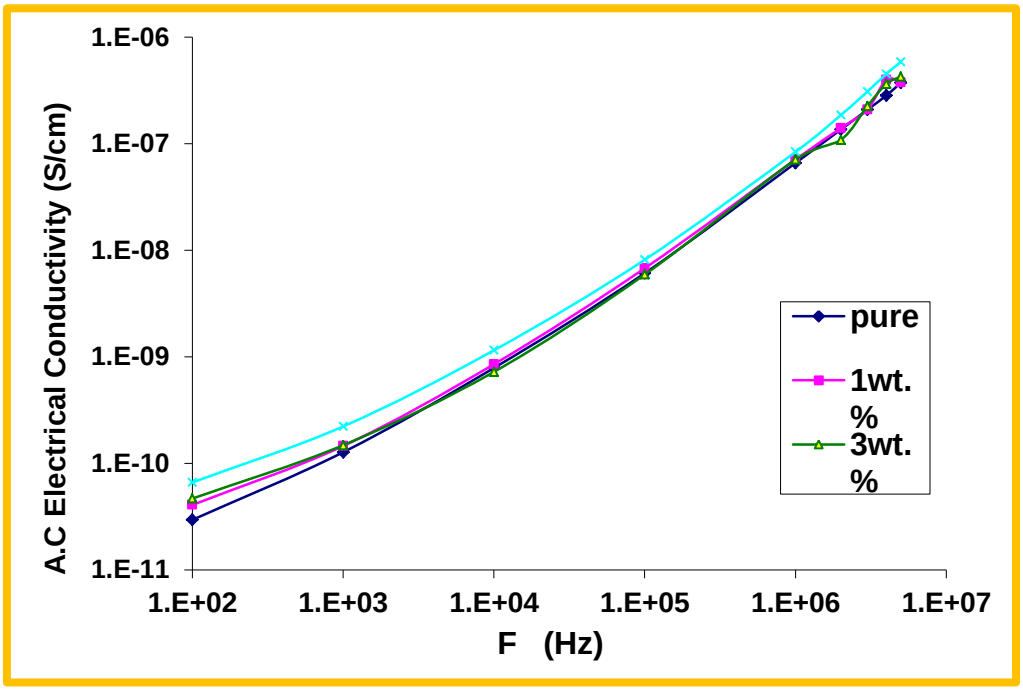

Figure(4.35): Variant of the A.C electrical with frequency for (PVP/PVA / $Cu_{0.1} Ni_{0.9} FeO_3$) nanocomposites.

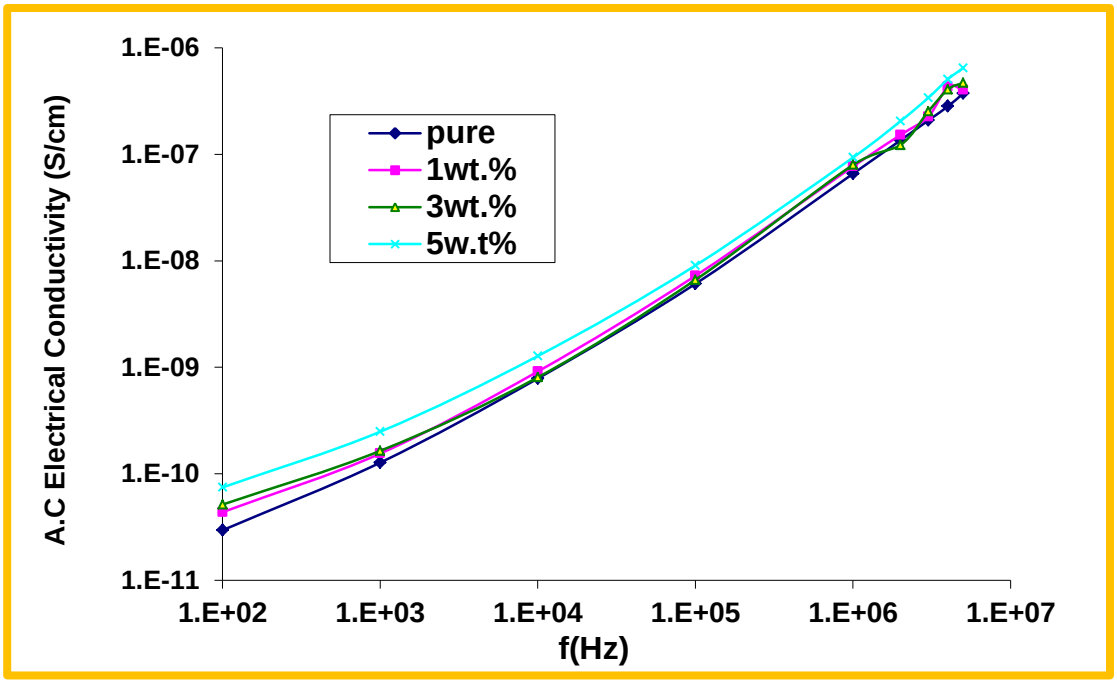

Figure(4.36): Variation of the A.C electric with frequency for (PVP/PVA/ $Cu_{0.3}Ni_{0.7}FeO_3$) nanocomposites.

4.5 Microwave Attenuation

In order to obtain materials with a attenuation of electromagnetic waves, their reflection loss must be reduced to the lowest possible value. Figs.(4.35, 4-36) show the relationship between the reflection loss of the prepared materials with frequency range (4-7) GHz for the $Cu_x Ni_{1-x}FeO_3$ with(x=0.1 and 0.3). From this figures, it is observed that the reflection loss shows greater while the content of 5wt % of FeO_3 to the nanocomposite. The reflection loss reaches to (-16, -13 and -11 dB) at frequency 5.3 GHz respectively for the $Cu_x Ni_{1-x}FeO_3$ with x=0.1 and reflection loss reaches to (-13.1,-12 and -10 dB) at frequency 5.3 GHz respectively for the $Cu_x Ni_{1-x}FeO_3$ with x=0.3. Thus, have obtained materials with a low reflection loss that can be used as attenuators of microwaves emitted by mobile for devices within the S-band. This result agree with researcher [140].

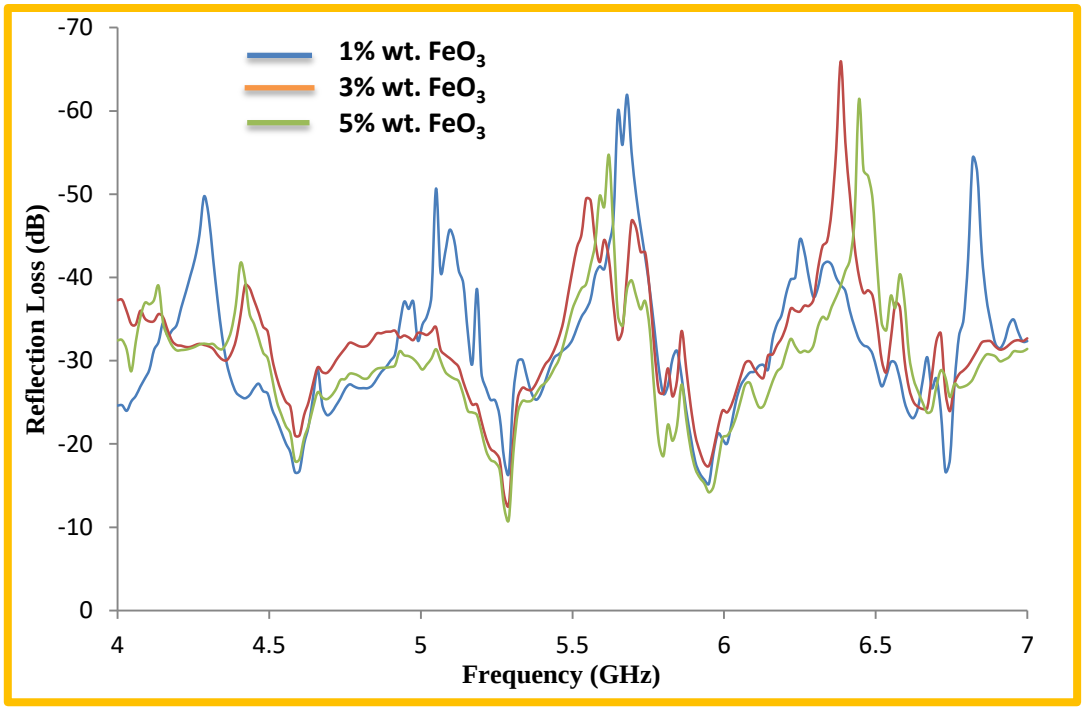

Figure(4.37) The variance of reflectivity loss with frequency for (PVP/PVA/$Cu_{0.1}$ $Ni_{0.9}FeO_3$) nanocomposite

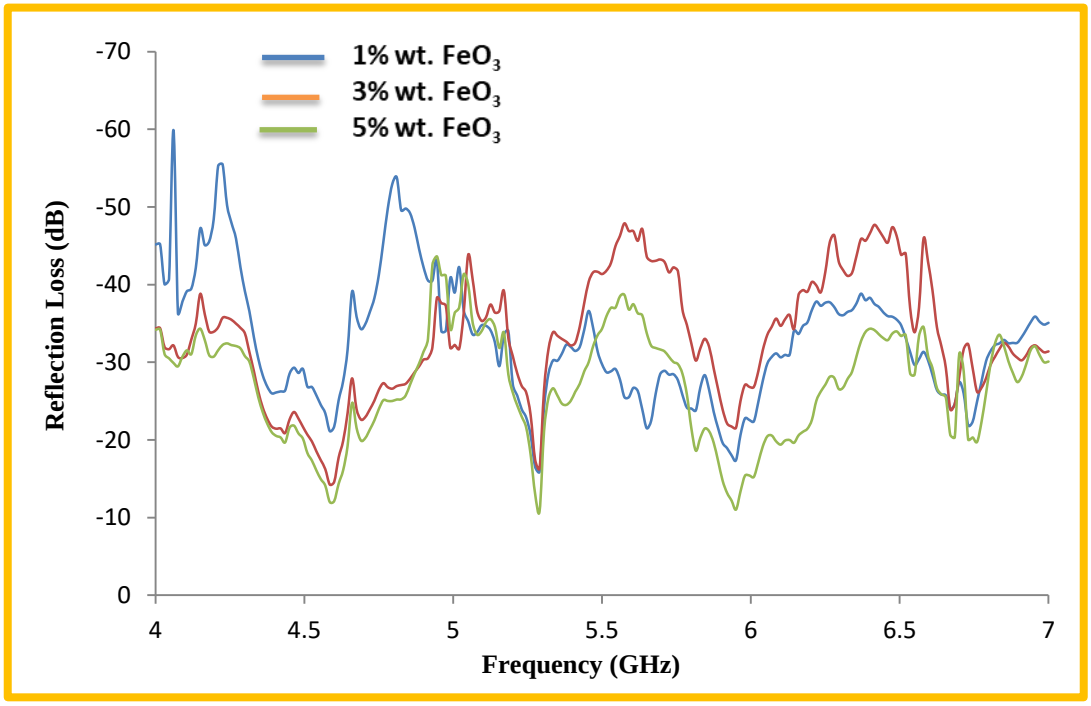

Figure(4.38) The variance of reflectivity loss with frequency for (PVP/PVA/$Cu_{0.3}$ $Ni_{0.7}FeO_3$) nanocomposite

4.6 Conclusions

The following points are concluded:

1- The XRD results showed that all films are polycrystalline in nature with a cubic structure of ferrite at the degree of calcination of powder ferrite $Cu_x Ni_{1-x}FeO_3$ with x=0.1 and 0.3 at a temperature of 1200 ℃.

2- The ferrite $Cu_x Ni_{1-x} FeO_3$ with x=0.1 and 0.3 forms a continuous network within the PVP/PVA composite at concentrations of (1 ,3 and 5) wt %. percent, as shown by FESEM and optical microscope photos.

3- The (PVP/PVA) polymer matrix has no interactions with ferrite $Cu_x Ni_{1-x} FeO_3$ with x=0.1 and 0.3, as shown by FTIR spectra showing shifts in certain bonds and changes in intensities.

4- The absorbance increases with increasing concentration of ferrite $Cu_x Ni_{1-x} FeO_3$ with x=0.1 and 0.3 within (PVP/PVA) polymer matrix. Because of the increased density of the films, and this means an increase of atoms and ions in the light path and increase the absorbance, while the transmittance and energy gap for $C_xNi_{1-x} FeO_3$ nanocomposite decrease with the increasing of the Ferrite concentrations nanoparticles.

5- The absorption coefficient, extinction coefficient, refractive index, real and imaginary parts of optical conductivity are increasing with the increase of the weight percentages of ferrite nanoparticles.

6- The dielectric constant and loss increase with increasing the concentration of ferrite $Cu_x Ni_{1-x}FeO_3$ with x=0.1 and 0.3 inside (PVP/PVA) polymer matrix and decrease through increasing of frequency of the applied electrical field, while the

A.C increase through increasing of the ferrite concentration $Cu_x Ni_{1-x}FeO_3$ with x=0.1 and 0.3 inside (PVP/PVA) polymer and also increase with frequency.

7- When conducting examinations for the attenuation of microwaves within the frequency range (4-7) GHz for different concentration of $Cu_x Ni_{1-x}FeO_3$ with x=0.1 and 0.3 inside (PVP/PVA) polymer. The ability of this nanocomposite to be attenuators of microwaves emitted within the S-band.

8-The energy gap for all concentrations is lower than the ratio 0.3 for all 0.1 concentrations and for all permitted and prohibited transfers

.4.7 Future Works

The following suggests for future work:

1- Study effect of ferrite materials on the physical properties for (PVA-CMC-ferrite)

2. Effect of the prepared ferrite nanoparticle material on Structural, optical and electrical properties of (PMMA).

3. Study the influence of temperature on the optical and electrical properties($Mn_x Fe_{1-x} Fe_2O_4$)(PS-ferrite) nanocomposites.

4. Study of microwaves attenuation of (NR/SBR/ferrite) Rubbery nanocomposites.

5. preparation and study the thickness effect on attenuation properties for (CMC-PVP-ferrite) within the frequency range (3-8 GHz).

REFERENCES

REFERENCES

[1] G. A. Kontos, A. L. Soulintzis, P. K. Karahaliou, G. C. Psarras, S. N. Georga, C. A. Krontiras and M. N. Pisanias, "Electrical relaxation dynamics in TiO_2-polymer matrix composites", Express Polymer Letters ,Vol .1,No 12, pp. 781-789,(2007).

[2] S. Mustafa," Engineering Chemistry", Library of Arab Society for Publication and Distribution, Jordan, (2008).

[3] S. Hossain, "Optical properties of polymers and their applications." (2019).

[4] T. M. Beraada, and G. A. Al-Adam. "The Updated Chemistry of Large Molecules." University of Basrah, College of Science (1989).

[5] A. Long ," Composites Forming Technologies" , Cambridge University, England , (2007).

[6] S. S. Pendhari, T. Kant and Y. M. Desai, " Application of polymer composites in civil construction": A general review. Composite structures, 84(2), 114-124,(2008).

[7] P. Ajayan , L. Schadler and P. Braun, " Nanocomposite science and technology Wiley VCH", (2003) .

[8] N. Malhotra, K. Sheikh and S. Rani, "A Review on Mechanical Characterization of Natural Fiber Reinforced Polymer Composites. Journal of Engineering Research and Studies, 3, 75-80.(2012).

[9] L. L. Zhai, L. G. P. and W. Y .Wang. "Effect of nano-Al_2O_3 on adhesion strength of epoxy adhesive and steel" International Journal of Adhesion and Adhesives;28:23 .(2007).

[10] P. R. Singh , M .Zhang and D. Chan "Toughening of a brittle thermosetting polymer: Effects of reinforcement particle size and volume fraction" J. Mater. Sci. 37, 371.*(*2002)

[11] R. R. Nagavally, "Composite materials-history, types, fabrication techniques ,advantages, and applications." Int J Mech Prod Eng 5.9: 82-7(2017).

[12] J. Furer "Growth of Single-Wall Carbon Nanotubes by Chemical Vapor Deposition for Electrical Devices", Ph. D thesis, Basel University (2006).

[13] K.T. Ramesh, "Nanomaterials Mechanics and Mechanisms", The Johns Hopkins University, USA,PP.3, (2009).

[14] D. Liu, W. Wu, Y. Qiu, S. Yang, S. Xiao, Q. Q. Wang, L. Ding, and J. Wang ,"Surface functionalization of ZnO nanotetrapods with photoactive and electro-active organic monolayers", J. of Langmuir, Vol.24, pp.5052-5059, (2008)

[15] C. Sun," Controlling the rheology of polymers/silica nanocomposites", thesis, Eindhoven University of Technology, (2010).

[16] M. Arifitekhar, "Introduction to Composite Materials", Copyright © 2010, ASM International, (1999).

[17] J.J. Smit and P.H.F. Morshuis," Thermal and electrical properties of nanocomposites, including material processing",Ph.D. thesis, Sai-Petersburg State Electrotechnical University 'LETI', Russia, (2012).

[18] F.L.Martien,"Encyclopedia of Polymer Science and Engineering", Wiley,New York, (1986).

[19] Z. Ping ,Q .T. Nguyen, and J. Neel," Polymer. advanced. Technology Macromolecule Chemistry and Physics .,No. 195,pp.21,(1994).

[20] M. T. Razzak, S. P. Dewi, Lely, H., & E. Taty ,"The characterization of dressing component materials and radiation formation of PVA–PVP hydrogel. Radiation Physics and Chemistry", 55(2), 153-165(1999).

[21] D. C. H. Liu , D. J. Liaw, B. Y. Liaw , C. H. Tsai, J. H. Ho & T. I. Ho , " Effects of gamma radiation on various polyimides". Journal of the Chinese Chemical Society, 47(4A), 583-588(2000).

[22] H. D. Wu, I. D. Wu& F. C. Chang . "The interaction behavior of polymer electrolytes composed of poly (vinyl pyrrolidone) and lithium perchlorate ($LiClO_4$). Polymer, 42(2), 555-562(2001).

[23] M.R. Shaik, M. Kuniyil, M. Khan, N. Ahmad, A. Al-Warthan, M. R. H. Siddiqui and S. F. Adil , "Modified Polyacrylic Acid-Zinc Composites: Synthesis, Characterization and Biological Activity", Molecules, Vol.21, PP.292, (2016).

[24] Sekisui Specialty Chemicals America.. Salvo polyvinyl alcohol. A versatile high-performance polymer(2009).

[25] Liu, D. C. H., Liaw, D. J., Liaw, B. Y., Tsai, C. H., Ho, J. H., & Ho, T. I. "Effects of gamma radiation on various polyimides". Journal of the Chinese Chemical Society, 47(4A), 583-588,(2000).

[26] V. Bühler . "Polyvinylpyrrolidone excipients for pharmaceuticals: povidone, crospovidone and copovidone". Springer Science & Business Media(2005).

[27] J. Chen, Y. Li, Y. Zhang & Y. Zhu, "Preparation and characterization of graphene oxide reinforced PVA film with boric acid as crosslinker". Journal of Applied Polymer Science, 132(22).(2015).

[28] Z.W. Abdullah, Y. Dong, I.J. Davies, S. Barbhuiya "PVA, PVA blends and their nanocomposites for biodegradable packaging application" Polym Plast Technol Eng , 56 (2017).

[29] K. Kreft , B.Kozamernik, & U.Urleb,. Qualitative determination of polyvinylpyrrolidone type by near-infrared spectrometry. International journal of pharmaceutics, 177(1), 1-6(1999).

[30] C. C. DeMerlis & D. R. Schoneker. Review of the oral toxicity of polyvinyl alcohol (PVA). Food and chemical Toxicology, 41(3), 319-326(2003).

[31] N. Limpan , T. Prodpran , S. Benjakul, & S. Prasarpran,. Influences of degree of hydrolysis and molecular weight of poly (vinyl alcohol)(PVA) on properties of fish myofibrillar protein/PVA blend films. Food hydrocolloids, 29(1), 226-233 (2012).

[32] C. C. DeMerlis , & D. R. Schoneker," Review of the oral toxicity of polyvinyl alcohol (PVA). Food and chemical Toxicology, 41(3), 319-326(2003).

[33] Celanese," Celvol Polyvinyl Alcohol A Versatile High-Performance Polymer" Published,(2007).

[34] R. C. Buchanan, (Ed.). Ceramic materials for electronics. CRC press(2018).

[35] J. Allouche "Synthesis of Organic and Bioorganic Nanoparticles Springer-Verlag London, PP.27-74, (2013).

[36] N. Sanpo , C. Wen , C. C. Berndt & J. Wang. Antibacterial properties of spinel ferrite nanoparticles. Microbial pathogens and

strategies for combating them: science, technology and education. Spain: Formatex Research Centre, 239-250, (2013).

[37] S. M. Ali Ridha, "X-ray Studies and Electrical Properties of the Zinc-substituted Copper Nano-ferrite Synthesized by sol-gel Method," Int. J. Compos. Mater., vol. 5, no. 6, pp. 195–201, (2015).

[38] C. B. Carter and M. G. Norton, Ceramic Materials: Science and Engineering. Springer New York,ISBN:9781461435235,(2007).

[39] R. Louh, T. G. Reynolds and R. C. Buchanan , "Ferrite Ceramics," Dekker, Marcel New York, Ceramic Materials for Electronics, vol. 3, (1986).

[40] V. Rangarajan, Materials Science, McGraw-Hill Publishing

Company Limited, New Delhi, (2004).

[41] N. A. K. M. M. ALMAMMORI, The effect of sintering time on the magnetic properties. Iraqi journal of mechanical and material engineering, 100(first conf./eng. coll.) (2009).

[42] C.W. Chen." Magnetism and Metallurgy of Soft Magnetic Materials" North-Holland PublishIing Company pp368-372 (1977)

[43] G. Alex, Modern Ferrite Technology, 2nd ed., Pittsburgh, PA, USA, Springer, (2006).

[44] K. H. J. Buschow and F. R. Boer, " Physics of Magnetism and Magnetic Materials", Kluwer Academic Publishers, New York, , pp34 - 35 (2004).

[45] S. H. Al-Nesraway, , M. H. Al-Maamori, and J. M. Al-Issawe. "Preparation of a rubber nanocomposite (Silicone Rubber-Ferrite) for

protect human from bioeffects of microwave emitted from mobile devices." Journal of Bionanoscience 12.5: 645-651,(2018).

[46] K. T. Arul, E. Manikandan, R. Ladchumananandasivam & M. Maaza, Novel PVA polymer based nanostructure with ferrities co-doped with nickel and cobalt ions for Magneto-Sensor application.

[47] S. Mirzaee and S. F. Shayesteh. "Ultrasound induced strain in ultrasmall $CoFe_2O_4$@ polyvinyl alcohol nanocomposites." Ultrasonics sonochemistry 40 583-586. (2018).

[48] M. T. Ramesan, T. Anjitha, , K. Parvathi, , T. Anilkumar & G. Mathew, "Nano zinc ferrite filler incorporated polyindole/poly (vinyl alcohol) blend: Preparation, characterization, and investigation of electrical properties. Advances in Polymer Technology, 37(8), 3639-3649 (2018).

[49] S. Mallesh and V. Srinivas, "A comprehensive study on thermal stability and magnetic properties of MnZn-ferrite nanoparticles," J. Magn. Magn. Mater., vol. 475, no. November 2018, pp. 290–303,(2019), doi: 10.1016/j.jmmm..11.052 ,(2018).

[50] T. Kaewmanee, S. Wannapop , A. Phuruangrat , T. Thongtem, , O. Wiranwetchayan, W. Promnopas & S. Thongtem , Effect of oleic acid content on manganese-zinc ferrite properties. Inorganic Chemistry Communications, 103, 87-92(2019).

[51] R. Sagayaraj, T. Dhineshkumar, Prakash, A., Aravazhi, S., Chandrasekaran, G., Jayarajan, D., & Sebastian, S. Fabrication, microstructure, morphological and magnetic properties of W-type ferrite by co-precipitation method: Antibacterial activity. Chemical Physics Letters, 759, 137944. (2020).

[52] T. A. Taha, A. Hassona, S. Elrabaie, & M. T. Attia, Dielectric spectroscopy of PVA-$Ni_{0.5}$ $Zn_{0.5}$ Fe_2O_4 polymer nanocomposite films. Journal of Asian Ceramic Societies, 8(4), 1076-1082. (2020).

[53] A. H. Alshammari, & T. A. Taha, Structure, thermal and dielectric insights of PVC/PVP/$ZnFe_2O_4$ polymer nanocomposites. The European Physical Journal Plus, 136(12), 1-13(2021).

[54] M. S. Toman and S. H. Al-nesrawy. "New Fabrication (PVA-CMC-PbO) Nanocomposites Structural and Electrical Properties." NeuroQuantology 19.4: 38(2021).

[55] A. A. Abid, S. H. Al-nesrawy, and Ali R. Abdulridha. "New Fabrication (PVA-PVP-C. B) Nanocomposites: Structural and Electrical Properties." Journal of Physics: Conference Series. Vol. 1804. No. 1. IOP Publishing, (2021).

[56] K. Sangsuriyonk, N. Paradee, K. Rotjanasuworapong& A. Sirivat, Synthesis and characterization of Co_xFe_{1-x} Fe_2O_4 nanoparticles by anionic, cationic, and non-ionic surfactant templates via co-precipitation. Scientific Reports, 12(1), 1-11(2022).

[57] R. O. Gould and W. Massa, Crystal Structure Determination. Springer Berlin Heidelberg,(2013).

[58] Lee, Myeongkyu " X-Ray diffraction for materials research: from fundamentals to applications" CRC Press, (2017).

[59] S. M. Sze, Y. Li & K. K. Ng, Physics of semiconductor devices. John wiley & sons (2021).

[60] K. Praveena, K. Sadhana, S. Bharadwaj, and S. R. Murthy, “Development of nanocrystalline Mn-Zn ferrites for high frequency

transformer applications," J. Magn. Magn. Mater., vol. 321, no. 16, pp. 2433–2437, 2009, doi: 10.1016/j.jmmm.2009.02.138.

[61] S. H. Abud, Z. Hassan, and F. K. Yam, "Enhancement of structural and optical properties of porous in0.27Ga0.73N thin film synthesized using electrochemical etching technique," Int. J. Electrochem. Sci., vol. 7, no. 10, pp. 10038–10046, (2012).

[62] S. Sudjatmoko, W. Wirjoadi, and B. Siswanto, "Influence of Substrate Temperature on Structural, Electrical and Optical Properties of ZnO:Al Thin Films," Atom Indones., vol. 35, no. 2, 2011, doi: 10.17146/aij.(2009).

[63] A. Khorsand Zak, W. H. Abd. Majid, M. E. Abrishami, and R. Yousefi, "X-ray analysis of ZnO nanoparticles by Williamson-Hall and size-strain plot methods," Solid State Sci., vol. 13, no. 1, pp. 251–256, 2011, doi: 10.1016/j.solidstatesciences.2010.11.024.

[64] R. Cik, H. Che F. Choo and Azillah Fatimah Othman Nor. "Field Emission Scanning Electron Microscope (FESEM) Facility in BTI." (2015).

[65] P. Gnauck, V. Drexel, and J. Greiser, A New high resolution field emission scanning electron microscope with variable pressure capabilities, Micrsocopy and Microanalysis, 7 : 880 (2001).

[66] D.C. Joy and J.B. Pawley, High resolution scanning electron microscopy, Ultra microscopy, 47: 80-100, (1993) .

[67] A.V. Crewe and P.S.D Lin, Production of a field emission source, In Progress in Optics XI (Eds. Wolf E.) North Holland : 225-246, (1973).

[68] J. Pawley, & H. Schatten, (Eds.). Biological low-voltage scanning electron microscopy. Springer Science & Business Media(2007).

[69]M. F. AL-Mudhaffer, M. A. Nattiq and M. Ali Jaber, "Linear optical properties and energy loss function of Novolac: Epoxy blend film", Scholars Research Library, Archives of Applied Science Research, Vol. 4, No. 4, PP.1731-7140(2012).

[70] A. Telser, “Fundamentals of Light Microscopy and Electronic Imaging,” Shock, vol. 17, no. 5, p. 442,(2002).

[71] A. Ramírez-hernández, C. Aguilar-flores, and A. Aparicio-saguilán, “Fingerprint analysis of FTIR spectra of polymers containing vinyl análisis en la huella dactilar de espectros FTIR de polímeros que contienen etileno,” Rev. DYNA, vol. 86, no. 209, pp. 198–205, 2019 .

[72] Rodríguez, Margarita P. Q. "Fourier transform infrared (FTIR) technology for the identification of organisms" Clinical Microbiology Newsletter, Vol.22, No.8, pp.57-61, (2000).

[73] S. Wei Fu, "Research on the characterization of hydrogenated silicon thin film using constant photocurrent method", Thesis M.Sc, Department of Optics and Photonics, National Central University, China,(2009).

[74] O.Stenz," The physics of thin film optical spectra", An Introduction, Winzer laer Str. 10, 07745 Jena Germany, PP.71-72, (2005).

[75] C. Mwolfe, N. Holouyak,and G. B. Stillman, "Physical Properties of Semiconductor", prentice Hall, New York, (1989)

[76] J.I. Pankove, "Optical Process in Semiconductors", Dover Publishing, Inc., New York ,(1971).

[77] Y. N. Al-Jamal, "Solid State Physics", Al-Mosel University, 2nd Ed., Arabic Version, (2000).

[78] A. G. Nilens "Deep imparity in Semiconductors" Wily-Inter Science Pubication, (1973) .

[79] J. I. Pankove "Optical processes on semiconductors Dover publication" Inc. New york, (1971)

[80] C. Kittel and Paul M. "Introduction to solid state physics" New York: Wiley, Vol.8., (1996)

[81] Peinke, Joachim, Jürgen P., Otto E. R. and Ruedi S. "Semiconductor physics" In Encounter with Chaos, Springer, Berlin, Heidelberg, pp.9-41, (1992).

[82] Jaffe J. E. and Alex Z. "Electronic structure of the ternary pnictide semiconductors ZnSiP 2, ZnGeP 2, ZnSnP 2, ZnSiAs 2, and MgSiP 2." Physical Review B, Vol. 30, No.2, p.741,(1984).

[83] F.A. Jenkins and H.E. White, "Fundamentals of Optics", 4th Ed., McGraw-Hill, Inc., (1981).

[84] Bonnell, D. A., Huey, B., & Carroll, D. In-situ measurement of electric fields at individual grain boundaries in TiO2. Solid State Ionics, 75, 35-42(1995).

[85] L. L. Kazmerski, " polycrystalline and Amorphous Thin Flims and Devices" ACadmic Press, New York, (1980).

[86] Marien J., Wagner T., Duscher G., Koch A. and Rühle M. "Nb on (110) TiO2 (rutile): growth, structure, and chemical composition of the interface" Surface science, Vol.446, No.3, pp.219-228, (2000)

[87] Tintu, R., Saurav, K., Sulakshna, K., Nampoori, V. P. N., Radhakrishnan, P., & Thomas, S. Ge28Se60Sb12/PVA composite films for photonic applications. Journal of Non -Oxide Glasses, 2(4), 167-174(2010)..

[88] M. H. Hassouni , K. A. Mishjil, S. Chiad and N. F. Habubi, "Effect of Gamma Irradiation on the Optical Properties of Mg doped CdO Thin films deposited by Spray Pyrolysis", International Letters of Chemistry, Physics and Astronomy, Vol. 11, PP. 26-37,(2013).

[89] P. Barber, S. Balasubramanian, Y. Anguchamy, S. Gong,A.Wibowo, H. Gao, H. J. Ploehn and H. C. zur Loye, 2009, "Polymer Composite and Nanocomposite Dielectric Materials for Pulse Power Energy Storage", Materials Journal, Vol. 2, PP.1697-1733.

[90] T. Putjuso and P. Sangarun, 2012, " Influence of Annealing on the Giant Dielectric Properties of CuO Ceramics Prepared by a Simple PVA Sol-Gel", KKU Research Journal, Vol.17, No. 2, PP. 203-210.

[91]M. Akram, A. JAVED and T. Zahra, 2005, "Dielectric Properties of Industrial Polymer Composite Materials", Turk Journal of Physics, Vol. 29, PP. 355- 362.

[92] R. Hule and D. J.Pochan,2007,"Polymer Nanocomposites for Biomedical Applications", Journal of MRS BULLETIN, Vol. 32, PP. 354-358.

[93] S. Kitouni . " Dielectric Properties of Triaxial Porcelain Prepared Using Raw Native Materials Without Any Additions", Baikan Journal of Electrical & Computer Engineering, Vol.2, No.3, PP.128-131(2014) .

[94] S. Prasher, M. Kumer and S. Singh, "Analysis of Electrical Properties of Li3+ ion Beam Irradiated Lexan Polycarbonate", Asian Journal of Chemistry, Vol.21, No.10,PP.43-46 (2009).

[95] Micheli, D., Delfini, A., Marchetti, M., Gianola, P., Bertin, G., & Diana, R. Measurements of the outdoor-to-indoor attenuation of mobile phone signal. International Journal on Communications Antenna and Propagation (IRECAP), 4(6) (2014).

[96] A.Hamed, P.Mohammad A Study on the Effect of Temperature in Synthesis and Magnetic Properties of W-Type Hexaferrites Barium Nano Composites with Radar Wave Absorbing Properties Natural and Social Sciences, Vol.3, No.3 pp. 580-588,(2014)

[97] S. Vinayasree, M. A. Soloman, S.Vijutha, P. Mohanan, K.Philip, P. A. Joy, and M. R. Anantharaman Flexible microwave absorbers based on barium hexaferrite, carbon black, and nitrile rubber for 2– 2GHz applications J. Appl. Phys. 116, P.P.024902 (2014).

[98] E. J.Silvia, G. B.Paula, A. H.Carlos and A. V.Leandro r hexaferrite Ni ferrite nanocomposites magnetic behavior and microwave absorbing properties in the X-band Materials Chemistry and Physics, Volume 157, Pages 124–129,(2015).

[99] Gao, Y., Wang, Z., Pei, J., & Zhang, H. Structure and magnetic properties correlated with cation distribution of Ni_{0}. 5-x$Mo_{x}Zn_{0}$. $5Fe_{2}O_{4}$ferrites prepared by sol-gel auto-combustion method. Ceramics International, 44(16), 20148-20153(2018).

[100] M. A. Ahmed, K. E.-S. Rady, K. M. El-Shokrofy, A. A. Arais, and M. S. Shams, “The Influence of Zn²⁺ Ions

Substitution on the Microstructure and Transport Properties of Mn-Zn Nanoferrites," Mater. Sci. Appl., vol. 5, no. 13, pp. 932–942, 2014, doi: 10.4236/msa..513095(2014).

[101] S. Irfan, M. Ajaz-Un-Nabi, Y. Jamil, and N. Amin, "Synthesis of Mn_{1-x} $Zn_xFe_2O_4$ ferrite powder by co-precipitation method," IOP Conf. Ser. Mater. Sci. Eng., vol. 60, no. 1, , doi: 10.1088/1757-899X/60/1/012048 (2014).

[102] C. Murugesan and G. Chandrasekaran, "Structural and Magnetic Properties of Mn1−xZnxFe2O4 Ferrite Nanoparticles," J. Supercond. Nov. Magn., vol. 29, no. 11, pp. 2887–2897doi: 10.1007/s10948-016-3604-1(2016).

[103] M. Gupta, M. Gupta, Anu, R. K. Mudsainiyan, and B. S. Randhawa, "Aqueous Ammonia as „CPCA" in Sol-gel Combustion Method for Nanofabrication of CdFe2O4," Mater. Today Proc., vol. 3, no. 2, pp. 319–324, doi: 10.1016/j.matpr.2016.01.076. (2016).

[104] Carvalho, A. J. Felix, E. Trovatti, and C. Alvarez Casale. "Polystyrene/cellulose nanofibril composites: fiber dispersion driven by nanoemulsion flocculation." Journal of Molecular Liquids 272 387-394,(2018).

[105] E. Masoud, M. El-Bellihi, A. A., Bayoumy, W. A., & E. S. Abdelazeem . Structural, optical, magnetic, and electrical properties of nanospinels containing different molar ratios of cobalt and aluminum ions. Ionics, 23(9), 2417-2427.29, 2417, (2017).

[106] J. R. Babu and K. Vijay kumar, "Studies on structural and electrical properties of NaHCO3 doped PVA films for electrochemical cell applications," Int. J. ChemTech Res., vol. 7, no 1,pp. 171–180, Jan. 2015.

[107] N. Elmarzugi1, T. Adali, A. Bentaleb, E. I. Keleb, A. T. Mohamed and A. M. Hamza, 2014, " Spectroscopic Characterization of PEG-DNA Biocomplexes by FTIR", Journal of Applied Pharmaceutical Science, Vol. 4, No. 8, PP. 6-10.

[108] N. Arsalani, H. Fattahi and M. Nazarpoor. " Synthesis and characterization of PVP-functionalized superparamagnetic Fe3O4 nanoparticles as an MRI contrast agent", Journal of eXPRESS Polymer Letters Vol.4, No.6, PP. 329–338 (2010).

[109] D. Kumar, S. Karan Jat, P. K. Khanna, N. Vijayan, S.Banerjee "Synthesis Characterization andStudies of PVA/Co-Doped ZnO Nanocomposite Films", International Journal of Green Nanotechnology, Vol. 4, PP.408–416(2012).

[110] A. Pal Indolia and M. S. Gaur, "Optical Properties of Solution Grown PVDF-ZnO Nanocomposite Thin Films", Journal of Polymer Research, Vol. 20, No. 43, PP. 1-8(2013).

[111] P. Phukan and D. Saikia, "Optical and Structural Investigation of CdSe Quantum Dots Dispersed in PVA Matrix and Photovoltaic Applications", International Journal of Photoenergy, Vol. 2013, Article ID 728280, 6 pages (2013).

[112] Y. Feng, N. Dong, G. Wang, Y. Li, S. Zhang K. Wang, L. Zhang, W. J. Blau, and J. Wang, "Saturable absorption behavior of free-standing graphene polymer composite films over broad wavelength and time ranges", Journal of Optics Express, Vol.23, No.1, PP.559-569 (2015).

[113] E. Fortunati, F. Luzi, D. Puglia, R. Petrucci, J. Kenny and L. Torre, "Processing of PLA nanocomposites with cellulose

nanocrystalsextracted from Posidonia oceanica waste: Innovative reuse of coastal plant", Journal of Industrial Crops and Products, Vol. 67, PP.439 – 447 (2015).

[114] G. A. M Amin and M. H. Abd-El Salam, "Optical, dielectric and electrical properties of PVA doped with Sn nanoparticles", Journal of Materials Research Express, Vol. 1, PP.1-8 (2014).

[115] N. B. Rithin Kumar, Vincent Crasta, and B.M. Praveen ,"Advancement in Microstructural, Optical, and Mechanical Properties of PVA (Mowiol 10-98) Doped by ZnO Nanoparticles", Physics Research International Journal, Vol. 2014, Article ID 742378, 9 pages (2014).

[116] S. Salman, N. Bakr and M. H. Mahmood, "Preparation and study of some optical properties of (PVA- $Ni(CH_3COO)_2$)composites", International Journal of Current Research, Vol. 6, Issue, 11, PP.9638-9643.(2014).

[117] A. Hashim, & A. Jassim .Novel of biodegradable polymers-inorganic nanoparticles: structural, optical and electrical properties as humidity sensors and gamma radiation shielding for biological applications. Journal of Bionanoscience, 12(2), 170-176(2018).

[118]A.M. Abdelghany, E.M. Abdelrazek and D. Rashad, "Impact of in situ preparation of CdS filled PVP nano-composite", Journal of Spectrochimica Acta Part A: Molecular and Biomolecular Spectroscopy, Vol. 130, PP.302–308 (2014).

[119] D. Hegazy, M. Eid and M. Madani, "Effect of Ni Nano particles on Thermal, Optical and Electrical Behaviour of Irradiated PVA/AAc Films", Arab Journal of Nuclear Science and Applications, Vol.47, No. 1, PP.41-52(2014).

[120] Z. Hossein Esfahani Mahshad Ghanipour and Davoud Dorranian ," Effect of dye concentration on the optical properties of red-BS dye-doped PVA film", Journal of theoretical Applied Physics, Vol.8, No.139, PP. 117-121|(2014).

[121] G. Attia and M.F.H. Abd El-kader" Structural, Optical and Thermal Characterization of PVA/2HEC Polyblend Films", International Journal of Electrochemical Science, Vol.8, PP. 5672 - 5687 (2013).

[122] A. M. El Sayed and W. M. Morsi, 2014, " α-Fe2O3 /(PVA + PEG) Nanocomposite Films; Synthesis, Optical, and Dielectric Characterizations", Journal of Materials Science, Vol.49, PP.5378–5387

[123] O. Gh. Abdullah, "Influence of Barium Salt on Optical Behavior of PVA Based Solid Polymer Electrolytes", European Scientific Journal, Vol.10, No.33,2014.

[124] N. K. Abbas, M. A. Habeeb, and A. J. Kadham Algidsawi, , "Preparation of Chloro Penta Amine Cobalt(III) Chloride and Study of Its Influence on the Structural and Some Optical Properties of Polyvinyl Acetate", International Journal of Polymer Science, Vol., Article ID 926789, 10 pages (2015).

[125] A. Hashim, "Enhanced Structural, Optical, and Electronic Properties of in 2 O_3 and Cr_2 O_3 Nanoparticles Doped Polymer Blend for Flexible Electronics and Potential Applications. “Journal of Inorganic and Organometallic Polymers and Materials, PP 1-13, (2020).

[126] D. Vaishnav1 and R. K. Goyal, , " Thermal and Dielectric Properties of High Performance Polymer/ZnO Nanocomposites",

IOP Conf. Series: Journal of Materials Science and Engineering, Vol. 64, PP.1-11,(2014) .

[127] A. Srivastava, K. Kumar Jana, P. Maiti, D. Kumar, and O. Parkash, " Investigations on Structural, Mechanical, and Dielectric Properties of PVDF/Ceramic Composites", Journal of Engineering, Vol. 2015, Article ID 205490, 9 pages(2015).

[128] H.N. Chandrakala, Shivakumaraiah, H. Somashekarappa, R. Somashekar, S. Chinmayee and Siddaramaiah," Poly(Vinyl Alcohol)/Zincoxide-Ceriumoxide Nanocomposites: Electrical, Optical, Structural and Morphological Characteristics",Indian Journal of Advances in Chemical Science, Vol. 2, PP. 103-106(2014).

[129] D. Pradhan, R. N. P. Choudhary, B. K. Samantaray, , " Studies of Dielectric Relaxation and AC Conductivity Behavior of Plasticized Polymer Nanocomposite Electrolytes", International Journal Electrochemical. Science, Vol.3, P. 597 – 608 (2008).

[130] S. Satapathy , P. K. Gupta , K. B. R. Varma ,and P. TiwariandV. Ganeshan,"Study on Dielectric Behavior of Lithium Tantalate (LT) Nanoparticle Filled Poly vinylidene Fluoride(PVDF) Nanocomposites", Ins. of Sci. India,(2008).

[131] A. Goswami, A. K. Bajpai, J. Bajpai, and B. K. Sinha, “Designing vanadium pentoxide-carboxymethyl cellulose/polyvinyl alcohol-based bionanocomposite films and study of their structure, topography, mechanical, electrical and optical behavior,” Polym. Bull., vol. 75, no. 2, pp. 781–807, (2018).

[132] K. Rajesh, V. Crasta, N. B. Rithin Kumar, G. Shetty, and P. D. Rekha, “Structural, optical, mechanical and dielectric properties of

titanium dioxide doped PVA/PVP nanocomposite," J. Polym. Res., vol. 26, no. 4,pp1-10,(2019).

[133] S.C. Mishra, "Dielectric Behavior of Bio-Waste Reinforced Polymer Composites", Global Journal Of Engineering Science And Researches, Vol. 1, No.9, P. 32-44, (2014).

[134] S. Ju1, M. Chen1, H. Zhang and Z. Zhang, " Dielectric properties of nanosilica/low-density polyethylene composites: The surface chemistry of nanoparticles and deep traps induced by nanoparticles", Journal of eXPRESS Polymer Letters Vol.8, No.9, PP. 682–691,(2014).

[135] G. Chakraborty, K. Gupta, D. Rana and A. Kumar Meikap , "Dielectric relaxation in polyvinyl alcohol – polypyrrole –multiwall carbon nanotube composites below room temperature", Advances in Natural Sciences, Vol. Vol.4, PP. 1-4, (2014).

[136] A. Goswami, A. K. Bajpai, J. Bajpai, and B. K. Sinha, "Designing vanadium pentoxide-carboxymethyl cellulose/polyvinyl alcohol-based bionanocomposite films and study of their structure, topography, mechanical, electrical and optical behavior," Polym. Bull., vol. 75, no. 2, pp. 781–807, (2018).

[137] K. Rajesh, V. Crasta, N. B. Rithin Kumar, G. Shetty, and P. D. Rekha, "Structural, optical, mechanical and dielectric properties of titanium dioxide doped PVA/PVP nanocomposite," J. Polym. Res., vol. 26, no. 4,pp1-10, (2019).

[138] P. Vasudevan, S. Thomas, K. Arunkumar, S. Karthika and N. Unnikrishnan, " Synthesis and dielectric studies of poly (vinyl pyrrolidone) /titanium dioxide nanocomposites",

Journal of Materials Science and Engineering, Vol. 73, PP. 1-4, doi:10.1088/1757-899X/73/1/01 ,(2015).

[139] I. Tantis, G. Psarras and D. Tasis, "Functionalized graphene poly(vinyl alcohol) nanocomposites: Physical and dielectric properties", Journal of eXPRESS Polymer Letters, Vol.6, No.4, PP.283–292, (2012).

[140] Lu, Honglong, et al. "The effect of polymer polarity on the microwave absorbing properties of MWNTs." RSC advances 5.80: 64925-64931(2015).

الخلاصة

في هذه الدراسة ، تم تحضير $Cu_x\ Ni_{1-x}FeO_3$ مع $x = 0.1$ و 0.3 عند درجة حرارة 1200^oC بواسطة طريقة الترسيب لأنها تعطي تجانسًا كبيرًا لجزيئات المسحوق.

وضحت حيود الاشعة السينية بتكوين طور المغزلي المكعب للوجه (FCC) عند درجة الكلسنة لمسحوق الفرايت $Cu_x\ Ni_{1-x}\ FeO_3$ مع $x = 0.1$ و0.3. بعد ذلك تم اضافة تراكيز مختلفة من الفرايت (1 ,3 و5) %wt إلى مركب البولي فينيل بيروليدون (PVP)/ بولي فينيل الكحول (PVA).

من المجهر الإلكتروني الماسح للانبعاثات الميدانية (FESEM) وصور المجهر الضوئي أظهرت الفرايت $Cu_xNi_{1-x}\ FeO_3$ مع $x = 0.1$ و 0.3 تشكل شبكة مستمرة داخل مركبات PVP/PVA وتنزاح الروابط معينة وتغيرات في شدة يمكن رؤية روابط معينة في طيف فورير للتحول الطيفي بالأشعة تحت الحمراء (FTIR) ، مما يدل على عدم وجود تفاعلات بين مصفوفة البوليمر (PVP / PVA) والفرايت $Cu_xNi_{1-x}FeO_3$ مع ($x = 0.1$ و 0.3) على التوالي.

من الخواص البصرية, تزداد الامتصاصية بزيادة تركيز الفرايت $Cu_x\ Ni_{1-x}FeO_3$ مع ($x = 0.1$ و 0.3) و تنخفض مع زيادة الطول الموجي لجميع عينات المتراكب النانوي ، بينما تقل النفاذية مع زيادة تركيز الفرايت وتقل مع زيادة الطول الموجي $Cu_x\ Ni_{1-x}FeO_3$ مع ($x = 0.1$ و 0.3)داخل مصفوفة بوليمر (PVP / PVA) . فجوة الطاقة تتناقص مع زيادة تركيز الفرايت $Cu_x\ Ni_{1-x}FeO_3$مع $x = 0.1$ و 0.3 داخل مصفوفة بوليمر (PVP / PVA) .زيادة معامل الامتصاص، معامل الخمود, معامل الانكسار، ثابت العزل الحقيقي والخيالي والتوصيلية البصرية مع زيادة تركيز الفرايت $Cu_x\ Ni_{1-x}FeO_3$ مع $x = 0.1$ و 0.3 داخل مصفوفة البوليمر(PVP / PVA).

الخواص الكهربائية للتيار المتناوب مثل ثابت العزل والفقد العزلي تزداد مع زيادة تركيز الفرايت $Cu_x\ Ni_{1-x}FeO_3$ مع $x = 0.1$ و 0.3 داخل مصفوفة بوليمر (PVP / PVA) وتنخفض مع زيادة

تردد المجال الكهربائي المطبق بينما تزداد الموصلية الكهربائية مع زيادة تركيز الفرايت $Cu_x Ni$ $_{1-x}FeO_3$مع x = 0.1 و 0.3 داخل بوليمر / PVP) PVA) وتزداد أيضًا مع التردد.

توهين الموجات المايكروية داخل نطاق التردد (4-7) جيجاهرتز لتركيز مختلف من $Cu_x Ni_{1-}$ $_xFeO_3$مع x = 0.1و 0.3 داخل بوليمر(PVP / PVA) .قدرة هذا المركب النانوي على توهين الموجات المايكروية المنبعثة داخل النطاق الحزمة S .

جمهورية العراق
وزارة التعليم العالي والبحث العلمي
جامعة بابل
كلية التربية للعلوم الصرفة
قسم الفيزياء

تصنيع ووصف المتراكبات النانوية (PVA-PVP-فرايت) وتطبيقاتها

رسالة مقدمة

إلى مجلس كلية التربية للعلوم الصرفة في جامعة بابل وهي جزء من متطلبات نيل درجة الماجستير في التربية / الفيزياء

من قبل الطالب

علي جاسم محمد مصارع

بكالوريوس تربية فيزياء

(جامعة بابل -2007)

بأشراف

أ . د . سمير حسن هادي

1443 هـ **2022 م**